2015

INTERFACIAL ENGINEERING OF BIOMASS HYDROLYSIS BY CELLULASE ENZYMES AND MECHANISTIC MODELING OF HYDROLYSIS OF CELLULOSE SUBSTRATES

Ravinder Kumar Garlapalli
University of Kentucky, rga225@uky.edu

STUDENT AGREEMENT:

I represent that my thesis or dissertation and abstract are my original work. Proper attribution has been given to all outside sources. I understand that I am solely responsible for obtaining any needed copyright permissions. I have obtained needed written permission statement(s) from the owner(s) of each third-party copyrighted matter to be included in my work, allowing electronic distribution (if such use is not permitted by the fair use doctrine) which will be submitted to UKnowledge as Additional File.

I hereby grant to The University of Kentucky and its agents the irrevocable, non-exclusive, and royalty-free license to archive and make accessible my work in whole or in part in all forms of media, now or hereafter known. I agree that the document mentioned above may be made available immediately for worldwide access unless an embargo applies.

I retain all other ownership rights to the copyright of my work. I also retain the right to use in future works (such as articles or books) all or part of my work. I understand that I am free to register the copyright to my work.

REVIEW, APPROVAL AND ACCEPTANCE

The document mentioned above has been reviewed and accepted by the student's advisor, on behalf of the advisory committee, and by the Director of Graduate Studies (DGS), on behalf of the program; we verify that this is the final, approved version of the student's thesis including all changes required by the advisory committee. The undersigned agree to abide by the statements above.

Ravinder Kumar Garlapalli, Student

Dr. Stephen E. Rankin, Major Professor

Dr. Thomas Dziubla, Director of Graduate Studies

INTERFACIAL ENGINEERING OF BIOMASS HYDROLYSIS BY CELLULASE ENZYMES AND MECHANISTIC MODELING OF HYDROLYSIS OF CELLULOSE SUBSTRATES

DISSERTATION

A dissertation submitted in partial fulfillment of the
requirements for the degree of Doctor of Philosophy
in the College of Engineering at the University of
Kentucky

By

Ravinder Kumar Garlapalli

Lexington, Kentucky

Director: Dr. Stephen Rankin, Professor of Chemical and Materials Engineering

Lexington, Kentucky

ABSTRACT FOR DISSERTATION

INTERFACIAL ENGINEERING OF BIOMASS HYDROLYSIS BY CELLULASE ENZYMES AND MECHANISTIC MODELING OF HYDROLYSIS OF CELLULOSE SUBSTRATES

Lignocellulosic biomass is a sustainable and renewable energy resource that can be converted to fuels and other commodity chemicals, but this conversion is currently limited by its recalcitrance to enzymatic degradation. Because of this recalcitrance, the major challenges in the commercialization of enzymatic hydrolysis processes are the relatively low hydrolysis rates, limited cellulose conversion under some conditions, and high cost of enzymes.

Enzymatic hydrolysis is influenced by the structure of the biomass after pretreatment and the mode of enzyme action, but has also been shown to be enhanced by surfactant additives. The objective of this work was to elucidate the mechanism of hydrolysis by studying the activity of cellulase enzymes and the effects of non-ionic surfactant Tween-80 on the interactions of model cellulose (varying in surface morphology and crystallinity) and lignin films with cellulases. The primary tool used to measure the binding and activity of cellulase enzymes derived from *Trichoderma reesei* was a quartz crystal microbalance with dissipation monitoring (QCM-D). The nonionic surfactant Tween-80 was found to reduce the adsorption of cellulases onto all types of cellulose films. Tween-80 had no significant effect on hydrolysis of amorphous LiCl/DMAc cellulose films whereas the hydrolysis rate decreased with increase in Tween-80 concentration for type II crystalline NMMO cellulose films. On lignin, co-adsorption of Tween-80 and cellulase resulted in an apparent net reduction in the amount of cellulase adsorbed on lignin. Sequential adsorption experiments suggested that Tween-80 was able to reduce and displace adsorbed cellulases. Thus, Tween-80 was found to compete effectively with cellulase enzymes for binding to hydrophobic surfaces such as lignin without significantly impeding hydrolysis of cellulose, which explains how it is able to enhance overall conversion for bulk biomass hydrolysis.

To gain fundamental understanding of the hydrolysis process, a kinetic model based on the processive action of cellulase enzymes was developed and applied to QCM-D data. The model makes a distinction between surface cellulose units and bulk sites that only become accessible as hydrolysis proceeds. The model predictions during binding and enzymatic hydrolysis under various scenarios are discussed along with future possible work.

Keywords: Cellulose, Enzymatic hydrolysis, Tween-80, Lignin, Adsorption, Kinetics

Ravinder Garlapalli

10/29/2015

INTERFACIAL ENGINEERING OF BIOMASS HYDROLYSIS BY CELLULASE ENZYMES AND MECHANISTIC MODELING OF HYDROLYSIS OF CELLULOSE SUBSTRATES

By
Ravinder Kumar Garlapalli

Dr. Stephen E Rankin

(Director of Dissertation)

Dr. Thomas Dziubla

(Director of Graduate Studies)

10/29/2015

(Date)

ACKNOWLEDGEMENTS

I alone can only take a small portion of the credit for the completion of this chapter in my life. I would like to extend my gratitude to the many people who made this possible. First of all, I am extremely happy to record my profound gratitude to my advisors, Dr. Stephen E. Rankin and Dr. Barbara L. Knutson for their valuable guidance, sustained interest and constant support through the years. Their great motivation and encouragement inspired me to not only try out new ideas but also dig into the fundamental scientific questions behind every project I worked on throughout my graduate career at University of Kentucky. I would also like to thank my advisory committee members Dr. Sue Nokes and Dr. Thomas Dziubla for their time and constructive feedback on my work.

I gratefully acknowledge the Kentucky Science and Engineering Foundation and USDA Biomass Research and Development Initiative for the financial support that made my PhD work possible.

I would like to acknowledge all the current and former members from both Dr. Rankin and Dr. Knutson research groups for their friendship and assistance. In particular, I would like to thank Dr. Suvid Joshi, Dr. Saikat Das, and Dr. Hsin-Fen Li and to be doctor's Suraj Nagpure, Syed Islam, Shanshan Zhou, for their generous help with my research and for creating a nice working environment.

I would also like to thank all my friends who directly or indirectly helped me and incredibly supportive for sharing the hard times and making the most of the good times. I am extremely fortunate to be surrounded by a group of highly motivated and wonderful friends that became a part of my life and made my time in Lexington enjoyable.

Finally, I am extremely thankful to my family for their unconditional love, encouragement, support and prayers in all the phases of my life. No words can explain how grateful I am and how fortunate I feel.

Table of Contents

List of Tables

List of Figures

CHAPTER 1

INTRODUCTION

Transition from a society dependent on fossil fuels to renewable resources is viewed as an important contribution to the development of a sustainable industrial society and effective management of greenhouse gas emissions[1]. The production of ethanol and commodity chemicals from lignocellulosic biomass promises to decrease fossil fuel use and increase domestic markets for agriculture and forestry commodities [1-3]. Primary consideration involves the production of ethanol from renewable resources as it represents an important, renewable liquid fuel for motor vehicles that can be blended with gasoline [4]. The use of ethanol and gasoline mixture as an alternative motor fuel has been steadily increasing around the world for a number of reasons. Domestic production and use of ethanol for fuel can decrease dependence on foreign oil, reduce trade deficits, create jobs in rural areas, reduce air pollution, and reduce global climate change carbon dioxide buildup. Biofuels derived from plant sources are not generally regarded as sources of greenhouse-gas emissions because the amount of carbon dioxide emitted during their use is equivalent to that of absorbed by plants during photosynthesis [5].

Interest in ethanol from biomass such as corn starch emerged in the 1970s when the price of fossil fuel rose. In the United States, the Energy Independence and Security Act (EISA) of 2007 mandate the production of 16 billion gallons (136.27 L) per year of bioethanol by the year 2022 [6]. Biofuel production grew exponentially reaching a capacity of 13.5 billion gallons (as of 2010) making the U.S. the world's leading biofuel producer and exporter. In the U.S., bioethanol is primarily produced from corn starch

feedstock. Although corn-based based-ethanol is a promising substitute to gasoline production mainly in the transportation sector, the amount available is not sufficient to replace a considerable portion of the one trillion gallons of fossil fuel presently consumed worldwide each year. Furthermore, the ethical concerns about the use of food crops as fuel raw materials have encouraged research efforts to work on more acceptable sources containing lignocellulosic biomass that are derived mainly from agricultural residues, industrial wastes, forest biomass and other inedible feedstock alternatives [7, 8]. As a result, abundant availability and renewability of lignocellulosic biomass has made it a topic of much interest and motivated research in use of lignocellulosic biomass as a source of energy via breakdown to sugars that can then be converted to fuels. For this purpose, enzyme systems from fungi have been widely investigated for the depolymerization of cellulosic biomass into monosaccharide building blocks [3].

One of the major limitations of enzymatic hydrolysis is the consistently high cost of the enzymes involved in the conversion of the cellulose component of biomass into fermentable sugars. This is primarily due to the comparatively high enzyme loadings commonly required to overcome the substrate features and enzyme related factors limiting effective hydrolysis [9-11]. For any enzyme source, developing economically viable cellulosic ethanol processes will require making significant inroads to overcome the factors that limit hydrolysis of biomass [12]. Efforts to reduce the costs by improving the activity of cellulase enzymes to catalyze the hydrolysis of cellulose have been hindered by incomplete understanding of enzyme-substrate interactions. In this work, we address the biophysics of the action of the enzymes on model biomass surfaces, with a

goal of establishing clear links between the biomass surface chemistry and interactions with cellulase enzymes and additives used in hydrolysis systems.

1.1 Lignocellulose biomass

Lignocellulosic biomass is an attractive material for bioethanol fuel production since it is the most abundant renewable resource. There are several groups of raw materials that are differentiated by their origin, composition and structure such as forestland materials include mainly woody biomass namely, hardwoods and softwoods; agricultural residues that cover food and non-food crops and grasses such as switch grass; and municipal and industrial wastes from residential or non-residential sources such as food wastes and paper mill sludge [13, 14].

Lignocellulose consists of plant cell wall materials primarily made up of cellulose, hemicellulose and lignin. Cellulose and hemicelluloses make up approximately 70% of the entire biomass and are tightly linked to the lignin component through covalent and hydrogen bonds that make the structure highly robust and resistant to enzymatic treatment. Table 1.1 presents biochemical compositions for several suitable feedstock materials for bioethanol production.

1.2 Cellulose, Hemicellulose and Lignin

Cellulose is a linear polysaccharide of glucose residues (D-anhydroglucopyranose) linked by β-1, 4 glucosidic bonds formed between the carbon atoms C(1) and C(4) of adjacent glucose units. Anhydrocellobiose is the repeating unit of cellulose in which the adjacent glucose moieties are rotated 180° with respect to their

immediate neighbors. The neighboring glucose residues interact via intra-molecular hydrogen bonds, which give rigidity to the chains, and the polymer chains link via inter-molecular hydrogen bonds to form microfibrils which results in crystalline cellulose. The microfibrils are bound together by van der Waals forces and hydrophobic interactions [15] and are embedded within hemicellulose and lignin to form the basis of the plant cell wall. Figure 1.1 shows the structure and composition of cellulose fibers. Cellulose consists of both crystalline and amorphous forms and its supramolecular chemistry is complex due to varying patterns of inter and intra chain hydrogen bonds. Four different polymorphs of cellulose are known, namely cellulose I, II, III and IV some of which contain sub-classes. Cellulose I is the form found in nature and occur in two polymorphs I_α and I_β. Cellulose II is formed from cellulose I either by regeneration (dissolution and deposition of cellulose) or mercerization. Cellulose III_1 and III_{11} are obtained by treatment of cellulose I or II with liquid ammonia or amines. Cellulose IV is formed by heating cellulose III[16, 17].

Hemicellulose consists of different monosaccharide units and is a highly branched polymer composed primarily of hexose (glucose, galactose and mannose) and pentose (xylose and arabinose) units [18, 19]. Its backbone chain is primarily composed of xylan β (1-4) linkages that include xylose and arabinose. It is chemically bonded and serves as an interface between the lignin and cellulose.

Lignin is a rigid aromatic network biopolymer with a high molecular weight bonded via covalent bonds to cellulose and hemicellulose conferring rigidity and a high level of compactness to the plant cell wall [20]. Lignin is composed of three phenolic

monomers of phenyl propionic alcohol namely, coumaryl, coniferyl and sinapyl alcohol. Extensive cross-linking and structural heterogeneity of lignin provide mechanical support to the plant cell wall and allows lignin to act as a barrier to protect the cells against microbial attack [11, 21]. This causes difficulty in the breaking of biomass into its components and blocks the exposure of cellulosic matter to enzymes. Lignin components substantially deactivate cellulase enzymes and hence influence enzymatic hydrolysis. This negative impact caused by lignin has led to interest in lowering the lignin inhibitory effect [22]. For example, the adsorption of cellulases to lignin requires a higher enzyme loading because this binding generates a non-productive enzyme attachment and limits the accessibility of cellulose to cellulases.

1.3 Biomass conversion process

Lignocellulosic biomass can be converted into fuels and chemicals via two different approaches, biochemical or thermochemical conversion [23]. Thermo-chemical conversion involves partial oxidation to produce carbon monoxide (CO) and hydrogen (H_2), which can be catalytically converted to alcohols, hydrocarbons and other products. While thermochemical conversion is an established process for any hydrocarbon source, it is relatively energy-intensive because it requires high temperature processing for both syngas generation and for catalytic generation of products. Biological conversion of biomass involves enzymatic hydrolysis of cellulose and hemicellulose to sugars that are subsequently fermented into alcohol and other valuable products. Biochemical conversion of lignocellulosics to bioethanol consists of four major unit operations: pretreatment, hydrolysis, fermentation and product separation. A simplified process description of biochemical lignocellulose conversion is shown in Figure 1.2.

1.3.1 Pretreatment

The first step in bioconversion of lignocellulose to bioethanol is size reduction and pre-treatment. Pretreatment is aimed at degrading the protective layers to facilitate enzymatic hydrolysis of carbohydrate-based components. At the molecular level, access to the cellulose chains of microfibrils is restricted by lignin and hemicellulose. In the pretreatment step the recalcitrance is reduced by depolymerizing and solubilizing hemicellulose, thereby exposing the cellulose chains which can then be hydrolyzed by cellulases [24]. A successful pre-treatment must meet the following requirements [9, 25, 26]: (i) maximize digestibility of lignocellulose material or the ability to subsequently form sugars by hydrolysis, (ii) avoid degradation or loss of carbohydrates, (iii) avoid formation of byproducts inhibitory to subsequent hydrolysis and fermentation processes, (iv) have a low capital and operating cost compared to product of interest, and (v) work for a variety of feedstocks.

Several different pretreatment methods have been used to remove the recalcitrant cell wall material of lignocellulosic biomass, namely, mechanical, biological or thermochemical. There has been considerable advancement in development of pretreatment processes, and many reviews are available that provide detailed overviews of the types of pretreatments available [25, 27, 28]. Table 1.2 illustrates some of the pretreatment methods that have been examined over the years. An ideal pretreatment process would involve complete separation and isolation of each component from a lignocellulosic substrate; however, pretreated lignocellulosic substrates usually contain some amount of hemicellulose and lignin associated with the cellulosic rich stream obtained after pretreatment. Although most of these treatments can liberate

hemicellulose and cellulose from the cell wall, some of them remain economically unfeasible due to key technical issues.

1.3.2 Hydrolysis

When pretreatment is complete, the biomass is prepared for hydrolysis (a process also known as saccharification). During this reaction, the polysaccharide chains of cellulose and hemicellulose are hydrolyzed into fermentable monomer molecules for conversion to bioethanol. There are two different types of hydrolysis processes that involve either acidic (dilute or concentrated sulfuric acid) or enzymatic hydrolysis. Dilute acid hydrolysis (1-3% sulfuric acid) requires a high temperature of 200-240 °C to disrupt cellulose crystals [29]. It is followed by hexose and pentose degradation and formation of inhibitory compounds like furfural, hydroxymethyl furfural (HMF), acetic acid and formic acid which impacts sugar recovery and ethanol yields [7]. Unlike dilute acid hydrolysis, concentrated acid hydrolysis (70% sulfuric acid) is not followed by high concentrations of inhibitors and produces a high yield of free sugars (90%), however, it requires large quantities of acid as well as costly acid recycling, which makes it commercially less attractive [30]. These issues have driven development of research to improve enzymatic hydrolysis. Enzymatic hydrolysis of natural lignocellulosic materials is a very slow process and results in solubilization of less than 20% of the originally present glucan; therefore some form of pretreatment to increase accessibility to enzymatic hydrolysis is included in most process concepts for biological conversion of lignocellulose. Pre-treatment, under appropriate conditions, retains nearly all of the cellulose present in the original material and allows close to theoretical yields upon enzymatic hydrolysis [31]. Enzymatic hydrolysis uses cellulolytic enzymes produced

from microorganisms to catalyze the depolymerization of cellulose into glucose oligomers, dimers, and monomers. *Trichoderma reesei* is one of the most efficient and productive fungi used to produce industrial grade cellulolytic enzymes. During the enzymatic hydrolysis of cellulosic substrates, several factors restrict the sustained catalytic activity of the cellulase mixture. It has been suggested that these limitations are due to both substrate- and enzyme-related factors which will be discussed later in this chapter [32]. The cost of bioethanol production from lignocellulosic materials is relatively high when based on current technologies, and the main challenges are low glucose yield and the high cost of the hydrolysis process [7].

1.3.3 Fermentation and Product recovery

The hydrolysate obtained from the hydrolysis step can be fermented by microorganisms to produce ethanol. Industrial yeast *Saccharomyces cerevisiae* has been utilized in corn-based and sugar-based industries as the primary fermentative strain for bioethanol production [33]. One of the challenges associated with fermentation is the effective use of sugars other than hexose. In response to this inability of *Saccharomyces cerevisiae* to ferment pentose sugars, extensive efforts have been employed to develop genetically engineered microorganisms that are capable of fermenting pentose and hexose sugars simultaneously. Subsequently, bioethanol obtained from a fermentation conversion requires further separation and purification of ethanol from water through a distillation process. Fractional distillation is a process implemented to separate ethanol from water based on their different volatilities. Thus, water can be separated via a condensation procedure and ethanol distillate captured at a concentration of >95% [34].

1.4 Cellulases

Cellulases refer to a complex of enzymes produced from fungi and bacteria that synergistically hydrolyze cellulose into its constituents, monosaccharide (glucose) and disaccharide (cellobiose). Many microorganisms in nature produce a set of enzymes capable of degrading cellulose, but only a few microorganisms are particularly recognized for their efficiency. Among these, *Trichoderma reesei* (*T. reesei)* soft-rot fungi have been extensively investigated for the depolymerization of cellulosic biomass into monosaccharide building blocks [3, 35, 36]. This complex was crudely pictured as an enzyme known as 'C_1' decrystallizing cellulose, followed by a consortium of hydrolytic enzymes, known as 'C_x', which break down cellulose to glucose [35]. This early concept of cellulase activity has been modified and the combined action these enzymes is now described in terms of three major classes of cellulase enzymes: first, endoglucanases which act randomly on soluble and insoluble cellulose chains; second, exoglucanases, which include cellobiohydrolases (CBHs) that act processively to preferentially liberate cellobiose from the ends of cellulose chain; and finally, β-glucosidases, which liberate D-glucose from cellobiose [37].

Cellulases secreted by *T. reesei* consist of two cellobiohydrolases, Cel 7A (CBH I) and Cel 6A (CBH II), five endoglucanases Cel 7B (EG I), Cel 5A (EG II), Cel 12A (EG III), Cel 61A (EG IV), Cel 45A (EG V) and two β-glucosidases[38]. The enzymes involved in the hydrolysis of lignocellulose are called glycosyl hydrolases (GH). These enzymes can be further classified into families with structurally-related features arising from individual amino acid sequences and maintained in the Carbohydrate-Active Enzymes Database (CAZy) for GH enzymes and other relevant carbohydrate-active

proteins [39, 40]. Presently, 133 glycosyl hydrolase families have been identified. Cellualses are modular enzymes that are composed of independently folded, structurally and functionally discrete units referred to as domains or modules. Most cellulolytic enzymes contain two domain structure consisting of a catalytic domain (CD) and a cellulose binding domain (CBD – or carbohydrate binding module, CBM), which are bound together by a flexible linker [41]. Crystal structures have been determined for the catalytic domain structures of *T. reesei* CBH I, CBH II and EG I. The structural differences of the catalytic domains of cellobiohydrolases and endoglucanases suggest that their action on cellulose substrates is dictated by the shape of their active site. Endoglucanases have an open active site, which enables action in the middle of the glucan chain, while exoglucanases have tunnel shaped structure which hydrolyze only chain ends [36, 42]. The open cleft structure of EGs and the tunnel structure of CBHs are shown in Figure 1.3.

Cellulase binding onto crystalline cellulose has been widely studied with the main focus on cellulose binding module (CBM)-cellulose interactions. It is generally accepted that the primary role of CBM is to facilitate physical contact of the enzyme to the cellulose, increasing the effective concentration of the enzyme at the substrate. Cellulose surfaces have hydrophilic and hydrophobic faces. The cellulose surface is often considered highly hydrophobic because of hydrogen bonding among cellulose chains. On the hydrophobic faces, pyranose rings are fully exposed at the fibril surface. Cellulases interact with the cellulose surface through the cellulose binding domain and the catalytic domain. CBMs are currently distributed into families, ranging from small peptides (30-40 amino acids) to modules consisting of over 200 residues [43, 44].

There are several basic surface and intermolecular forces which control the adsorption of proteins onto solid/liquid interfaces. These interactions are usually non-covalent, i.e. mediated by hydrogen bonding, electrostatic or hydrophobic interactions. The most hydrophobic residues in proteins are those containing aromatic groups like tryptophan, phenylalanine and tyrosine. When these are exposed at the surface of the protein molecule, they form binding sites through hydrophobic interaction and hydrogen bonding. Fungal CBMs from *T. reesei* belong to family 1 and are characterized by a small wedge shaped fold featuring a cellulose binding surface with three exposed aromatic residues. Sequence comparison of *T. reesei* CBMs have shown that the three conserved tyrosines (Y5, Y31 and Y32) are involved in the binding to cellulose [45]. The aromatic rings in these amino-acid residues are spaced so that they may stack with every other pyranose rings on a cellulosic chain [46]. In a study by Lehtio *et al*. [47] binding of family 1 and family 3 CBMs was shown (by transmission electron microscopy) to occur preferentially on the hydrophobic (110) planes of Valonia cellulose (I_α) and more recently *T.reesei* Cel 7A was shown to degrade crystalline cellulose exclusively from the hydrophobic faces of a cellulose crystals [48]. Nimlos *et al*. [49] demonstrated with molecular simulation that the CBM from *Tr*Cel7A binds preferentially to the hydrophobic surfaces. They also suggest that family 1 CBM may also be able to transfer from hydrophilic crystal surfaces, to hydrophobic surfaces. Palonen *et al*. [50] observed that CBMs greatly increase enzyme binding to cellulosic surfaces, although the catalytic modules are also capable of low binding to cellulose. The overall efficiency of cellulases is markedly enhanced by the presence of CBMs. Additionally, Lehito *et al*. [47] observed fully reversible binding of family 1 CBM to crystalline cellulose at 4 °C. Reversibility of

CBM binding to the cellulose is an important issue as it will allow the hydrolysis reaction to proceed longer by reducing the enzyme loss due to unproductive binding.

The presence of hydrophobic groups on cellulases can also lead to general adsorption and non-productive binding to cellulose or lignin. Several authors have identified the negative consequences of enzyme binding to the lignin fraction of lignocellulose [51-56]. Non-productive enzyme adsorption onto the lignin components in biomass is a major inhibitory mechanism preventing efficient hydrolysis of the cell wall carbohydrates. The phenomenon is detrimental for process economics, since higher enzyme loadings are required to overcome the inhibitory effect and enzyme recycling is hindered after a completed reaction [57]. Palonen *et al*. [58] showed that the carbohydrate binding modules (CBMs) of *T. reesei* enzymes, Cel7A and Cel5A, significantly increase enzyme binding onto lignin and indicated that hydrophobic interactions are involved in non-productive binding to lignin. In a study by Börjesson *et al*. [59] *Tr*Cel7B (EG I) was found to bind more onto isolated lignin than *Tr*Cel7A (CBH I), although the catalytic modules of both enzymes bound to lignin to a similar degree. The difference in binding of the full-length enzymes was explained by the more hydrophobic character of the *Tr*Cel7B CBM. Three types of interactions have been suggested to mediate enzyme binding onto lignin: hydrophobic interactions [58-61], ionic interactions [51], and hydrogen bonding interactions [51, 62, 63]. However, the exact mechanisms by which cellulases interact with lignin and result in the reduction in hydrolysis effectiveness have yet to be fully resolved.

It would be beneficial to be able to decrease the non-productive adsorption of cellulases to lignin in commercial hydrolysis applications. It has been reported that the addition of additives such as proteins and surface active chemicals (surfactants) to the reaction mixture can decrease the non-productive binding of cellulases onto lignin and block the binding sites from the enzymes [59, 60]. Addition of BSA into the reaction mixture has been shown to increase the hydrolysis of lignocellulosic materials presumably because the BSA adsorbed to the lignin leaving more cellulase available for conversion [60, 64]. Anionic and non-ionic surfactants [60, 65] as well as lignosulphonates [66] have also been shown to improve the enzymatic hydrolysis of lignocellulose. Pretreatment of lignocellulosic biomass in the presence of additives prior to enzymatic hydrolysis has been shown to decrease the cellulase enzyme concentration required to achieve a desired conversion [67, 68]. A possible mechanism for the improved hydrolysis was suggested to be reduced non-productive enzyme adsorption to lignin. Despite the research carried out on this topic, more information about the effect of additives on binding of cellulases to cellulose and lignin is still required.

1.5 Factors affecting enzymatic hydrolysis of cellulose

The typical time course of the enzymatic hydrolysis of the lignocellulosic material is characterized by a rapid initial rate of hydrolysis followed by slower and/or incomplete hydrolysis. There are several factors that have been identified to affect the enzymatic hydrolysis of cellulose due to the heterogeneous nature of the hydrolysis process (enzymes are dissolved in liquid phase and cellulose exists as a solid phase). These

factors are divided into two groups: enzyme related factors and substrate related factors [32].

Several factors associated with the nature of the cellulase enzyme system have been suggested to be influential during the hydrolysis process. These include end product inhibition, thermal deactivation, synergism, adsorption and irreversible adsorption of enzymes. Synergy between cellulolytic enzymes occurs when the combined action of two or more enzymes leads to a higher rate of action than the sum of their individual actions [32]. The two most often reported synergy types involve cooperative action of either *endo*-glucanses (EG) and *exo*-glucanses (CBH), in so called endo-exo synergy [69], or the two complementary CBHs, i.e. acting from the reducing and the non-reducing end of the cellulose chain, in exo-exo synergy [70, 71]. Studies regarding synergy between purified cellulolytic enzymes confirm that the synergy between enzymes can be of significant benefit in increasing the hydrolysis rate, but the effect is substrate-dependent, with some enzyme mixtures showing cooperative action on amorphous substrates, but not on microcrystalline cellulose.

End-product inhibition is an important enzyme related factor influencing the hydrolysis process. The cellulase complex is inhibited by cellobiose, a dimer of glucose. The effects of product inhibition have been studied extensively [72-74], but the actual inhibition mechanism are still under debate. The magnitude depends strongly on the source of enzymes, the enzyme-substrate ratio [72], and the nature of the substrate [38]. One of the most important parameters for the design and operation of bioreactors for lignocellulosic conversion is enzyme dosing of the cellulase enzymes to obtain high

specific rates of cellulose conversion. As a general rule, the conversion of the substrate increases with increase of enzyme concentration, but the increase in conversion is not proportional to the increase of enzyme loading (Figure 1.4) [75]. Converse *et al*. [76] observed reduction in the activity and the concentration of the adsorbed enzyme and proposed a slow deactivation of the adsorbed enzyme to be the rate limiting factor. At the current conversion rates for enzymatic hydrolysis, one needs to use a high enzymatic loading to achieve conversion rates high enough to make the implementation of this technology feasible. There is a need to develop alternative techniques so as to obtain higher conversion rates at lower enzyme loading.

To better understand the enzymatic depolymerization of cellulose, it is important that the general chemical and physical features of the cellulose substrates be accurately understood. Structural substrate characteristics play key roles in determining both the rates and degree of hydrolysis and these include: crystallinity of cellulose, degree of polymerization, available/accessible surface area, structural organization and presence of associated materials such as hemicellulose and lignin [32, 77].

Crystallinity of cellulose is considered to be an important structural parameter that affects enzymatic hydrolysis [77-79]. Based on the change of the degree of crystallinity during enzymatic hydrolysis it has been suggested that the amorphous component of cellulose is hydrolyzed first leaving the more recalcitrant crystalline component to be hydrolyzed, thus resulting in an increased crystallinity index and possibly explaining the slowdown in hydrolysis rate [77]. However, some researchers think that crystallinity of cellulose may not be a key factor determining the rate of enzymatic hydrolysis [32, 36,

80, 81]. One reason for the controversy is that different types of cellulose with different degrees of crystallinity have been employed in different studies. In addition, it has been suggested that treatments that were found to cause a change (decrease) in crystallinity also resulted in an increase in specific surface area, which may have been the cause of any increase in hydrolysis rate [82]. Some researchers concluded that pore size of the substrates compared to the diameter of enzyme molecules is the main structural factor influencing enzymatic hydrolysis extent [83, 84]. Grethlein *et al*. [83] showed that initial rate of the hydrolysis by cellulolytic enzyme of *T.reesei* is correlated with pore volume of the substrate. A relationship between accessible surface area of pores and digestibility was also found [85]. The effect of the degree of polymerization (number of glycosyl residues per cellulose chain) is essentially related to crystallinity. It has been reported that the degree of polymerization of the cellulose substrates is marginally reduced by various cellulase components following hydrolysis. However, regardless of the substrate being hydrolyzed, there seems to be a "leveling off" of the cellulose degree of polymerization, which is correlated with the increased recalcitrance of the residual (crystalline) cellulose [32]. Also, removal of lignin and hemicellulose by the pretreatment methods results in extensive changes in the structure and accessibility of cellulose. Their removal leaves the cellulose more accessible and more open to swelling on contact with cellulases. Even though the factors that affect cellulose hydrolysis substantially have been identified, it is important to stress that many factors are interrelated during a hydrolysis process, and as a result, the influence of each factor is difficult to quantify in isolation. Consequently, digestibility of biomass is highly dependent on the contribution of the composition of the

substrate, type of pretreatment, and dosage and efficiency of the enzymes used for hydrolysis.

1.6 Mechanistic modeling

Given the complexity of enzymatic degradation of cellulose, the multiple enzymes involved and changing substrate features, the enzymatic cellulose hydrolysis process is one of the bottlenecks and the key cost center in the commercialization of cellulosic ethanol production. Most studies are being conducted to reduce the cost by improving the understanding of the process, testing enzymes and various substrates under different conditions to determine optimal hydrolysis conditions. Among the many aspects of enzymatic hydrolysis, understanding of the mechanism and enzymatic kinetics is important and can be used as a forecasting tool in designing more economical saccharification processes [86]. There are two principle approaches to modeling cellulose hydrolysis by cellulase enzymes, empirical and mechanistic modeling [36, 86]. Empirical models, based on experimental results relate the factors using a mathematical correlation, without any insight into the underlying mechanism. These are easy to develop and are useful in enzyme characterization and substrate preparation but require large sets of experimental data [75, 87-89]. The second approach involves formulation of mechanistic models which attempt to capture some of the underlying phenomenon with simplifying assumptions. Rate expressions are described using Michaelis-Menten type enzyme kinetics with or without considering the effects of enzyme adsorption and product inhibition. An extensive summary of the models of enzymatic hydrolysis of cellulose from the perspective of the development of an aggregate understanding of the action of the cellulase enzymes is presented elsewhere [36, 86]. These models are reasonably

accurate in predicting cellulose hydrolysis. However, a key limitation of most models is that while adsorption, substrate reactivity and accessibility change throughout conversion, these kinetic models often do not consider dynamic changes in properties that directly affect the enzyme-substrate interactions and rate of hydrolysis.

Rate expressions generally described using Michaelis-Menten (MM) type enzyme kinetics that hold good for homogenous enzymatic reactions in solution cannot be directly applied since cellulose is an insoluble substrate. Due to insoluble nature of cellulose, large fractions are not exposed to cellulases in the reaction mixture during the hydrolysis. Few studies have described the cellulose polymers as cellulose chains embedded in a solid substrate. Zhou *et al*. [90] used time scale analysis to study the synergistic behavior of exo- and endo-acting cellulases and examined the hydrolytic time evolution of a solid substrate. Levine *et al*. [91] described the cellulose polymers as individual discrete species, essentially tracking the concentration for each chain length. Griggs *et al*. [92] developed a kinetic model describing the distinct mode of action of the cellulase enzymes, distribution of chain lengths for the insoluble cellulose substrate using a population balance approach. Although these models improved our understanding of cellulose hydrolysis, some are validated using experimental data from the literature which tend focus on one specific aspect of the hydrolysis process to the exclusion of other simultaneously occurring phenomenon. It is necessary to consider many factors which affect the rate and extent of hydrolysis of biomass for developing mechanistic models such as the effect of enzyme adsorption, substrate heterogeneity and product inhibition. In this work, a mathematical model is designed in a way to appropriately describe the hydrolysis process, identify and understand the most crucial aspects of the hydrolysis

process, and consequently lead towards suggestions how to improve the hydrolysis process.

1.7 Research hypothesis and approach

Designing methods to enhance cellulose hydrolysis and enzyme recovery requires a mechanistic understanding of the interplay that the CBM, the surface chemistry of the substrate, and the effect of additives on binding on hydrolysis. Based on the binding studies of family 1 CBDs by molecular dynamics [49], transmission electron microscopy [47], and atomic force microscopy [48] it can be proposed that the CBMs interact with surfaces rich in hydrophobic and aromatic character. We hypothesize that non-productive binding may occur on other surfaces rich in hydrophobic and aromatic character, such as lignin, and the adsorption of binding inhibitors (additives) to those sites for non-productive binding may provide molecular leverage for displacement of cellulases onto productive sites. Control of productive cellulase binding is relevant to enzyme recovery as well as maximizing hydrolysis activity. In dilute fungal cellulases, reversibility of CBD binding has been found to range from about 25% to 100% depending on species, substrate and conditions of saccharification [93, 94]. The approach in the literature to reducing nonproductive binding focuses primarily on genetic manipulation of enzymes and feedstock [95]. In this work, we propose to use the surface science approach to model surfaces (thin films) and investigate the binding of cellulase enzymes to cellulose and lignin, and the role of surfactants to suppress the binding cellulases to surfaces differing in surface chemistry. We hypothesize that this approach will be more capable of being generalized to reverse engineer the best pretreatment of biomass to favor the appropriate surface for controlled binding.

The advent of advanced techniques to synthesize an array of model thin films coupled with analytical methods provides real-time detection of enzyme adsorption and enzymatic hydrolysis of cellulose. Recently, surface sensitive techniques such as quartz crystal microbalance with dissipation monitoring (QCM-D) [96-98], ellipsometry [99], neutron reflectometry [100] and surface plasmon resonance (SPR) [101] have been applied to monitor hydrolysis of cellulose thin films as well as enzyme binding onto cellulose or lignin at the interfacial level. Among the surface analysis techniques, QCM-D is the widely used technique for hydrolysis and enzyme binding studies of lignocellulose substrates including pure cellulosic films [96, 98], cellulose-lignin bicomponent films [97] and films made of lignocellulosic nanofibrils [102], and protein binding on lignin films [55, 103]. QCM-D is a highly sensitive balance; it measures small changes in the resonant vibration frequency of a quartz crystal sensor under electrical simulation due to the mass addition (adsorption) or loss (degradation) onto the crystal. In addition to measuring changes in frequency due to adsorbed material it also measures dissipation in signal after ceasing electrical stimulation which gives a measure of the viscoelasticity of the adsorbed layer.

This dissertation addresses enzyme-substrate interactions in biomass hydrolysis with an overall goal of quantifying at the interfacial level, the binding of cellulase enzymes to cellulose and lignin in response to the surface chemistry and the presence of binding inhibitors. Many bulk adsorption and activity studies have been performed with various enzymes and substrates, and suggest that additives (e.g. polyethylene glycol [59], bovine serum albumin [64] or surfactants [60]) can enhance both conversion to sugars and enzyme recovery particularly when lignin is present. While a variety of surfactants,

proteins and polymers have been used to promote desorption of *T. ressei* cellulases, we propose to use the most common nonionic based polyethylene glycol based surfactant, Tween-80. More specifically, the aims of this work were to:

1. Prepare model cellulose films differing surface chemistry (morphology and crystallinity) and measure binding and activity of cellulases on these films.
2. Measure the effects of binding inhibitors (surfactants) on binding and activity of cellulases.
3. Prepare model lignin films and measure the binding of cellulases to those films to identify and test inhibitors to nonproductive cellulase binding to lignin.

In this document, chapter 2 outlines the key instrumental techniques used to complete this research. Chapter 3 reports the experimental procedures used to prepare model cellulose films differing in surface chemistry following the binding and activity of cellulases to those films studied using QCM-D. Three kinds of model cellulose films were prepared in this work by dissolving cellulose in various solvents. The films are named after the solvent used for dissolution or the surface morphology of the cellulose films, specifically as NMMO, LiCl/DMAc and cellulose nanocrystal (CNC) films. Data obtained in the experimental studies were compared and evaluated against a mechanistic mathematical model describing the hydrolysis process. Chapter 4 reports the effects of nonionic surfactant Tween-80 on binding and cellulase hydrolytic activity on NMMO and LiCl/DMAc cellulose films. In chapter 5, an experimental method used to prepare model lignin films was described and the effects of Tween-80 on cellulase binding to

lignin films are reported. Chapter 6 reports the effect of enzyme concentration on hydrolysis of NMMO cellulose films followed by fitting the experimental data to the surface kinetic model. Finally, chapter 7 reports the conclusions and a suggestions for future work.

1.8 Figures and Tables

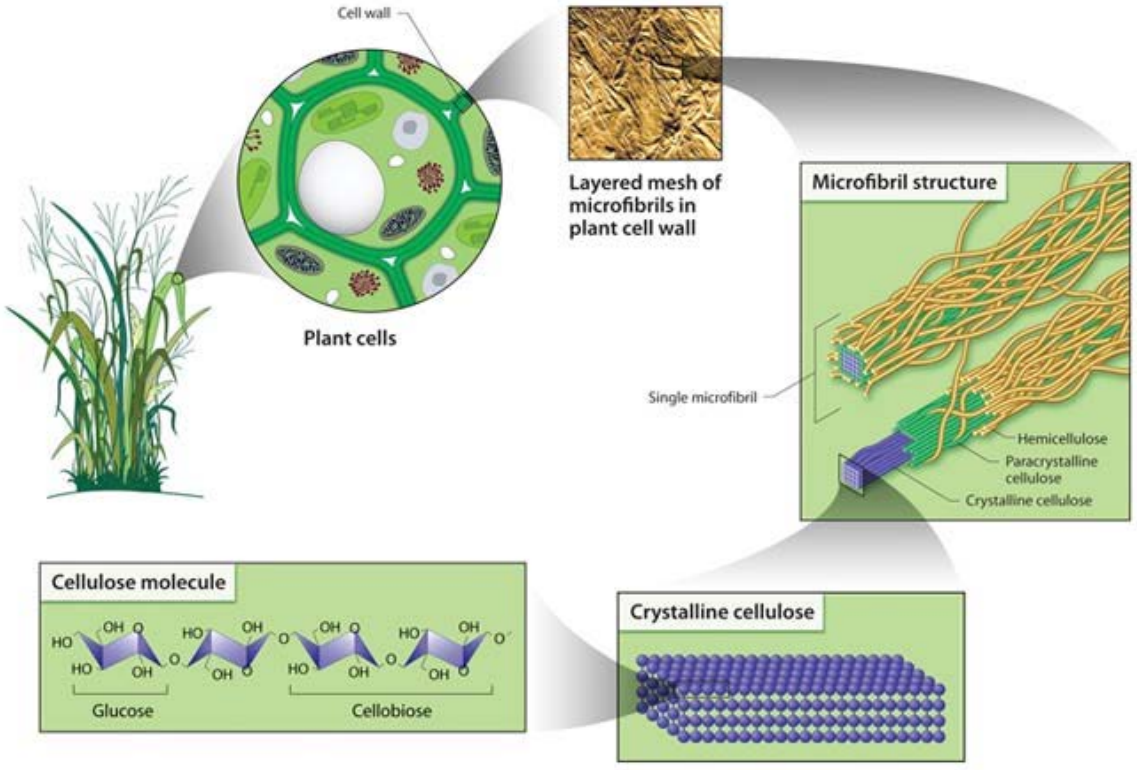

Figure 1.1. Schematic presentation of cellulose fiber structure [Reproduced with permission from the U.S. Department of Energy Genomic Science program, available at http://genomicscience.energy.gov [104]].

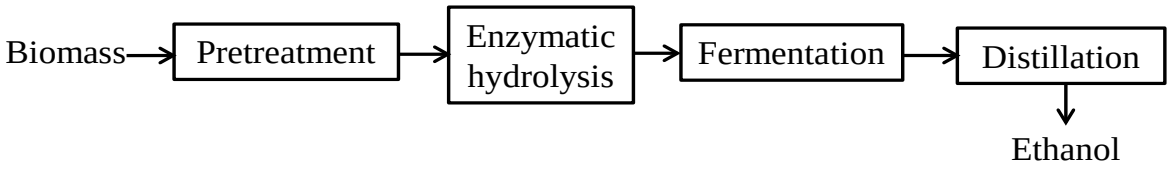

Figure 1.2. Schematic overview flowsheet for the biochemical conversion of biomass to bioethanol.

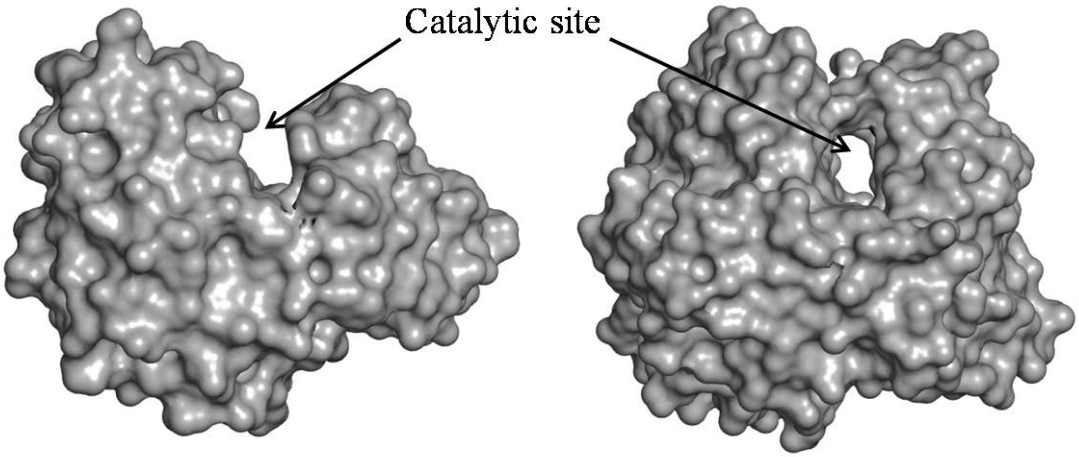

Figure 1.3. Three dimensional surface representations of the active sites of endoglucanases E2 from *T.fusca* (left) and exoglucanase CBH II from *T.reesei* (right) [105]. [Molecular surface diagrams prepared using PyMOL Molecular Graphics System, Schrodinger LLC, version 1.1r1].

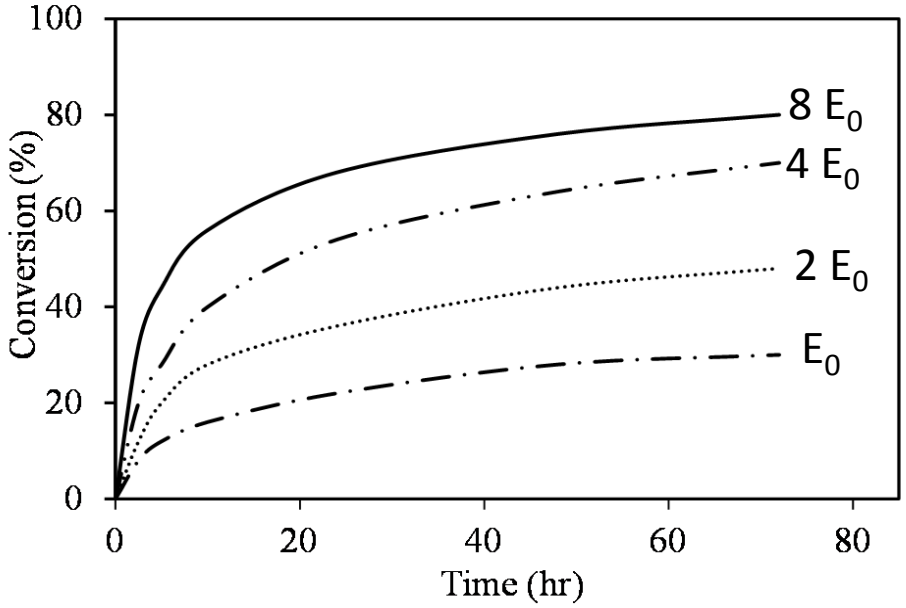

Figure 1.4. Effect of different initial enzyme concentration on reaction progress. The plots are generated to demonstrate the conversion vs time progress for different enzyme loadings, the data are not from hydrolysis experiments (Similar trends reported by Sattler *et al*., 1989).

Table 1.1. Typical biochemical compositions of potential lignocellulosic biomass feedstocks (% dry weight) [Adapted from Limayem and Ricke [106]].

Feedstock	Cellulose	Hemicellulose	Lignin	Others
Agricultural residues	37-50	25-50	5-15	12-16
Hardwood	45-47	25-40	20-25	0.8
Softwood	40-45	25-29	30-60	0.5
Grasses	40-55	35-50	-	-
Switch grass	40-45	30-35	12	-

Table 1.2. Various methods for pretreating lignocellulose biomass and their characteristics

Pretreatment	Characteristics	Ref
Acid treatment	- Practical and simple technique. - Does not require thermal energy. - Effective hydrolyze of hemicelluloses with high sugar yield. - Synthesis of furfural/hydroxymethyl furfural toxic inhibitors - Requires recovery steps	[26, 107]
Alkaline treatment	- High total sugar yield including pentose and hexose sugars. - Effective against hardwood and agricultural residues. - High pressure and temperature hinder chemical operation. - Commercial scalability problem - Formation of salts of calcium and magnesium	[108-110]
Ammonia fiber explosion (AFEX)	- Effective against agricultural residues mainly corn stover without formation of toxic end-products. - Not suitable for high-lignin materials. - Costly and requires ammonia recovery	[111-114]
Organosolv treatment	- Pure lignin obtained and used as value added product - Solvents inhibit enzymatic hydrolysis - Removal of solvents necessary to reduce operational costs	[115, 116]
Steam explosion with catalyst	- Effective against agricultural residues and hardwood. - High hemicelluloses fractions removal - Not really effective with softwood	[117-119]
Sulfite pretreatment to overcome recalcitrance (SPORL)	- Effective against high-lignin materials, both softwood and hardwood. - Highest pretreatment energy efficiency - Minimum of inhibitors formation - High cost of chemical recovery systems	[120, 121]
Alkaline wet oxidation	- The combination of oxygen, water, high temperature and alkali reduce toxic inhibitors. - High delignification and solubilization of cellulosic material - Low hydrolysis of oligomers - Formation of acids which act as enzyme inhibitors	[122, 123]
Fungal bioconversion	- Environmentally friendly - Low use of energy and chemicals - A part of fermentable sugars are utilized as carbon source - Slow process	[124, 125]

CHAPTER 2

METHODS AND MATERIALS

This chapter gives an outline of the principles of the key instrumental techniques used in this work, including Atomic Force Microscopy (AFM), ellipsometry, Quartz Crystal Microbalance with Dissipation (QCM-D), X-ray Photoelectron Spectroscopy (XPS) and X-ray Diffraction (XRD).

2.1 Atomic force microscopy (AFM)

Atomic force microscopy (AFM) is most often used to obtain topographical information about a surface with nanometer-level resolution. Developed in the mid-1980s, AFM has become one of the most successful tools in surface science. The basic components of an AFM are depicted in Figure 2.1. A sharp tip at the free end of a cantilever is brought into contact with the sample surface. The tip interacts with the surface, causing the cantilever to bend. A laser spot is reflected from the cantilever onto a positon-sensitive diode detector. As the cantilever bends, the positions of the laser spot changes. In idealized experimental conditions (e.g. in ultrahigh vacuum), when the cantilever tip approaches the sample surface, Van der Waals forces start acting upon it. Figure 2.2 shows a schematic of the expected interaction forces as the tip approaches the sample. At the right side of the curve the tip and sample are separated by a large distance. As they approach, the tip and sample atoms first weakly attract each other. This zone of interaction is known as the “non-contact” regime. Closer still, in the “intermittent contact” regime, the repulsive van der Waals force becomes important. When the distance between tip and sample is just a few angstroms, the forces balance, and the net

force drops to zero. When the total force becomes positive (repulsive), the atoms are in the contact regime.

Depending on the type and size of surface being imaged, several different AFM operating modes, namely, contact and dynamic modes are possible [126, 127]. The dynamic mode is further divide into tapping and non-contact modes. In the contact mode the AFM tip scans the surface in contact with surface. In the dynamic mode the cantilever is vibrating at or near its resonance frequency and measuring the changes in amplitude or frequency near the sample. In this work, the non-contact mode is used, and is discussed in detail.

The noncontact mode works via the principle of "amplitude modulation" detection. The corresponding detection scheme exploits the change in the amplitude '*A*' of the oscillation of a cantilever due to the interaction of a tip with a sample. The mechanism of noncontact AFM can be understood in terms of a force gradient model [128]. According to this model, in the limit of small *A*, a cantilever approaching a sample undergoes a shift in its natural frequency, f_0, towards a new value given by

$$f_{eff} = f_0 \left(1 - \frac{F'(z)}{k_0}\right)^{1/2} \qquad (2.1)$$

where f_{eff} is the new effective resonance frequency of the cantilever of nominal stiffness k_0 in the presence of a force gradient $F'(z)$ due to sample. The quantity z represents an effective tip-sample separation while $df = f_{eff} - f_0$ is typically negative, for the case of attractive forces. If the cantilever is initially forced to vibrate at an $f_{set} > f_0$, then the shift in the resonance spectrum of the cantilever towards lower frequencies will cause a

decrease in the oscillation amplitude at f_{set} as the tip approaches the sample. This change in A is used as the input in the non-contact feedback. To obtain an image in non-contact mode, the user initially chooses a value A_{set} as the set-point such that $A_{set} < A(f_{set})$ when the cantilever is far away from the sample. The non-contact feedback then moves the cantilever closer to the sample until its instantaneous oscillation amplitude, A, drops to A_{set} at the user-defined driving frequency f_{set}. At this point the sample can be scanned in the x–y plane with the control system keeping $A = A_{set}$ = constant in order to obtain an image.

AFM is a non-destructive technique capable of operation in a variety of environments, including insulated, fluid, and high vacuum conditions. Additionally, the only requirements for the substrate are a clean, flat, near defect-free surface. The dimensions of the AFM tip affect the resolution of the AFM image. Sharper tips with a small radius of curvature yield higher resolution images because the tip dimensions are typically smaller than the features on the surface. Because AFM can yield high resolution images in a number of different environments and using a variety of underlying substrates, AFM measurements has been applied to a wide range of synthetic and biopolymer films [129, 130]. Non-contact mode has the advantage that the tip never makes contact with the sample and therefore cannot disturb or destroy the sample. Both topographic images (dependent on the height of the cantilever above the surface) and phase contrast images (dependent on the rate of energy dissipation due to the interaction of the cantilever with the surface) are used to observe sample features. In this work, tapping mode AFM was used to characterize the dimensions and homogeneity of cellulose films and to characterize the changes in cellulose model surface structure and

morphology before and after enzymatic hydrolysis. In this work, an Agilent 5500 scanning probe microscope from Agilent Technologies, Palo Alto, CA, USA was used. The images were scanned in non-contact mode in air using silicon cantilevers (Tap300Al-G from Budget sensors, Bulgaria) and the resonant frequency of the cantilever was 300 ± 100 kHz. No image processing was done except flattening, which was performed using Gwyddion software (version 2.20).

2.2 Ellipsometry

Ellipsometry is a non-destructive optical technique that provides information useful in determining the optical parameters (refractive index, *n*, and extinction coefficient, *k*) and thickness of thin films [131]. Ellipsometry measures a change in polarization as light reflects or transmits from a material structure. The experimental setup consists of a light source, polarization analyzer, sample, and detector. The light source is polarized, creating a known ellipticity (ρ) – the ratio between the *s*- and *p*-polarized light. As light hits the surface, it is split into reflected and refracted components dependent upon the optical properties (e.g. polarizability) and thickness of the film. Relative to the incident beam, the reflected light has shifted amplitudes and phases as determined by an analyzer and detector, as illustrated in Figure 2.3. The principal equation in ellipsometry relates the ellipticity to the experimentally determined change in the amplitude (ψ) and the phase (Δ) of the polarized light:

$$\rho = \tan(\Psi)\, e^{i\Delta} = \frac{r_p}{r_s} \qquad (2.2)$$

The amplitudes of the *s* and *p* components, after reflection normalized to their initial value, are denoted by r_s and r_p, respectively. Application of the Fresnel equations to the case depicted in Figure 2.3 yields the ratio r_p/r_s given by Equations. 2.3 and 2. 4, where the subscripts refer to the layer above and below each interface (0 for air and 1 for the film).

$$r_p = \frac{n_1 cos\theta_0 - n_0 cos\theta_1}{n_1 cos\theta_0 + n_0 cos\theta_1} \qquad (2.3)$$

$$r_s = \frac{n_0 cos\theta_0 - n_1 cos\theta_1}{n_0 cos\theta_0 + n_1 cos\theta_1} \qquad (2.4)$$

where *n* is the refractive index. However, ellipsometry is an indirect method in that the experimentally determined values of ψ and Δ must be coupled with models that fit the optical parameters as a function of the film thickness. The optical and thickness parameters of the model are tuned until the calculated and experimentally measured ψ and Δ values agree, thereby yielding the refractive index, extinction coefficient, and thickness of the film [131]. Normally, a model analysis must be performed. Direct inversion of Ψ and Δ is only possible in very simple cases of isotropic, homogeneous infinitely thick films. In all other cases a layer model must be established, which considers the optical constants (refractive index) and thickness parameters of all individual layers of the sample including the correct layer sequence. Using an iterative procedure (least-squares minimization) unknown optical constants and/or thickness parameters are varied, and Ψ and Δ values are calculated using the Fresnel equations.

In short, the procedure is as follows. First, a measurement is performed to collect information about the sample in the form of ellipsometric angles. Second, a model is built

up using what is known about the measured sample to define a layered structure with layer thicknesses and optical properties as close to the real values as possible. In the case of materials with known optical properties, database values from earlier measurements can be used in the model. In the case of materials with unknown optical properties, the refractive index is often described using Cauchy relationship. The Cauchy relationship is given as,

$$n(\lambda) = A + \frac{B}{\lambda^2} + \frac{C}{\lambda^4} \qquad (2.5)$$

where the three terms A, B and C are adjusted to match the wavelength-dependent refractive index of the material. Third, some of the parameters (film thickness, optical properties) in the model are defined as variables, to be changed in the fitting process. Fourth, the mean square error (MSE) value is calculated, which is used as a measure for the quality of the fit. Fifth, the parameters defined as variables are changed using an optimization algorithm in order to decrease the MSE value. Step four and five are repeated until a minimum value of the MSE is reached. The calculated Ψ and Δ values, which match the experimental data best, provide the optical constants and thickness parameters of the sample. In this work, the thickness of the films was measured using a variable angle spectroscopic ellipsometer (M-2000, JA Woollam Co., Inc.).

2.3 Quartz crystal microbalance with dissipation (QCM-D)

QCM-D a nanomechanical acoustic-based analytical technique, provides *in situ*, real-time characterization of the interactions at solid/air and solid/liquid interfaces and is widely used in the areas of materials science, biophysics, and environmental and life sciences [132]. With QCM-D, simultaneous measurement of resonance frequency change

and energy dissipation change is performed by periodically switching off the driving power of oscillation of the sensor crystal and recording the decay of damped oscillation as the adsorption and/or structural changes take place at sensor crystal surface. While the changes in frequency provide information about the changes in mass, the changes in dissipation provide structural information about the viscoelastic properties of adsorbed films in real time. The minimum detectable mass change is typically ~1 ng cm^{-2}. A quartz crystal microbalance (QCM) crystal consists of a thin quartz disc sandwiched between a pair of metal electrodes typically composed of gold (Figure 2.4). The piezoelectric behavior, or the mechanical stress caused by application of electrical current, of quartz is the basis of the QCM. During a QCM experiment, an external driving oscillating circuit is applied to the quartz crystal through its gold electrodes and excites the crystal. The crystal starts to oscillate in shear mode at its fundamental resonant frequency. An applied stress, such as a change in the mass on the crystal or the medium contacting the crystal surface, leads to a change in the resonant frequency of the oscillating crystal [133-135].

In 1959, Sauerbrey [136] reported results regarding the adsorption of rigid thin films onto the surface of a quartz electrode in the gas phase and derived an equation relating the frequency shift, Δf, of an AT-cut oscillating piezoelectric crystal induced by added mass. This relationship is now known as the Sauerbrey equation:

$$\Delta m = \frac{-C_f}{n}\Delta f = -\frac{A\sqrt{\rho_q \mu_q}}{2nf_0^2}\Delta f \qquad (2.6)$$

where Δm is the mass per unit area, n is the index of the frequency overtone, Δf is the change in frequency, C_f is a constant (0.177 $mg \cdot m^{-2} \cdot Hz^{-1}$ for a 5 MHz crystal), A is the active area of measurement, ρ_q is the density of quartz, μ_q is the shear modulus of quartz,

and f_0 is the resonant frequency of the bare crystal and is dependent on the cut and thickness of the quartz [137]. For the QCM-D used in this work, the fundamental resonant frequency (e.g. n = 1) is ~5 MHz. Higher resonant frequencies for the oscillating crystal are possible (e.g. 15, 25, 35 MHz), where the higher resonant frequency is the product of the fundamental frequency (e.g. 5 MHz) and an odd overtone number (n = 3, 5, 7, 9…).

Strictly speaking, the Sauerbrey equation can only be used to estimate the mass change of a *rigid* adsorbed layer on the resonator surface in air or vacuum. When a viscoelastic film is deposited on the resonator surface in liquid medium, the oscillation of the resonator is expected to be damped by the adsorbed layer. If the damping in the deposited film becomes sufficiently large, the linear relationship between Δf and Δm is no longer valid. Therefore, another parameter is defined to characterize the viscoelastic properties of the adsorbed layer. The energy dissipation during the oscillation of resonator can be described with the dissipation factor (D) [138]

$$\Delta D = \frac{E_{dissipated}}{2\pi . E_{stored}} \qquad (2.7)$$

where $E_{dissipated}$ is the energy dissipated during one oscillation, and E_{stored} is the energy stored due to elastic deformation. A larger value of D reflects the formation of a softer and more swollen layer, whereas a smaller D indicates a relatively rigid and dense layer adsorbed on the resonator surface [139]. In this work, all of the studies on the cellulase behavior at the cellulose surface are conducted on a quartz crystal microbalance with dissipation (QCM-D) from Q-sense AB. When the quartz resonator is immersed in a

Newtonian fluid the frequency response of the resonator can be quantitatively described by the Kanazawa-Gordon equation [140]

$$\Delta f = -f_0^{3/2} \frac{(n\rho_l\eta_l)^{1/2}}{(\pi\rho_q\mu_q)^{1/2}} \qquad (2.8)$$

where ρ_l and η_l are the density and viscosity of the fluid, respectively. On the other hand the change in dissipation factor in a Newtonian fluid can be expressed as [141]

$$\Delta D = 2\left(\frac{f_0}{n}\right)^{1/2} \frac{(\rho_l\eta_l)^{1/2}}{(\pi\rho_q\mu_q)^{1/2}} \qquad (2.9)$$

Equation 2.8 and 2.9 show that Δf and ΔD are related not only to the inherent properties of the quartz crystal but also to the solvent viscosity and density.

Since the Sauerbrey equation is not valid for the viscoelastic layer, theoretical representations based on Voigt model can be applied in such situations [142]. Assuming that the adsorbed layer is surrounded by a semi-infinite Newtonian fluid under no-slip conditions and is homogenous with a uniform thickness, the complex shear modulus (G) of the adsorbed layer can be described by

$$G = G' + iG'' = \mu_f + i2\pi f\eta_f \qquad (2.10)$$

where *G'* is the storage modulus, *G"* is the loss modulus, μ_f is the shear modulus of the film, η_f is the viscosity of the film, and *f* is the frequency of oscillation. Application of the Voigt model to the case of a single layer of viscoelastic polymer adsorbing to a model

surface from bulk solution leads to the following expressions for the frequency Δf and dissipation ΔD changes:

$$\Delta f \approx \frac{1}{2\pi\rho_0 h_0}\left\{\frac{\eta_3}{\sqrt{\frac{2\eta_3}{\rho_3\omega}}} + h_1\rho_1\omega - 2h_1\left(\frac{\eta_3}{\sqrt{\frac{2\eta_3}{\rho_3\omega}}}\right)^2 \frac{\eta_1\omega^2}{\mu_1+\eta_1^2\omega^2}\right\} \qquad (2.11)$$

$$\Delta D \approx \frac{1}{\pi f\rho_0 h_0}\left\{\frac{\eta_3}{\sqrt{\frac{2\eta_3}{\rho_3\omega}}} + 2h_1\left(\frac{\eta_3}{\sqrt{\frac{2\eta_3}{\rho_3\omega}}}\right)^2 \frac{\eta_1\omega^2}{\mu_1+\eta_1^2\omega^2}\right\} \qquad (2.12)$$

where ρ_0 is the density of the quartz crystal, h_0 is the crystal thickness, η_3 and ρ_3 refer to the viscosity and density of the bulk fluid in contact with soft film, and h_1, ρ_1, μ_1 and η_1 denote the thickness, density, shear modulus and viscosity of the soft film, respectively. Consequently, application of the Voigt model to data obtained from a QCM-D yields quantitative thickness, shear modulus, and viscosity values of the soft film [142]. For solid surfaces coated with a polymer layer immersed in liquid media, the interfacial properties would be significantly influenced by the polymer behavior at the interfaces. So far, the characterization and analysis of cellulose behavior at the solid/liquid interfaces still remain a great challenge, particularly for the dynamic polymer behavior. Sauerbrey equation can be used to extract the areal mass density of the film if it is rigid; meaning the mass adsorbed on the surface is firmly attached with no oscillatory effect. To make the distinction more quantitative, the ratio of $\Delta D/(-\Delta f)$ is considered. If $\Delta D/(-\Delta f) < 4*10^{-7}$ Hz^{-1} for a 5 MHz crystal then the film can be approximated as a rigid [143]. In this study, the Sauerbrey equation is valid because the ratio of $\Delta D/(-\Delta f)$ was relatively small ($1\text{-}5*10^{-7}$) during cellulase and Tween-80 treatments on cellulose and lignin films.

2.3 X-ray photoelectron spectroscopy

X-ray photoelectron spectroscopy (XPS) is one of the most established methods for determining the elemental composition and the chemical state of solid surfaces and thin films. XPS exploits x-ray photons to excite electrons from the core levels of the atoms of a solid into the vacuum, thus probing the electronic structure with sensitivity to elemental composition and chemical state. A typical setup involves an ultra-high vacuum chamber containing a monochromatic X-ray source, sample, electron analyzer, and electron detector. XPS is based, in principle, on a very simple process. When a solid surface is irradiated with soft x-ray photons, an incident photon of energy $h\omega$ can be absorbed by an electron with binding energy E_B below the vacuum level: the entire photon energy is transmitted to the electron, which is then promoted to an unoccupied state above the vacuum level. As a result, photoelectrons are ejected into the vacuum with kinetic energy E_K.

$$E_K = h\omega - E_B - \Phi_w \qquad (2.13)$$

Here, Φ_w is the work function of the material and represents the minimum energy required to remove an electron from the solid; it can be seen as an energy barrier that electrons need to overcome in order to escape from the surface into the vacuum. The ejected electrons can originate from core levels or from the occupied portion of the valence band; however, due to the relatively high photon energy (typically in the range between 100-200 eV and 2000eV), attention is primarily focused on core level electrons. A typical XPS spectrum is obtained at a given photon energy by recording the number of photoelectrons as a function of the kinetic energy and can be plotted as a function of the

binding energy by making use of Equation 2.13. The spectrum consists of a succession of distinct lines, reflecting the sequence of occupied core levels in the system under investigation. Since the binding energies of core levels are different for and characteristic of each element, and no two elements share the same set of binding energies, photoemission spectra can serve as "fingerprints" of the respective elements [144]. The binding energy is also sensitive to the oxidation state of the nucleus, and in some cases to bonding configurations (for instance for carbon) and therefore can provide additional information about the state of the surface. In this work, analysis was conducted using a Thermo Scientific K-Alpha photoelectron spectrometer using monochromatic Al Kα radiation with photon energy of 1486.6 eV. The measurement was carried out by placing the films at an angle of ~45° relative to the incident beam.

2.4 X-ray diffraction

X-ray scattering techniques are a family of non-destructive analytical techniques which reveal information about the crystallographic structure, chemical composition, and physical properties of materials and thin films. These techniques are based on observing the scattering intensity of an x-ray beam hitting a sample as a function of incident and scattered angle, polarization, and energy. X-ray diffraction techniques are based on the principle of the interference of the diffracting monochromatic X-ray beams from structures that have a long range order. The comprehensive description of scattering from crystals is given by the dynamic theory of diffraction [145]. W. L. Bragg observed that for a certain specific wavelengths and incident angles, crystalline solids produced intense peaks (Bragg peaks) of reflected x-rays and explained this result by modeling the crystal as a set of discrete parallel planes separated by a constant parameter known as the

interplanar distance (*d*). It was proposed that the incident x-ray diffraction would produce a Bragg peak if their reflections off the various planes interfered constructively. This gives the formula for Bragg condition: $n\lambda = 2d \sin\theta$, where, θ is the scattering angle, λ is the characteristic wave length and *n* is an integer. Figure 2.5 shows the schematic of the x-ray diffraction where the diffracted rays interfere.

In this work, X-ray diffraction (XRD) was performed on microcrystalline cellulose powder and model cellulose thin films using a Bruker D8 Advance instrument. The radiation source was Cu ($K\alpha$) radiation, with a wavelength of 1.54 Å. The angular scanning range was $2\theta = 2°$ to 40° with 0.02° steps. However, for thin films no crystallinity data was obtained using the conventional x-ray diffraction method. This may be a result of the small amount of material present in thin films, which makes it challenging to collect sufficient signal to measure crystallinity. Small crystallites also broaden x-ray peak, which provides an additional challenge. Grazing incidence wide angle x-ray scattering (GIWAXS) measurements were performed at Advanced Photon Source (Argonne National Lab, IL, USA) to measure the crystallinity of cellulose thin films with a more powerful source. GIWAXS uses a reflection geometry having a shallow angle of incidence of the x–ray beam onto the sample surface. The photons from the x-ray are scattered by the electrons in the atoms of the thin film which are then collected by a detector (Figure 2.6). Typically semicrystalline polymer films such as conjugated polymers are efficiently studied with GIWAXS [146, 147]. X-ray scattering from polycrystalline polymer films is considered to be complex due to the combination of disordered and packing defects in the crystalline domains and preferential orientation of the domains. For a given sample with a preferred out-of-plane orientation and isotropic

in-plane orientation, the diffraction pattern will consist of spots for each crystallographic plane for a narrow orientation distribution. If the films comprise of partial preferential orientation, scattering pattern will show arcing (Figure 2.7)[146]. Figure 2.8 (a, b, c) shows the GIWAXS scattering patterns exhibited for cellulose nanocrystal, NMMO and LiCl cellulose films.

2.5 Figures and Tables

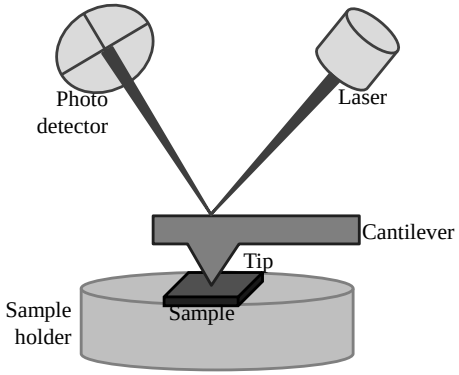

Figure 2.1. Schematic illustration of main components of AFM.

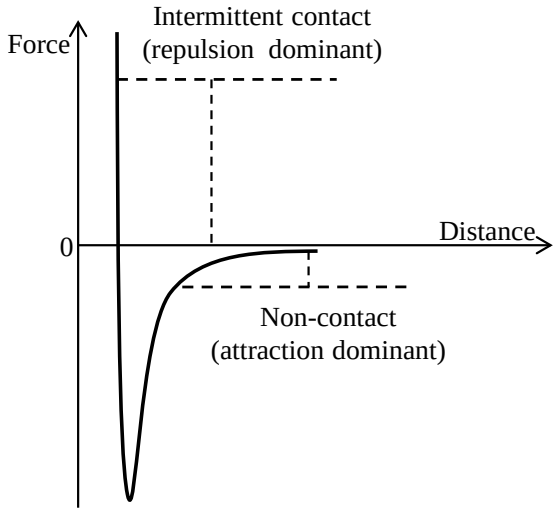

Figure 2.2. Typical force-distance curve for AFM measurement and schematic representing the zones of contact.

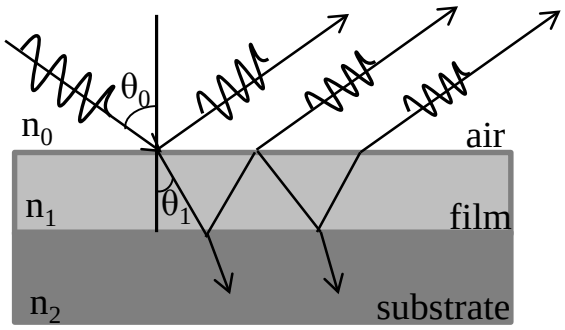

Figure 2.3. Schematic of an ellipsometry measurement, where polarized light reflects and refracts at each interface, which leads to multiple beams exiting from a thin film for each incident electromagnetic beam.

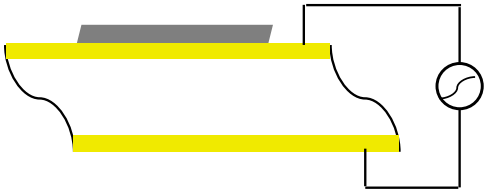

Figure 2.4. Schematic working principle of QCM in which voltage applied to a quartz crystal coated with gold induces oscillation whose frequency and dissipation characteristics are dependent on the adsorbed layer attached to one crystal face.

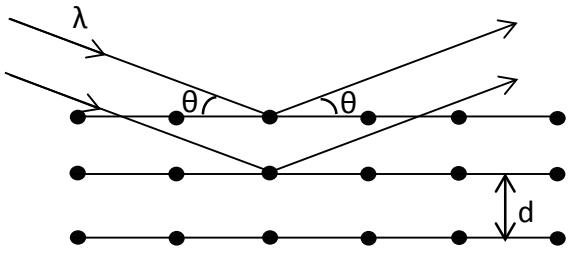

Figure 2.5. Schematic of Bragg diffraction in which incident photons of wavelength λ undergo constructive interference when they hit a material with atomic spacing *d* at incidence angle θ.

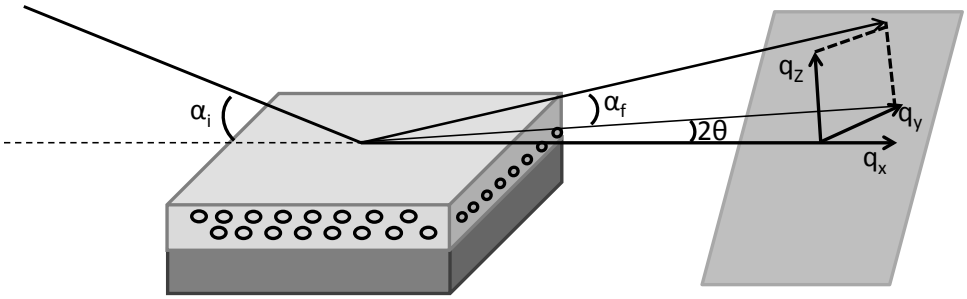

Figure 2.6. Schematic drawing of the experimental setup in GIWAXS geometry. The sample surface is placed horizontally. The incident angle denoted by α_i and the exit angle α_f.

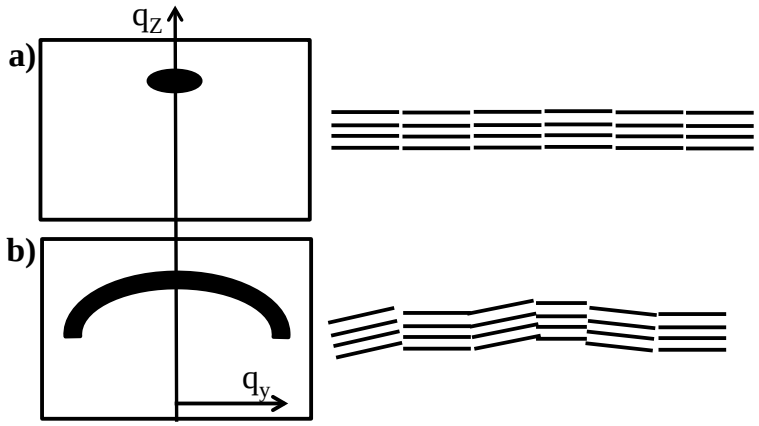

Figure 2.7. Illustrations of example diffraction patterns for different microstructures. a) Highly oriented films produce an ellipse (spot); b) Films with partial orientation produce an arc.

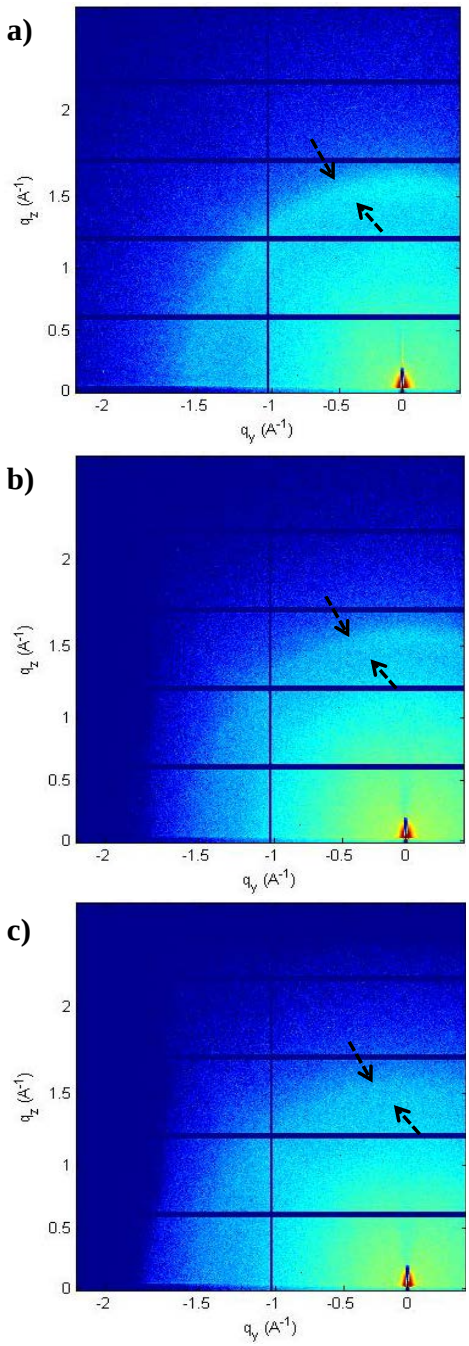

Figure 2.8. 2D-GIWAXS images of cellulose thin films. a) Cellulose nanocrystal film b) NMMO cellulose film (both films are partially orientated represented by arc pattern) c) LiCl cellulose film (the films have no orientation).

CHAPTER 3

ENZYMATIC HYDROLYSIS OF MODEL CELLULOSE FILMS: EFFECT OF SURFACE STRUCTURE AND MECHANISTIC MODELING OF ENZYMATIC HYDROLYSIS

3.1 Summary

Substrate properties have been speculated to be the limiting factor in hydrolysis of cellulose. To understand how cellulose structural properties impact cellulase-cellulose interactions, three kinds of model cellulose films with different surface structures and degrees of molecular ordering (crystallinity) were prepared by spin coating cellulose suspensions onto solid substrates and characterized using AFM. QCM-D was used to study the kinetic behavior of cellulases on those cellulose films. It was observed that the three cellulose surfaces were hydrolyzed in distinct ways and that the mechanism appeared to be influenced by the structure of the cellulose substrate. In this work, the kinetic behavior of hydrolysis was modeled using surface-based reaction kinetics; the distinct feature of the proposed model is that the cellulose substrate is considered to consist of bulk and exterior accessible surfaces with only a portion of cellulose substrate being accessible to enzymes at a given time. The time evolution of substrate accessibility to cellulases was modeled based on the cellulase mediated erosion of a cylindrical particle. The rate constants for the adsorption and cellulase hydrolysis (k_2) were obtained, which indicated that films deposited from LiCl/dimethylacetamide (amorphous, $k_2 = 2.22 \pm 0.35$ min^{-1}) were hydrolyzed 5 times faster than films deposited from N-methylmopholine-N-oxide (NMMO) (semi-crystalline, $k_2 = 0.44 \pm 0.11$ min^{-1}), while the

cellulose nanocrystal (CNC) (crystalline, k_2 = 0.029 ± 0.0002 min^{-1}) films were hydrolyzed very slowly suggesting that it is more difficult for the cellulase enzymes to hydrolyze crystalline cellulose substrates even when they present a high surface area for binding of enzymes.

3.2 Introduction

Enzymatic hydrolysis of plant carbohydrates has developed as the most prominent technology for conversion of lignocellulosic biomass to soluble sugars for subsequent fermentation into bioethanol [148]. Lignocelluloses are composed of cellulose, hemicelluloses and lignin in an intricate structure, which is recalcitrant to decomposition. This leads to difficulties within the conversion process. To reduce the recalcitrance of lignocellulosic biomass and make it more accessible to hydrolytic enzymes, researchers have developed a number of different biomass pretreatment methods as summarized in published reviews [28, 149, 150]. The principal framework of plant cells is cellulose, consisting of chains of glucose linked by β-1,4 linkages. Cellulose chains aggregate through hydrogen bonding and pyranose ring stacking into tightly packed crystalline elementary microfibrils, and these fibrils in turn are further aggregated into higher order supermolecular assemblies [16]. In plant cell walls, cellulose occurs in both crystalline and amorphous forms. The enzymatic hydrolysis of cellulose to glucose requires a system of cellulase enzymes working synergistically: endoglucanases randomly cleave internal bonds in the cellulose chain, exoglucanases (cellobiohydrolases) cleave off cellobiose from the reducing and non-reducing chain ends of the cellulose polymers and β-glucosidases convert cellobiose to glucose [151]. The factors that affect enzymatic

hydrolysis of biomass have been divided into two groups: biomass structural features (including chemical compositions and physical structure of lignocellulose) and enzyme mechanism. The chemical structural features are the compositions of cellulose, hemicellulose, lignin, and acetyl groups bound to hemicellulose. The physical structural features consist of accessible surface area, crystallinity, degree of polymerization, pore volume, and biomass particle size. Although structural features that limit the enzymatic hydrolysis of biomass have been widely studied, the molecular mechanisms of biomass recalcitrance are still not completely clear [32, 36].

The initial degree of crystallinity of cellulose is considered to be an important structural parameter that affects the rate of enzymatic hydrolysis [78, 79, 152, 153]. A completely amorphous sample is hydrolyzed much faster than partially crystalline cellulose [154]. This observation has led to the hypothesis that amorphous domains in a partially crystalline cellulose sample are hydrolyzed first, leaving crystalline parts at the end, thus resulting in an increased crystallinity index [79, 155]. However, some researchers think that crystallinity may not be a key factor determining the enzymatic hydrolysis, [32, 80, 81] thus making this a controversial theory. Another important criterion influencing the rate and extent of enzymatic hydrolysis of lignocellulose is surface accessibility [36, 83-85, 156-159], as the enzymatic hydrolysis of cellulose is a surface-dominated phenomenon, and direct physical contact between cellulose and cellulase enzymes is a prerequisite for hydrolytic reactions to occur. Cellulose particles have external and internal surfaces, the external surface area determined by overall fibril dimensions, and the internal surface area depending on capillary structure including intraparticle pores as well as interparticulate voids. Grethlein [83], showed that initial

enzymatic hydrolysis rates are strongly correlated with the reactive surface area available to enzymes, which greatly increases during pretreatment. It is likely that the enzymatic hydrolysis of cellulose can occur only on the external surface of the cellulose fibrils, Arantes and Saddler [156, 157] suggested that disruption of the highly ordered and tightly packed regions of the cellulose structure facilitates the exposure of inaccessible cellulose chains buried within these regions, thereby enhancing enzyme access to cellulose. They also suggested that the rate limiting step during hydrolysis is the limited accessibility of the enzymes to the cellulose chains due to the physical structure of the cellulose substrate. Recently, Hu *et al*. [160] studied the influence of various substrate physicochemical characteristics on the effectiveness of enzyme synergism. They observed a strong relationship between cellulose accessibility and the degree of synergism, with greater synergism observed on less-organized cellulose. Sinitsyn *et al*. [85] found a linear relationship between crystallinity index and accessible surface area with initial hydrolysis rate for pure cellulose substrates, but, in the case of lignocellulosic substrates, a linear correlation was observed only with accessible surface area. The fact that the cellulose structure affects cellulase activities has long been documented. However, determination of the key rate limiting factors for hydrolysis has remained challenging as the structure of cellulose depends on pretreatment methods and conditions. The goal of this study is to elucidate the relationship between cellulose structure and enzyme hydrolytic activity.

One approach which has been gaining traction for studying the effects of structural features of biomass at a more fundamental level is the use surface science techniques. Surface sensitive techniques such as quartz crystal microbalance with

dissipation monitoring (QCM-D) [96-98], ellipsometry [99], neutron reflectometry [100] and surface plasmon resonance (SPR) [101] have been applied to measure adsorption and activity of cellulases onto cellulose at the interfacial level. For this purpose thin films of lignocellulose biomass components have been prepared by dissolution or dispersion in various solvents, and adsorption and hydrolysis by cellulase enzymes measured using quartz crystal microbalance with dissipation (QCM-D) monitoring[96-98, 161-164]. In the present study, three kinds of model cellulose surfaces were prepared by dissolution of microcrystalline cellulose in three solvents systems: N-methylmorpholine-N-oxide (NMMO), dimethylacetamide / lithium chloride (LiCl) and sulfuric acid, and the last of which gives rise to cellulose nanocrystals (CNC). Ahola *et al*. [96] studied enzymatic hydrolysis kinetics of different cellulose structures using QCM-D. They found that nature of the cellulose substrate (crystallinity and morphology) significantly influence the hydrolytic activity of cellulase enzymes. Empirical equations based on QCM-D data were used to quantify and compare binding and hydrolysis rates among different substrates. However, empirical models are based on data correlation without explicit definitions for enzyme substrate interactions and provide limited mechanistic insight.

Previously, mechanistic models for enzymatic hydrolysis have been developed which include the cellulase adsorption onto cellulose described by a Langmuir equation and simplified representations of the solid cellulose substrate (as soluble, digestible and inert fractions)[86]. Recently, models have been developed in which the cellulose is represented as a heterogeneous substrate, having both exterior and interior surfaces. The time evolution of solid substrate morphology and enzymatic chain fragmentation were both considered in the work of Zhou *et al*.[90, 165, 166]. They found that cellulose

saccharification kinetics strongly depend on substrate morphology while at the same time morphology is affected by enzymatic degradation. Levien *et al*.[91] developed a non-equilibrium mechanistic model for cellulose hydrolysis that took into account surface area by modeling cellulose as polydisperse spheres. The ability to capture the rate of change in available surface area was demonstrated, but the model failed to capture the decrease in the rate of hydrolysis with time. Griggs *et al*.[92] developed a model using a population balance approach which provides a kinetic description of the evolution of the enzyme accessible cellulose by cellulase mediated erosion of a cylindrical particle comprised of cellulose chains. They suggested that an improved understanding of cellulose hydrolysis can be achieved by comparing the distribution of cellulose chain lengths measured experimentally to model results. In the present study, results from both mechanistic modeling and experimental studies will be employed to examine the rate of enzymatic hydrolysis of cellulose substrates and their dependence of crystallinity and accessibility. Surface based kinetic model was developed based on cellulose mediated erosion of cylindrical fiber that considers the action of cellulase enzymes on cellulose surfaces and the time evolution of substrate accessibility to cellulases. The model was fit to the QCM-D data to determine the model parameters. The effects of cellulose film structure on binding and activity; the kinetic rate constants that govern the adsorption and hydrolysis of cellulases on the cellulose surfaces are reported.

3.3 Materials and Methods

3.3.1 Materials: Microcrystalline cellulose (~20 μm) from Sigma Aldrich was used as the cellulose raw material. Sodium acetate (>99%), acetic acid (>99.7%), sulfuric acid (95-

98%), and N-methylmorpholine-N-oxide de (NMMO) (50 wt% aqueous solution) were purchased from Sigma Aldrich; lithium chloride (99.8%), methanol, water (deionized ultra-filtered), hydrogen peroxide (30%), concentrated ammonia hydroxide (25%), nochromix powder, and N,N-dimethylacetamide (DMAc) (≤0.01% water) from Fischer Scientific; and polyethyleneimine (average M_n~1200, 50 wt. % in water) and dimethyl sulfoxide (>99.8%) from Acros Organics. Commercial cellulase (Celluclast®, Sigma Aldrich) derived from *Trichoderma reesei* (> 700 EGU/g) in the form of an aqueous solution was used as the enzyme source. All reagents and the enzyme were used as received. Gold coated quartz sensors supplied by Q-Sense AB, Gothenburg, Sweden were used as the base supports for preparation of cellulose films for QCM-D experiments. Polished silicon wafers (500 μm thick) supplied by University Wafer, Boston, MA were used as base supports for ellipsometry measurements.

3.3.2 Cellulose films processed in a lithium chloride solution of dimethylacetamide (LiCl/DMAc): Microcrystalline cellulose was dissolved in LiCl/DMAc by an activation and dissolution method based on the procedure from Aulin *et al. [167]*. Activation helps in opening up the polymer chains to enhance the diffusion of the solvent. To accomplish this, 0.5 g of cellulose was immersed in 10 ml deionized water while stirring overnight to allow cellulose to swell. Thereafter, the suspension was filtered to remove water and then extracted with 10 ml methanol by immersion for 30 min with magnetic stirring followed by filtration. Methanol extraction was repeated a total of three times. The methanol exchange helps to expel the residual water, thus avoiding the collapse of the pore structure and enhancing penetration of DMAc. The cellulose was then solvent exchanged with DMAc by three rounds of immersion in 10 ml DMAc for 30 min with stirring

followed by filtration. This 0.5 g solvent exchanged cellulose was then added to 18 ml of DMAc which was heated to 160 °C, and then leaving the solution to cool to 100 °C. Then 1.5 g of LiCl was added to the mixture and then left to cool to 25 °C while stirring for 12-15 hours. The cellulose was diluted with 80 ml of DMAc to reduce the viscosity, heated to a temperature of 110 °C and then spin coated onto quartz sensors.

Prior to spin-coating the quartz sensors were first cleaned by UV ozone treatment (BioForce, Ames, IA) for 10 minutes, and then cleaned with a 5:1:1 mixture of water, ammonia (25%) and hydrogen peroxide (30%), heated to 75 °C for 15 minutes, and finally rinsed with deionized water. After rinsing with deionized water the sensors were then dried under a stream of nitrogen and underwent another 10 minutes of UV ozone treatment. This is consistent with the sensor cleaning protocols recommended by the manufacturer, Q-sense. Silicon wafers with a naturally occurring silicon oxide layer were also used as the base support for the preparation of cellulose films. Silicon wafers were cleaned in nochromix solution to remove organic residues from the wafer surface, then rinsed with deionized water and dried under nitrogen. The silicon oxide layer was obtained by oxidizing the silicon wafer in an oven at 1000 °C for 30 minutes [168]. Cleaned supports were then immersed in a diluted polyethyleneimine solution (1% in water) for 15 minutes before spin coating which served as an anchoring layer for cellulose deposition. Finally, the cellulose solution was spin coated onto the polymer coated sensors with a spin coater (WS-400BZ-6NPP/Lite, Laurell Technologies Corporation) at 3000 rpm for 45 seconds. The cellulose coated substrates were then placed in deionized water for 30 min to remove any excess LiCl and DMAc, dried in an

oven at 50 °C, and stored in a desiccator until used for characterization or QCM-D studies.

3.3.3 Cellulose films processed using N-methylmorpholine-N-oxide (NMMO): Cellulose films were deposited from NMMO using a method developed based on procedures reported by Gunnars *et al.* [168], Falt *et al.* [169] and Turon *et al.* [98]. The base supports were cleaned and coated with polymer as mentioned above before deposition of cellulose film. For the dissolution of cellulose, the as-received 50% aqueous NMMO solution (4.4 ml) was preheated to 115 °C before addition of cellulose powder (0.1 g). Cellulose was added to the preheated NMMO solution and care was taken so that the temperature did not rise above 125 °C. Solutions prepared at high temperatures (above 125 °C) turn dark, making them unusable. At low temperatures cellulose does not dissolve and appears to be a yellow cloudy solution, whereas a completely dissolved solution appears clear and brown in color. After the cellulose was dissolved, 13.5 ml DMSO was added to reduce the viscosity of the solution and to give an overall concentration of 0.5 wt. % cellulose. Cellulose films were prepared from this solution by spin coating onto polymer coated supports with spin coater at 3000 rpm for 45 seconds. The cellulose films were then precipitated in deionized water for 30 min, dried in an oven at 50 °C, and stored in a desiccator until used for characterization or QCM-D studies.

3.3.4 Cellulose Nanocrystal films: Colloidal suspensions of cellulose nanocrystals were prepared by sulfuric acid – catalyzed degradation of microcrystalline cellulose (20 μm). The concentration of sulfuric acid used was 64% (w/v) and the ratio of cellulose to acid was 1:8.75 (g/ml) [170, 171]. The suspension was hydrolyzed for 1 hr. at 45 °C. The

reaction was quenched at the end of the hydrolysis by adding 10-fold of deionized water, and then vigorously stirred for 10 min. The suspension was centrifuged (at 4500 rpm for 10 min, Eppendorf centrifuge, Model 5702) and washed with equal amount of deionized water to remove excess sulfuric acid. The centrifuge step was stopped after at least five washings, or until the supernatant became turbid. The resultant suspension was dialyzed in a regenerated cellulose tube with a cutoff molecular weight of 14,000 Da until the wash water maintained at constant neutral pH. The suspension was further dispersed by an ultrasound treatment with a micro-tip probe (Qsonica Sonicator, Model Q500) for 5 minute intervals for a total of 20 minutes. The ultrasonic treatment was carried out in an ice bath with intermediate cooling intervals to avoid overheating. The sulfur content of the nanocrystal powders was determined using X-ray photoelectron spectroscopy.

3.3.5 Cellulose Thin Film Characterization: The thickness of model cellulose thin films cast onto silicon wafers was measured using a variable angle spectroscopic ellipsometer (M-2000, JA Woollam Co., Inc.). The surface topography and material distribution of the cellulose thin films on QCM sensors (QSX301, Q-sense, Göteborg, Sweden) was characterized by AFM (Series 4500, Agilent Technologies). The support base and the cellulose thin layer coating on the sensor were scanned in tapping mode using a silicon cantilever (TAP 300AI-G, Budget Sensors) with a spring constant of 40 N/m and a driving frequency of 300 kHz. X-ray photoelectron spectroscopic (XPS) analysis was conducted using a ThermoScientific K-Alpha photoelectron spectrometer using monochromatic Al K-α radiation with photon energy of 1486.6 eV to determine the surface composition of the nanocrystal film. Grazing incidence wide angle x-ray scattering measurements of cellulose thin films were conducted at beamline 8-ID-E of

the Advanced Photon Source (Argonne National Laboratory, IL, USA) using 7.35 keV energy photons (1.6868 Å), with an incident angle at 0.2°. The beam size was 50 μm (V) x 100 μm (H). The cellulose films spin coated on silicon wafer were used for measurements. Line cuts were performed to obtain the intensity of the diffraction peaks as a function of 2θ by integration over a phi (φ) angle range between 10 – 20° in the out-of-plane direction.

3.3.6 Cellulose Thin Films/ Cellulase Interactions Measured by Quartz Crystal Microbalance with Dissipation (QCM-D): A quartz crystal microbalance (Q-Sense model E4) equipped with four temperature controlled flow modules was used to measure changes in mass per unit area and in the viscoelasticity properties of the cellulose thin films from the change in frequency (Δf) and dissipation (D) of the cellulose-coated quartz crystal resonator. The oscillation frequency and dissipation energy were measured simultaneously after the application of an AC voltage across the electrode, which caused the piezoelectric quartz crystal vibrate. The resonance frequency change ($\Delta \boldsymbol{f}$) is proportional to the mass absorbed on the crystal surface by the Sauerbrey equation [138]

$$\Delta m = \frac{-C_f}{n}\Delta f \qquad (3.1)$$

where, Δm is the mass per unit area, n is the index of the frequency overtone, Δf is the change in frequency, C_f is a constant (0.177 $mg \cdot m^{-2} \cdot Hz^{-1}$ for a 5 MHz crystal). The QCM-D acquires frequency signal at the fundamental resonance (5 MHz) and at a multiple of resonance (overtone frequency). The third overtone frequency was used to avoid edge effects (unstable frequency signal at the edge of the sensor measured at the fundamental frequency).

The mass change of cellulase thin films in response to cellulase activity was measured by QCM-D. Prior to contacting the cellulose thin films with cellulase, the cellulose-coated QCM sensors were equilibrated with an acetate buffer (0.1 M, pH 5) at a flow rate of 0.2 ml min^{-1} until a constant baseline frequency measurement was reached (< 2 Hz hr^{-1}). The temperature of the QCM chamber was controlled at 25 ± 0.02 °C. All liquid solutions were degassed for 30 min using an ultra-sonicator (Cole-Parmer 8890, IL) prior to injection into the flow cell. The enzyme solution was prepared by diluting the commercial cellulase mixture with acetate buffer (pH – 4.7, 0.1 M) 200 times, which is equal to a protein concentration of 45 mg/ml determined by Bradford assay. When enzyme solutions were injected (0.2 ml min^{-1}) into the QCM flow module containing the cellulose thin films, both cellulase binding and cellulose hydrolysis were monitored simultaneously. The change in oscillation frequency and dissipation energy was recorded throughout the experiment.

3.3.7 Model fitting and error analysis: To verify the proposed kinetic model (see below), the experimentally measured frequency change was fitted to the modeled frequency by nonlinear regression using the *lsqcurvefit* function in Matlab. The rate parameters in the model k_1, k_{-1}, k_2, α_0, A, and B (defined below) were estimated as explained in the Results section. The confidence intervals (95%) of the fitted parameters were determined using the *nlparci* function in Matlab and standard errors are reported.

3.4 Kinetic models

Cellulose fibril based kinetic model

The objective was to develop a kinetic hydrolysis model appropriate to cellulase enzyme activity on model cellulose thin films measured by QCM-D [96, 172]. The frequency change response by QCM-D is assumed to be proportional to the concentration of bound enzyme-substrate complex (ES) and the amount of cellulose substrate (S_T) present on the quartz sensor surface. Therefore, the frequency change (Δf) can be represented by Equation (3.2):

$$\Delta f = \underbrace{-\mathrm{A}[ES]}_{Enzyme\ adsorption} + \underbrace{\mathrm{B}([S_T]_0 - [S_T])}_{Hydrolysis} \qquad (3.2)$$

where, A and B are constants representing the frequency response to enzyme and cellulose units on the surface, respectively; [*ES*] is the concentration of cellulose-bound enzyme on the sensor; $[S_T]_0$ is the initial total concentration of cellulose on the sensor; and $[S_T]$ is the total concentration on the sensor at a given time. Note that binding of mass to the sensor causes a negative frequency change. Equation (3.2) is used to link the experimentally observed frequency changes to the changes in individual species at the sensor surface based on the model discussed below.

Unlike the traditional Michaelis-Menten enzyme kinetic scheme in which the enzyme (*E*) binds to the substrate (*S*) to form a substrate-bound enzyme (*ES*), and the enzyme is recovered after the product (*P*) is formed, the kinetic model developed here is based on the processive mechanism of cellulase enzymes. Several cellulase components form a cellulase cocktail which synergistically hydrolyses cellulosic substrates, and the nature of the cellulolytic enzyme system employed determines the mode of action of cellulase, activity of each enzyme component, and synergistic action among the enzyme components [173]. As it is difficult to distinguish the function of each component by QCM-D, the cellulase system is assumed to have a single combined activity in the

hydrolysis of cellulose and is represented as a single enzyme (E). The model is developed based on current theoretical understanding of processive cellulase action: first, the enzyme (*E*) binds to the unoccupied cellulose substrate (*S*) to form a productive enzyme substrate complex *(ES)*, where the enzyme is threaded with the cellulose chain and completes catalytic cycles releasing the product (*P*) until eventually the complex dissociates. The binding scheme may be reversible for the formation and dissociation of complex *ES*.

The distinct feature of the proposed model is that that rather than assuming that the substrate is easily accessible and that all sites are always available for binding and reaction, the cellulose substrate is considered to consist of bulk and exterior accessible surfaces with only a portion of cellulose substrate being accessible to enzymes at a given time. The exterior surface is gradually exposed as hydrolysis proceeds (structure represented in Figure 3.1a). The interfacial surface sites concentration is given by S_i. The surface concentration of cellulose is modeled to change with time as the hydrolysis progresses. As layers of substrate are solubilized, the reaction interface moves towards the interior of the substrate, new surface is exposed, and the total substrate concentration is reduced. The reaction scheme is presented in equations 3.3, 3.4 and 3.5 and the instantaneous concentration of available substrate (*S*) for enzyme binding is given by substrate balance at the interface in equation 3.6.

$$E + S \underset{k_{-1}}{\overset{k_1}{\longleftrightarrow}} ES \qquad (3.3)$$

$$ES \overset{k_2}{\rightarrow} ES + P - S_i \qquad (3.4)$$

$$S_{bulk} \rightarrow S_i \qquad (3.5)$$

$$[S_i] = [\mathrm{S}] + [ES] \qquad (3.6)$$

The above reaction scheme leads to differential equations for enzyme-bound and interfacial sites (equations 3.7 and 3.8).

$$\frac{\mathrm{d[ES]}}{\mathrm{dt}} = \mathrm{k_1[E][S]} - \mathrm{k_{-1}[ES]} \qquad (3.7)$$

$$\frac{\mathrm{d}[S_i]}{\mathrm{dt}} = -\mathrm{k_2} * [ES] + \text{rate of exposure} \qquad (3.8)$$

The rate of exposure of the new interfacial sites from bulk sites for a cylindrical cellulose particle is given by equation 3.9 (for the derivation see Appendix I):

$$rate\ of\ \ exposure = \mathrm{k_2} * \left(1 - \frac{[S_i]}{[S_T]}\right)^{1/2} * [ES] \qquad (3.9)$$

The rate of exposure is assumed to be equal to the rate of loss of bulk substrate:

$$\frac{\mathrm{d}[S_b]}{\mathrm{dt}} = -\mathrm{k_2} * \left(1 - \frac{[S_i]}{[S_T]}\right)^{1/2} * [ES] \qquad (3.10)$$

As the total cellulose substrate is considered to consist of interfacial and bulk sites (*i.e.*, $S_T = S_i + S_b$), the initial proportion of interfacial substrate to the total substrate concentration, α_0, is defined by equation 3.11.

$$\alpha_0 = \left[\frac{S_{i,0}}{S_{T,0}}\right] \qquad (3.11)$$

The parameters k_1, k_{-1}, k_2, α_0, A and B were obtained by fitting the frequency profile data to the model. The initial total substrate concentration was measured based on the amount of dry mass of cellulose coated on the sensor surface. The initial interfacial substrate concentration was calculated using equation 3.11. The initial bulk substrate concentration was calculated from the difference between initial total substrate concentration and initial interfacial substrate concentration.

Cellulose nanocrystals network based kinetic model

For films made up of discrete, uniformly accessible fibrils of cellulose, the mechanism of hydrolysis and the time evolution of substrate accessibility to cellulases was modeled based on a model build around cellulase mediated erosion of a cylindrical particle. For nanocrystalline films, it is instead assumed that the cellulose film is made of a network of cellulose nanocrystals with radius 'r' and length 'l' (structure represented in Figure 3.1b). If N_p is the number of particles per unit volume of film, S_i and S_T represents the surface site concentration (g/m^3) and total site concentration (g/m^3), If $\rho_{surface}$ is the surface density of cellulose (g/m^2) and $\rho_{cellulose}$ is the bulk density of cellulose (g/m^3). The rate of exposure and the change in radius of the nanocrystals are given by

$$rate\ of\ \ exposure = k_2 ES\left(1 - \frac{\rho_{surface}}{\rho_{cellulose} r}\right) \qquad (3.12)$$

$$\frac{\mathrm{d}[r]}{\mathrm{dt}} = -k_2 ES \frac{1}{\rho_{cellulose} N_p 2\pi r l} \qquad (3.13)$$

Detailed description of the terms and the derivation of rate of exposure are provided in Appendix II. These equations along with the rate expressions based on the reaction scheme detailed above are combined and solved to fit the frequency profile for the nanocrystal films.

3.5 Results and discussion

AFM topography images were recorded to determine the morphology and surface roughness of the cellulose films. Three types of cellulose thin films were prepared by dissolution or dispersion using different solvents. Figure 3.2 (a, c and e) illustrates AFM images of cellulose surface prepared from NMMO solution showing a fibrillar structure (referred to as NMMO films), from dimethylacetamide/lithium chloride solvent which

exhibits a non-fibrillar structure with no preferential orientation (referred to as LiCl films), and cellulose nanocrystal films which display randomly oriented nanocrystals with dimensions of about 20 nm in width by 200-400 nm in length (referred to as CNC films). The root mean square roughness (rms) of the cellulose films determined over an area of 1 μm × 1 μm. The thicknesses of the cellulose films measured using ellipsometry are listed in table 3.1. These structural features are consistent with those reported in literature [96].

Cellulose found in biomass after pretreatment is thought to be imperfect, and contain crystalline regions (crystallites) and amorphous regions. A parameter termed the crystallinity index has been used to describe the relative amount of crystalline material. Figure 3.3 shows the XRD spectrum of microcrystalline powder, with peaks assigned to indicate their crystal lattice assignments, assuming the I_β phase is aligned with the fiber axis. Crystallinity index was calculated from the ratio of the height of the (002) peak (I_{002})and the height of the minimum (I_{AM}) between the (002) and the (101) peaks by method proposed by Segal *et al*. [174]. Using this method the Crystallinity index of microcrystalline cellulose powder was calculated to be 80%. Efforts to determine the crystallinity of model cellulose films using conventional x-ray diffraction were unsuccessful due to small amount of cellulose material present in the films and possibly broadening of the reflections due to reduction in the mean crystallite size. Therefore, grazing incidence wide angle x-ray scattering technique using synchrotron radiation was used to characterize the degree of crystallinity of model cellulose films. The diffraction patterns of the model cellulose films obtained were very diffuse. Analysis of the diffraction patterns indicated that the NMMO and CNC films showed a broad peak

between 2θ value of 20° and 25° corresponding to the (002) crystal plane of cellulose crystal I organization. The 101 peak between 13° and 18° was not observed for these cellulose films. The crystallinity index of the NMMO and CNC films was not calculated due to lack of a complete diffraction pattern data for the films. However, cellulose films prepared using similar procedures were reported to show type I crystal organization for nanocrystal films and type II crystal organization for NMMO films. It was also reported that the degree of crystallinity was higher for CNC films than for NMMO films [167]. Though the data collected here is not sufficient to provide information about the crystalline form of cellulose films, the presence of the 002 peak obtained confirms that the NMMO and CNC films have some degree of crystallinity. The LiCl films did not show any diffraction patterns using the grazing incidence wide angle x-ray scattering technique suggesting that the films lack crystalline ordering which was consistent with results observed in literature [167].

To investigate the effect of the structure and morphology of different cellulose model films, the binding and cellulose degradation kinetics were studied using QCM-D. Initially all the cellulose films were allowed to equilibrate with flowing buffer solution to attain a baseline frequency (ΔF= 0 Hz). Following this, the buffer solution was replaced with cellulase enzyme solution (200 times diluted cocktail in 0.1 M acetate buffer, pH 4.7 at 25°C). Figure 3.4 displays the typical frequency and dissipation profiles obtained with QCM-D after enzyme injection, which consists of a rapid binding phase indicated by a sharp drop in frequency (addition of mass) followed by more gradual increase in frequency (mass loss) due to enzymatic hydrolysis.

The change in dissipation reveled information about the changes in the viscoelasticity (and by inference morphology) of the film. Initially, steady baseline dissipation was reached suggesting a stable equilibrated film of cellulose, when the enzyme solution was injected a rapid increase in dissipation was observed indicating the adsorption of soft enzyme and its coupled water. The dissipation reached maximum at a certain point following the minimum in frequency followed by a decrease as the cellulose film gets depleted resulting in a more rigid surface [98]. The maximum is most likely due to further softening of the film as hydrolysis begins and new interfacial sites are exposed.

Figure 3.4a shows the frequency profile of cellulase binding and hydrolysis on NMMO cellulose film. As seen in the Figure 3.4a a minimum frequency drop of -50 Hz was observed when the cellulase mixture initially absorbed onto the NMMO cellulose surface. At the minimum, the rates mass change due to adsorption and hydrolysis are equal and after the initial adsorption stage, the frequency increases until reaching a plateau. Figure 3.4b, shows that during the enzymatic degradation of LiCl film, a similar trend is observed to the one observed for NMMO film. The minimum frequency drop was observed to -40 Hz. However, the hydrolysis was completed much faster (in ~10 min) than for NMMO cellulose films (60 min) after the enzyme binding. For CNC films, though the enzyme adsorption and hydrolysis phases were observed (Figure 3.4c), the trends were different compared to NMMO and LiCl cellulose films. The magnitude of the drop in minimum frequency was -690 Hz suggesting the enzyme clearly adsorbed much more onto the CNC films, and subsequent degradation of the film was much slower. The magnitude of the change in dissipation profile also showed a rapid increase indicating a

thick and dissipative enzyme layer on the nanocrystal film. The structure and morphology changes of the cellulose films after enzyme treatment were investigated with AFM (Figure 3.2. b, d, and f) and it was found that the roughness was reduced considerably by hydrolysis: from 12 nm to 2.56 nm for NMMO, 1.88 nm to 0.87 nm for LiCl, and 8 nm to 3.43 nm for CNC films respectively. These results are consistent with previously reported studies of enzymatic hydrolysis of model cellulose films [96, 98, 164, 175]. The different trends in frequency and dissipation profiles observed for CNC films can be explained based on differences in the mechanism of binding and hydrolysis. Kittle *et al*.[175] investigated the water content of regenerated and nanocrystal films based on solvent exchange studies using QCM-D and showed that nanocrystal films contained five time more water than regenerated films, suggesting the nanocrystal films have higher porosity. They also studied the accessibility of these films using cellulase mixture as a probe and demonstrated that nanocrystals are more accessible than regenerated cellulose films. In another study, Jiang *et al*.[164] investigated the adsorption and hydrolysis of nanocrystal films with different sulfate group densities using QCM-D. They reported that sulfate groups slow down or inhibit the enzymatic hydrolysis of cellulose substrates. From XPS measurements on the CNC films used in this study, the sulfate ion concentration was determined to be negligible (<0.5%) suggesting that the effect of sulfate groups was not significant on enzymatic hydrolysis and larger adsorption of cellulase enzymes on the CNC surface is due to higher accessibility to the pore surface. Note that if the films were not dialyzed for a long enough time, residual sulfate groups were observed to inhibit hydrolytic activity, which is consistent with the observations of Jiang et al. [161].

Based on the time taken for the three films to hydrolyze, it can be qualitatively suggested that the CNC films were hydrolyzed much slower than the LiCl and NMMO films. However, quantitative measurements are not directly comparable due to the differences in the magnitude of frequency change due to binding and hydrolysis. In such cases, modeling the kinetics of binding and hydrolysis helps us to quantify and compare the kinetic parameters among different substrates. To describe the detailed molecular mechanisms occurring at the cellulose surface we developed a surface kinetic model based on the interactions between enzymes and degradable solid substrate, as described above. In this model, it is assumed that the enzyme (E) adsorbs to cellulose substrate (S) and complexes to form enzyme bound substrate complex (ES) in one concerted step, neglecting that the association process is likely to involve multiple distinguishable steps [176]. The substrate is represented as a cylindrical fiber with embedded cellulose chains and the model was focused on capturing the time course of available cellulose for hydrolysis. Initially a fraction of the total substrate (α_0) is assumed to be accessible at the start of the reaction and with hydrolysis of surface sites, new sites are exposed and the total substrate concentration is reduced. The developed model was fitted to match the QCM-D frequency data for all three films and determine the kinetic rate parameters (k_1, k_{-1}, k_2) and other model parameters (A, B, α_0). The model requires the specification of the interfacial and bulk substrate concentration. This is not trivial for an insoluble substrate coated in the form of a thin film, so here we use the dry mass of cellulose coated on the sensor surface measured by QCM-D in the absence of buffer as the measure of the total substrate concentration ($S_{T,0}$, g/m^2). Using the parameter $\alpha_{0,}$ the initial interfacial

substrate concentration was determined according to equation 3.11. Thus, the parameter α_0 gives us the measure of the initial accessible fraction of total substrate.

Figures 3.5, 3.6 and 3.7 show the best fit plots of the fibril-based model to experimental data for NMMO, LiCl and CNC films respectively. It was observed that the model fits the NMMO and LiCl cellulose film QCM data well. However, for the CNC film frequency profile was not perfectly captured. The time dependent concentration profiles of the ES complex, total substrate (S_T) and interfacial substrate (S_i) for all three films are provided in Figures 3.8, 3.9 and 3.10. Table 3.2 below shows the fitted parameters obtained from the model fitting.

For the same cellulase mixture, the hydrolysis rate constant for LiCl films (k_2 = 2.22 ± 0.35 min^{-1}) was found to be 5 times higher than for NMMO films (k_2 = 0.44 ± 0.11 min^{-1}). While the frequency profile of the CNC films was not fit perfectly by the fibril-based model, the estimated rate constant was found to be much lower (k_2 = 0.05 ± 0.01 min^{-1}) compared to LiCl and NMMO films, suggesting that it is indeed more difficult for the cellulase enzymes to hydrolyze the crystalline cellulose substrate. The rate of adsorption was found to be similar for NMMO and LiCl films, and α_0 which indicates the fraction of initial accessible substrate for enzyme binding was also similar order for NMMO (0.18) and LiCl (0.29) cellulose surfaces suggesting these films have similar binding affinity for cellulase enzymes. For the CNC films, α_0 was much larger (0.8) suggesting a higher accessible surface. The parameters A and B represent the frequency response to enzyme and cellulose units on the surface. As the frequency change due to the amount of cellulose coated on the sensor surface was converted into mass units using the Sauerbrey relation, the value of parameter B (or 1/B, g m^{-2} Hz^{-1}) is

ideally expected to be related to the Sauerbrey coefficient ($C = 1.7*10^{-4}$ g m^{-2} Hz^{-1}) which represents the cellulose units removed from surface due to hydrolysis. The value 1/B for NMMO (0.15 g m^{-2} Hz^{-1}) and LiCl (0.24 g m^{-2} Hz^{-1}) and CNC (0.64 g m^{-2} Hz^{-1}) films was much larger in magnitude compared to the Sauerbrey coefficient suggesting a correction factor might be needed to account for the exact amount cellulose units removed. . Similarly, the value of parameter A, which represents frequency change associated with enzyme occupied substrate and depends on the molecular weight of enzyme, was found to be similar for NMMO and LiCl films but different for CNC films. This difference suggests that the proposed fibrillar model may not consistently model the behavior of the CNC system and may need modifications to fit the frequency profile for CNC films.

The main distinctive feature of CNC films is that they consist of a network of nanocrystals having a defined surface area. To capture the adsorption and hydrolysis kinetics of CNC films with cellulases accurately, the cellulose film was considered as a porous film composed of a network of randomly oriented cellulose nanocrystals with radius ‘r’ and length ‘l’. The adsorption and hydrolysis mechanism was considered to be similar to the previous fibril-based model, and the time course of change in substrate concentration per unit volume of the cellulose nanocrystals was modeled. As the interfacial sites on the cellulose particles get hydrolyzed, new sites from the bulk are exposed thus resulting in a decrease of radius of the nanocrystals and an increase in total surface area. A detailed description of the rate equations and rate expressions is available in the model section. The parameters associated with the cellulose substrate are the initial surface accessible concentration $S_{i,0}$ (g/m^3) and the total substrate concentration $S_{T,0}$

(g/m^3). The surface density of cellulose is calculated assuming the substrate surface consists of homogenous lattice of cellobiose units. The surface density ($\rho_{surface}$) was calculated to be 183×10^{-5} g/m^2 (surface density calculation shown in Appendix III). The bulk density ($\rho_{cellulose}$) of cellulose was assumed to be 1.5 g/cm^3. The parameter N_p (defined as the number of particles per unit volume), radius r and the length of the particles l were manually adjusted by trial and error. Figure 3.11 shows the best fit of frequency obtained using a particle radius of 3 nm, length 500 nm and N_p 4.27×10^{16} particles/m^3. The enzyme binding and hydrolysis trends were captured using the cellulose nanocrystal network model with these parameters. Table 3.3 lists the kinetic parameters obtained using the cellulose nanocrystal network model for the nanocrystal film.

From the fitted parameter values it was observed that the hydrolysis rate constant ($k_2 = 0.029 \pm 0.0002$ min^{-1}) estimated using the cellulose nanocrystal kinetic model was of a similar order of magnitude compared to the fibril-based kinetic model ($k_2 = 0.05 \pm 0.01$ min^{-1}). Thus, it can be suggested that irrespective of the model used to match the QCM data, the results indicate that the crystalline structure of cellulose significantly slows down rate of hydrolysis. The reason is that crystalline substrates contain stronger inter-chain H bonds that need to be broken by the cellulase enzymes than in an amorphous substrate, which makes crystalline cellulose resistant to enzymatic hydrolysis. Beckham *et al.*[177] used free energy methods to calculate the amount of work that cellulases must conduct to decrystallize cellulose as a function of cellulose polymorph and showed that the decrystallization work for cellulose II and III chains is substantially lower than that for equivalent chains in cellulose I, which is in agreement with the results from the present study. The adsorption rate constant for the CNC films was found to be

smaller than for NMMO and LiCl films, suggesting hindered diffusion through the pores of the nanocrystalline films. The best fit was obtained using a particle radius of 3 nm even though the nanocrystals appeared to be much larger in dimension from the AFM image (Figure 3.2. d). This would be consistent with the nanocrystals being composed of smaller primary particles, although more detailed study would be required to confirm this. A large value for N_p was needed to provide a large initial surface area for the model to capture the enzyme binding extent. This indicates the binding and hydrolysis kinetics is strongly dependent on the accessible surface area and that this is an important parameter for enzymatic hydrolysis.

Irrespective of the film geometric model, the same enzyme adsorption and hydrolysis mechanism was assumed for all films. Enzyme binding is typically considered to be one of the important rate limiting factor in enzymatic hydrolysis, and the amount of surface bound cellulases has been shown to be directly correlated to cellulose hydrolysis rates [86, 178]. However, in the case of nanocrystal films, the high available surface area resulted in an increased enzyme binding, but this did not translate into an enhanced overall hydrolysis rate. The high degree of crystallinity was found to be most important factor dictating the slow hydrolysis rate (k_2). Thus, pretreatments that are able to both reduce crystallinity and increase accessibility of cellulose are likely to have the most benefit towards the overall rate of hydrolysis of cellulose.

All three substrates showed fast initial frequency increase due to hydrolysis followed by a decline in the hydrolysis rate throughout the completion of hydrolysis. The hydrolysis slowdown in bulk studies has previously been attributed to a loss of enzyme activity, either due to enzyme inactivation [76] or due to enzyme inhibition [72-74] by

hydrolysis products. However, in this work, neither enzyme degradation not product inhibition was required to quantitatively describe hydrolysis even to large extents of reaction. This suggests that a significant part of the decrease in hydrolysis rate is in fact due to hydrolysis-induced changes in the accessibility of the substrate itself. Zhang and Lynd et al.[36] stated that declining substrate reactivity is caused by the substrate heterogeneity during hydrolysis as a result of factors such as less surface area and fewer accessible chain ends. This suggests that the hydrolysis of cellulose is a complex phenomenon and the role of cellulose ultrastructure on the relationship between cellulase binding and activity is not straightforward. From this experimental investigation coupled with mathematical modeling, the physical structure and accessibility (which is differentiated simply by their surface accessible fraction) are considered to be the key factors determining reaction rate. However, substrate structural heterogeneity alone cannot explain the whole picture. The proposed models presented were not fully comprehensive in that they lacked consideration of the synergistic actions of individual cellulase components and enzyme deactivation mechanisms. Nevertheless, the models were able to capture trends in the hydrolysis of model cellulose film enzymatic hydrolysis kinetics based on simple geometric models that consider the effects of gradually exposing additional hydrolysable cellulose units as the hydrolysis reaction proceeds. This model allowed clear quantitative comparisons to be made in the rate coefficients for enzymatic hydrolysis (k_2) which showed that type I nanocrystalline cellulose is hydrolyzed by *T. reesei* cellulases about an order of magnitude slower than type II NMMO-derived cellulose, despite significantly higher accessibility to the enzymes. Amorphous LiCl/DMAc films show the greatest hydrolysis rate – about 5-50

times greater than for their crystalline counterparts, which is consistent with expected structural effects.

3.6 Conclusions

Model cellulose films with different morphology and crystallinity were prepared and used to investigate the enzymatic hydrolysis kinetics by monitoring the changes in frequency in situ using QCM-D. The experimental results showed qualitatively that the hydrolysis rate of CNC films was slower than NMMO and LiCl films despite a high level of enzyme binding, suggesting that the microstructure of the films has a significant effect on the binding and hydrolysis of cellulose. The larger drop in frequency upon cellulase binding on CNC films indicated that the nanocrystals films have a much higher surface area available for adsorption compared to the NMMO and LiCl cellulose films. A mechanistic model coupling enzyme binding and hydrolysis with exposure of new sites from embedded cellulose was developed to study the effect of cellulose structure on hydrolysis rate. The model prediction showed excellent agreement with experimental data and the hydrolysis rate constants obtained from fitting were consistent with qualitative results from experiments. The hydrolysis rate coefficient from the best-fit model of LiCl films ($k_2 = 2.22 \pm 0.35$ min^{-1}) was found to be larger than NMMO ($k_2 = 0.44 \pm 0.11$ min^{-1}) and CNC ($k_2 = 0.029 \pm 0.0002$ min^{-1}) cellulose films. From these results it can be suggested that drop in hydrolysis rate of cellulose in bulk studies may be due to the nature of the substrate becoming more recalcitrant as amorphous regions are consumed due to the strong H-bonding network of crystalline cellulose. In order to determine these parameters, two kinetic models were needed. For NMMO and LiCl

films, an approach assuming uniformly accessible cylinder-shaped particles was found to be successful, but this approach did not capture the binding features of the CNC films. A new cellulose nanocrystal network model was developed to capture the physical features of the substrate such as a large accessible surface area. A large number of nanocrystals per unit volume with a small initial radius (3 nm) of the cellulose particles were assumed to provide a large surface area and provide the best fit of the model to the QCM data. These results suggest that the ultrastructure of cellulose (crystallinity and morphology) and the accessibility of cellulose are both important factors determining the overall reaction rate. Based on these findings, we can speculate that pretreatments that increase accessibility of cellulose without reducing the crystalline fraction are not likely to be as successful as those able to increase both accessibility and amorphous cellulose content of biomass.

3.7 Figures and Tables

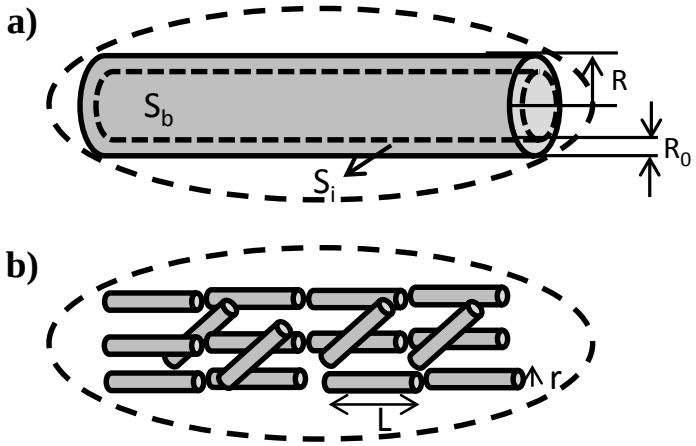

Figure 3.1. Schematic representation of the cellulose structure a) fibril based model – cellulose surface made of cellulose chains embedded inside a fiber structure, R_0 represents the thickness of the interfacial layer (S_i – interfacial layer), R represents the radius of the cellulose fiber (S_b – bulk cellulose) b) cellulose nanocrystal model – cellulose surface is made of randomly oriented nanocrystals of radius 'r' and length 'l'.

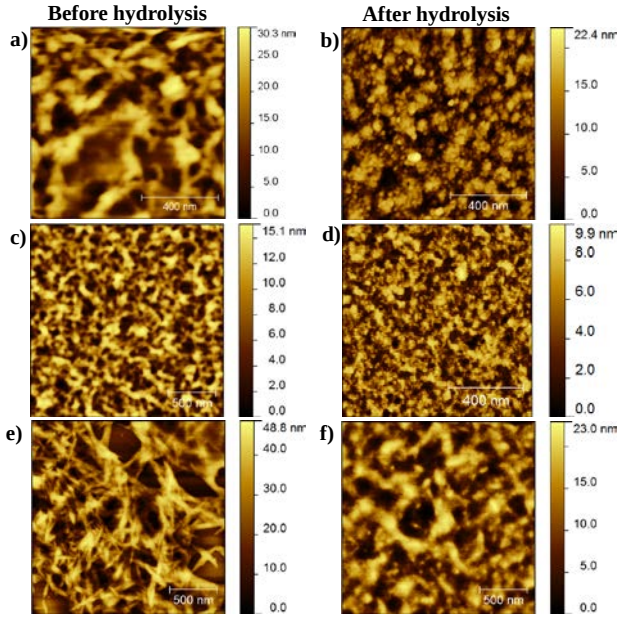

Figure 3.2. AFM images of model cellulose surfaces before and after hydrolysis of NMMO (a, b), LiCl (c, d) and CNC (e, f) films. The scale bars to the right of each image show the z-range.

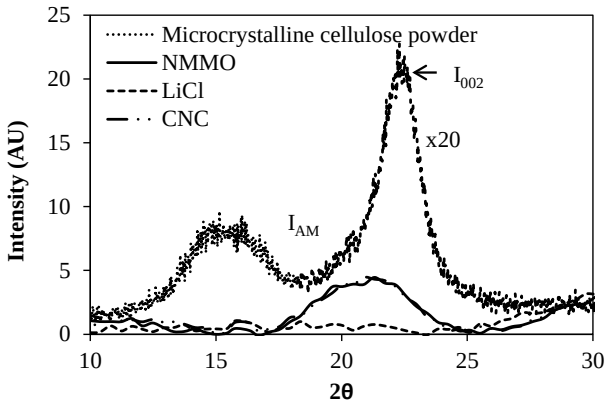

Figure 3.3. X-ray diffraction pattern of microcrystalline powder (using x-ray diffractometer) and grazing incidence wide angle x-ray scattering (GIWAXS) profiles of the cellulose films. 1D diffraction profile from GIWAXS data were obtained by performing line cuts over a phi (φ) angle range between 10 – 20° in the out-of-plane direction.

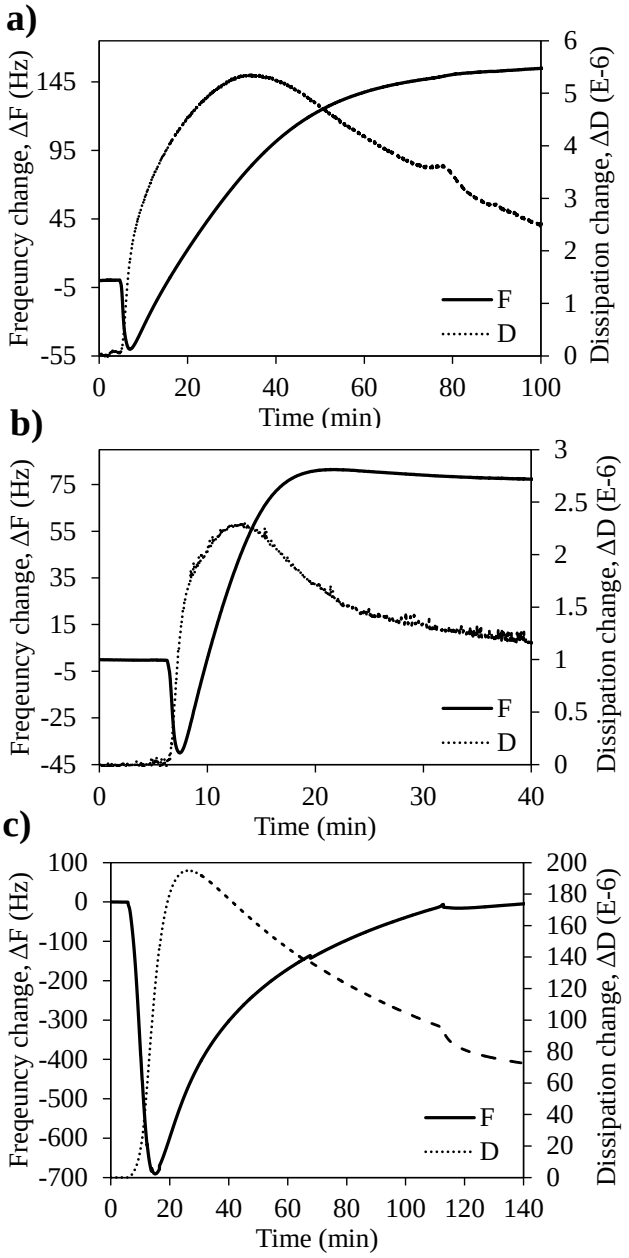

Figure 3.4. Frequency and dissipation profiles during the enzymatic hydrolysis of cellulose films by a 200x diluted *T. reesei* cellulase cocktail in pH 4.7 acetate buffer (0.1M) for a) NMMO b) LiCl and c) CNC.

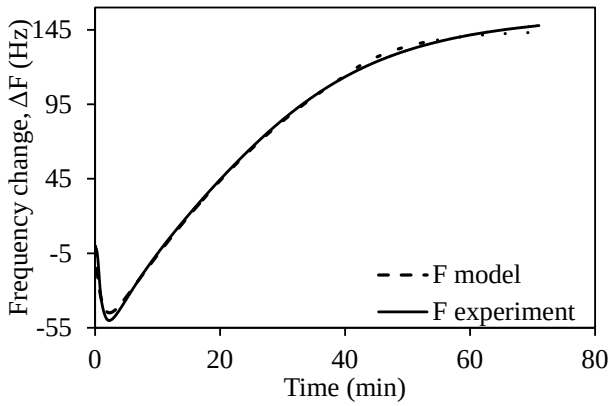

Figure 3.5. Fitting of the fibril based kinetic model with accessible sites generated by hydrolysis (dotted curve) to experimental frequency response QCM-D data (solid curve). The result for the NMMO film hydrolysis by cellulase at pH 4.7, 25°C.

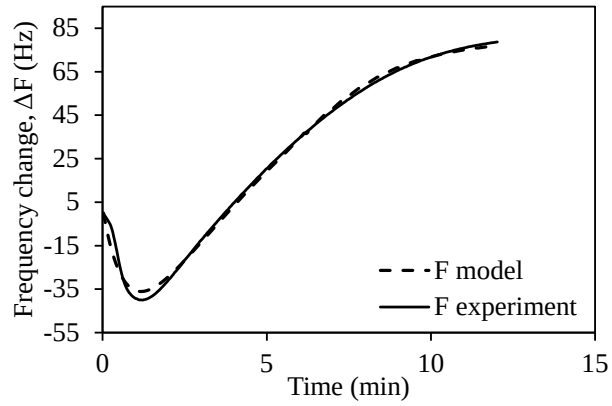

Figure 3.6. Fitting of the fibril based kinetic model with accessible sites generated by hydrolysis (dotted curve) to experimental frequency response QCM-D data (solid curve). The result for the LiCl film hydrolysis by cellulase at pH 4.7, 25°C.

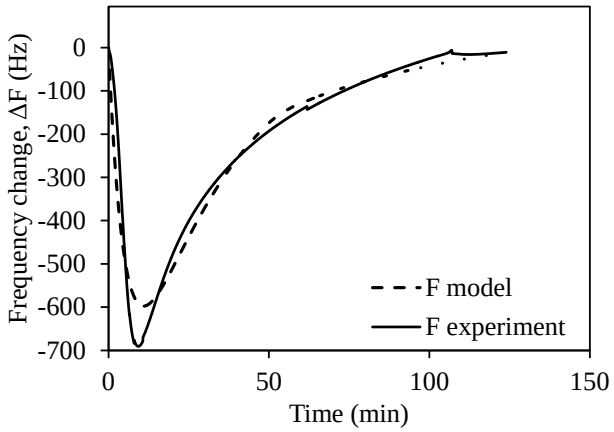

Figure 3.7. Fitting of the fibril based kinetic model with accessible sites generated by hydrolysis (dotted curve) to experimental frequency response QCM-D data (solid curve). The result for the CNC film hydrolysis by cellulase at pH 4.7, 25°C.

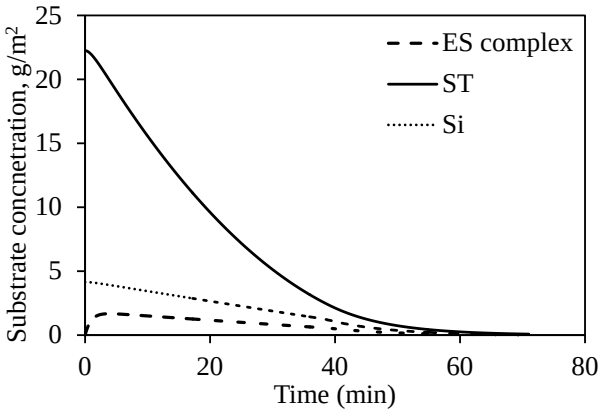

Figure 3.8. Model concentration profile of ES complex (dashed line), interfacial substrate concentration Si (dotted line) and total substrate concentration ST (solid line) for NMMO film hydrolysis by cellulase at pH 4.7, 25°C.

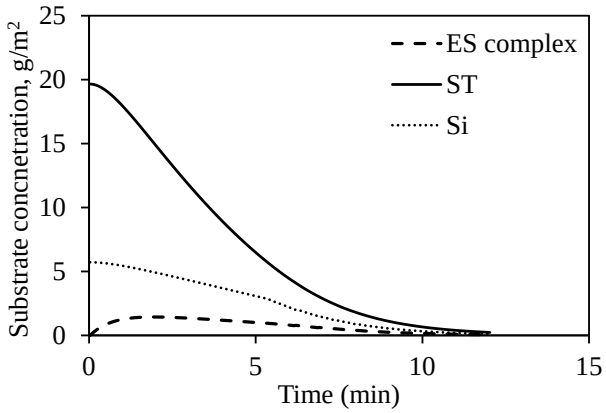

Figure 3.9. Model concentration profile of ES complex (dashed line), interfacial substrate concentration Si (dotted line) and total substrate concentration ST (solid line) for LiCl film hydrolysis by cellulase at pH 4.7, 25°C.

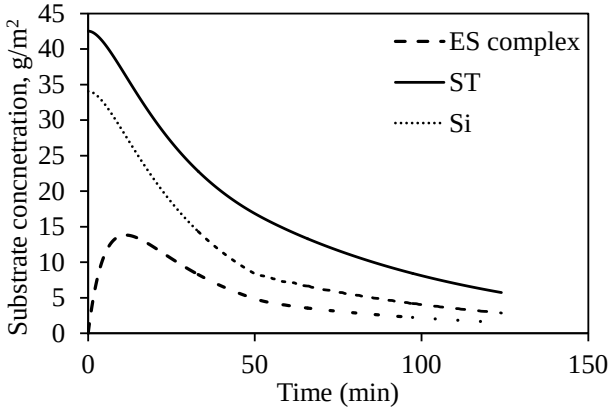

Figure 3.10. Model concentration profile of ES complex (dashed line), interfacial substrate concentration Si (dotted line) and total substrate concentration ST (solid line) for CNC film hydrolysis by cellulase at pH 4.7, 25°C.

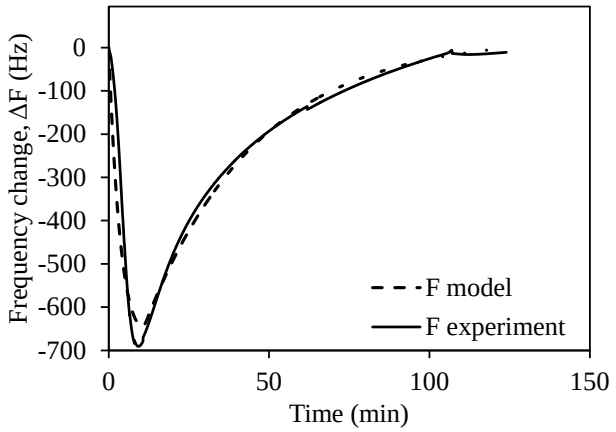

Figure 3.11. Fitting of the cellulose nanocrystal based kinetic model hydrolysis (dotted curve) to experimental frequency response QCM-D data (solid curve). The result for the CNC film hydrolysis by cellulase at pH 4.7, 25°C.

Table 3.1. Measurements of cellulose film roughness (AFM) and thickness (ellipsometry)

Cellulose film	Surface roughness rms (nm)	Thickness (nm)
NMMO cellulose	12 ± 2.45	51 ± 1
LiCl/DMAc cellulose	1.88 ± 0.1	39 ± 3
Nanocrystal cellulose	8.05 ± 0.1	57 ± 3

Table 3.2. Kinetic parameters obtained from the fitting of experimental frequency data with the modeled frequency for NMMO, LiCl and CNC films

Parameter	NMMO	LiCl	CNC
k_1 (mM min^{-1})	264±64	262 ± 25	65.5 ± 15.4
k_1 (min^{-1})	0.60 ± 0.12	1.08 ± 0.07	0.11 ± 0.02
k_2 (min^{-1})	0.44 ± 0.11	2.2 ± 0.35	0.05 ± 0.01
A (Hz g^{-1} m^2)	32.9 ± 8.8	34.0 ± 5.4	44 ± 13
B (Hz g^{-1} m^2)	6.49 ± 0.01	4.05 ± 0.35	1.56 ± 0.41
α_0	0.18 ± 0.006	0.29 ± 0.022	0.80 ± 0.05

Table 3.3. Kinetic parameters obtained using the cellulose nanocrystal network model for nanocrystal film

Parameter	Value
k_1 (mM min^{-1})	150 ± 4.5
k_1 (min^{-1})	0.0014 ± 0.01
k_2 (min^{-1})	0.029 ± 0.0002
A (Hz)	797 ± 30
B (Hz)	25.4 ± 1.3

CHAPTER 4

QUARTZ CRYSTAL MICROBALANCE WITH DISSIPATION MONITORING INVESTIGATION OF EFFECTS OF TWEEN-80 ON HYDROLYTIC ACTIVITY OF MODEL CELLULOSE SUBSTRATES

4.1 Summary

A number of studies have investigated the hydrolysis of lignocellulosic biomass in the presence of surfactants to understand the effects of surfactants on the enhancement of cellulose conversion. Several factors such as surfactant type, pretreatment type, lignin content, and hydrolysis conditions have been reported to affect hydrolysis process in the presence of surfactants. However, the mechanism for enhancement of enzymatic hydrolysis of cellulose by surfactants is still not clear. In this study, the role of non-ionic surfactant Tween-80 on enzymatic hydrolysis of cellulose is evaluated using a quartz crystal microbalance with dissipation modeling (QCM-D). Cellulose thin films with different surface morphology and crystallinity are used as substrates. Effects of Tween-80 on the adsorption of cellulases and hydrolysis are evaluated by changing the addition sequence of Tween-80. The results showed that the adsorption of cellulases is reduced on cellulose surfaces when Tween-80 is adsorbed onto cellulose surface prior to cellulase introduction. The hydrolysis rate showed no significant effect on hydrolysis of amorphous cellulose films deposited from a LiCl/dimethylacetamide solvent system whereas the hydrolysis rate decreases with increasing Tween-80 concentration (over the range from 0-8 mM) for semicrystalline fibrillar films derived from N-methylmorpholino-N-oxide. The effect of Tween-80 was found to be a function of cellulose substates and substrate type, but it is at best neutral; this suggests that the

positive effects of Tween-80 on lignocellulosic biomass are based on allowing redistribution of enzymes and reducing nonproductive binding rather than a direct enhancement of cellulose hydrolysis.

Keywords: Non-ionic surfactants, Cellulose, Cellulase, Adsorption, Enzymatic hydrolysis

4.2 Introduction

Enzymatic hydrolysis is an important and essentail step in the conversion of lignocellulosic material to bioethanol and other commodity chemicals. However, hydrolysis of lignocellulose into soluble and fermentable sugars is still cosnidered a major bottleneck in the biorefinery process . The extent and rate of hydrolysis are mainly limited by the recalcitrant and complex structure of lignocellulosic polymers (cellulose, hemicellulose and lignin) along with the requirement of high enzyme dosage in order to achieve a high rate and extent of cellulose conversion. Thus, in order to develop an effective process for conversion of cellulose into ethanol it is important to identify methods to increase enzyme effectiveness [9, 179, 180].

Different strategies have been applied to improve the effectiveness of the enzymes: improvement of pretreatment technologies to improve accessibility of cellulose to enzymes by removing lignin and hemicelluloses [26, 181]; screening of microorganisms for new lignocellulose degrading enzymes with better performance [182]; protein engineering [183]; and addition of additives to improve enzymatic hydrolysis and reduce the amount of enzyme needed [60, 184, 185]. Among the methods studied, the application of additives such as surfactants (e.g., Tween, poly(ethylene

glycol) (PEG)) and non-catalytic proteins (e.g., bovine serum albumin, BSA) represents a promising direction applicable to many cellulases (wild type and genetically modified), and has been widely investigated and shown in some studies to significantly increase the degree of enzymatic hydrolysis. Ooshima *et al.* [61] compared the effects of addition of non-ionic, anionic and cationic surfactants on the hydrolysis of different types of celluloses and found that non-ionic surfactants are most effective in improving cellulose conversion. In the presence of Tween-20 and Tween-80, the conversions of cellulose, xylan, and total polysaccharide from lime-pretreated corn stover were reported to increase by 42, 40, and 42 % (respectively) over 72 h of hydrolysis by cellulases from *Trichoderma reesei* [185]. Eriksson *et al*. [60] also reported that the addition of surfactants during enzymatic hydrolysis of steam-pretreated spruce increases the conversion of cellulose into soluble sugars, with nonionic surfactants being most effective. Kristensen *et al*. [180] reported that additives such as BSA, Berol 08, PEG 6000, and Tween 80 are all able to increase cellulose conversion. They reported that the degree of surfactant effect varied with the type and severity of pretreatment. Another study reported that addition of PEG increased both the efficiency of enzymatic hydrolysis of steam-pretreated spruce and the free cellulase activity in the hydrolysis supernatant [186]. Several mechanisms have been proposed to explain the enhancement of cellulase hydrolysis including: alteration of the substrate structure by surfactants to make it more accessible to enzymes [184, 185]; surfactants changing enzyme-substrate interactions to reduce non-productive adsorption of enzymes [60]; and surfactants increasing enzyme stability to prevent denaturation of enzymes and loss of activity during hydrolysis [184, 185].

Although additives have been reported several times to improve the hydrolysis of cellulose and lignocellulosic substrates, the results of other studies are mixed. Eriksson *et al*. [60] reported that surfactants only affected lignin-containing substrates but had no effect on delignified and cellulose substrates, which was interpreted as surfactant reducing unproductive binding of enzymes to lignin. In contrast, Ooshima *et al*. [61] reported that Tween-20 increased the conversion of Avicel by 35%. They attribute this effect to surfactant enhancing the synergistic action of endoglucanase and cellobiohydrolase on the surface of cellulose. Recently, Zhou *et al*. [187] reported that the conversion of pure cellulose is not consistently improved by surfactants and showed inhibition to cellulose conversion at high surfactant concentrations. They proposed that the interaction between surfactant and cellulases become significant in the late hydrolysis phase thus reducing the productive binding of cellulases onto cellulose and inhibiting the overall cellulase activity. So far, a mechanism that can consistently explain how and when surfactants affect enzymatic hydrolysis has not been developed.

Part of the reason that understanding of the enhancement in cellulose hydrolysis by surfactants is incomplete is that in most existing studies, the effect of surfactant was assessed by measuring the overall production of sugar after an arbitrary time or at completion of hydrolysis rather than by continuous kinetic measurements. The hydrolysis of cellulose into sugars by enzymes is a complex process that requires the adsorption of cellulase enzymes onto the cellulase surface followed by a hydrolysis process involving processive enzymes, desorption and enzyme reattachment. Studies focusing on sugar produced at a fixed time point are practically relevant (since batch processes of fixed duration are typically used for saccharification) but cannot

differentiate between the effects of surfactant on enzyme adsorption, the actual hydrolysis rate, and the desorption rate of enzymes. Prior studies have suggested that the rate of adsorption is rapid compared to the actual rate of hydrolytic activity of the enzymes, thus making the amount of adsorbed cellulase an important factor in the effectiveness of the reaction [188].

Most commercial cellulase enzymes for biomass hydrolysis are produced from *T.reesei* fungi comprised of three classes of enzymes exoglucanases (cellobiohydrolases), endoglucanases and β-glucosidases. Cellobiohydrolases CBH I and II constitute the major cellulase components, comprising up to 80% of the total protein content. CBH I and II hydrolyze cellulose processively from reducing and non-reducing ends releasing cellobiose. Cellobiohydrolase enzymes are modular proteins with two domain structures, a carbohydrate binding domain and a catalytic domain. The adsorption of cellulase enzymes to cellulose has been attributed to carbohydrate binding domains interacting with the hydrophobic face of cellulose [189]. If this is the case, cellulose binding domains may also be attracted to other hydrophobic surfaces that cannot be hydrolyzed, leading to nonproductive binding. Surfactants have been proposed to increase overall conversion by competing with enzymes for binding to hydrophilic surfaces, thus reducing the level of nonproductive binding. For pure cellulose, this could be either a positive or negative factor depending on the density of sites available for nonproductive binding.

Here, the hypothesis is directly tested that non-ionic surfactants bind to cellulose by hydrophobic interactions to reduce the non-productive adsorption of cellulases, and thereby enhance overall sugar production. Addressing these effects calls for a technique

capable of directly observing adsorption of and hydrolysis by cellulase enzymes at the surface of model biomass thin film substrates. Quartz crystal microbalance with dissipation monitoring (QCM-D) measurements have been shown to be such a technique [96, 98, 163, 190, 191]. Substrates consisting of model thin films of pure cellulose have allowed QCM-D to provide valuable information on the behavior of cellulose (for example swelling [17]) and make it suitable for *in situ* studies on enzymatic degradation of cellulose during simultaneous adsorption and degradation. Previous investigations have assessed the effect of substrate crystallinity[96], treatment conditions[98, 163] and the action of individual monocomponent cellulases [191] and cellulase mixtures [98] on the rate of hydrolysis. However, they did not address the effects of additives on cellulase interactions with model surfaces.

In this work, we report a study of the effects of Tween-80 on cellulase binding and hydrolysis of model cellulose substrates (NMMO and LiCl/DMAc cellulose films) using QCM-D. The non-ionic surfactant Tween-80 was chosen as a model additive because it was widely investigated and shown to be effective in enhancing overall sugar release from cellulose [60, 180, 185, 192, 193]. The specific aim of the present study is to quantify at the interfacial level the hydrolytic activity of cellulase and the binding of cellulase to cellulose in the presence of Tween-80. The effects of crystallinity of the cellulose surface will be investigated by preparing amorphous thin films (from LiCl/DMAc) and type II crystalline cellulose thin films (from NMMO) using different solvent systems. The mechanism of Tween-80 on saccharification will be investigated by comparing the hydrolysis behavior of *T. reesei* cellulases on the model cellulose films in the presence and absence of Tween-80. The addition sequence of Tween-80 will be

varied to investigate the ability of Tween-80 to compete with cellulase for binding, or to pre-saturate the surface to inhibit binding.

4.3 Materials and methods

NMMO and LiCl/DMAc cellulose films were used as model substrates in this study. Refer to section 3.3 (Chapter 3 Materials and methods) for the synthesis and characterization procedures employed. QCM-D measurements also followed the same approach as described in section 3.3, with the exception that Tween-80 was added at varying concentration and different sequences of addition, as described below.

4.4 Results and Discussion

The thickness of the cellulose films prepared from LiCl/DMAc and NMMO solvent systems were determined by ellipsometry to be 39 and 51 nm respectively. Figure 4.1 shows an AFM topographic image of cellulose surfaces on sensor surfaces scanned in tapping mode. The LiCl/DMAc cellulose films were uniform and displayed structured feature in the submicrometer scale with no preferential orientation. The NMMO cellulose films were non-uniform and displayed a fibrous structure. The rms surface roughness values were determined to be 1.88 ± 0.1 and 7.7 ± 0.5 nm for LiCl/DMAc and NMMO cellulose films respectively. The characteristics of these films are consistent with previous findings [167]. Because these morphological features match the literature upon which the synthesis procedures are based, we also presume that the crystal structures of the cellulose matches prior reports, in which LiCl/DMAc derived films were shown to be amorphous, and NMMO derved films were shown to be type II crystalline celluose [167].

As noted in Chapter 3, the films did not exhibit reflections in XRD, and GIWAXS only indicated the presence of crystallinity in the NMMO films but not multiple reflections that would be required for structure assignment. It may be that the crystallite size of our NMMO films is smaller than in the literature, which would have led to less distinct diffraction peaks.

Adsorption behavior of Tween-80 onto LiCl/DMAc cellulose surface was studied using QCM-D and is shown in Figure 2. The concentration range of Tween-80 used was varied from 0.38 mM to 15.26 mM. Initially, a buffer solution (0.1 M acetate) was passed continuously over the cellulose coated QCM sensor to obtain a steady baseline, and at this point frequency and dissipation were initialized to zero. Upon introduction of diluted Tween-80 solution, an immediate decrease in frequency was observed indicating adsorption of Tween-80 onto the cellulose surface. The adsorption was followed until a steady-state plateau was reached. After equilibrium was reached, the Tween-80 solution was switched to buffer solution and continuously rinsed to observe the desorption behavior. The desoprtion is represented by an increase in the frequency upon rinsing with buffer. The frequency change associated with desorption was quantified by taking the difference in the frequency after equilibration was reached upon rinsing and the frequency at the previous plateau. The frequency changes due to Tween-80 desorption were measured to be 1.45, 3.83, 9.90, 17.07, and 21.92 Hz for Tween-80 concentrations of 0.38, 0.76, 3.81, 7.63, and 15.3 mM. Upon rinsing with buffer the increasing magnitude of frequency change with Tween-80 suggests that the adsorption is mostly reversible, but that some residual Tween-80 remained.

The adsorption kinetics of Tween-80 on cellulose shows features that resemble non-ionic surfactant adsorption on hydrophilic [194, 195] and hydrophobic surfaces [196, 197]. Non-ionic surfactants are physically adsorbed and the adsorption is strongly affected by small changes in adsorbate concentration, molecular structure and temperature [198]. Torn *et al*. [199] studied the adsorption of non-ionic surfactants on cellulose surfaces and proposed that at low surfacatant concentrations both the head group and tail contribute to adsorption (since cellulose is amphiphilic) and that at high concentrations lateral attraction between surfactant molecules dominate adsorption. The frequency change due to adsorption of Tween-80 on LiCL/DMAc cellulose surfaces after reaching equilibrium was estimated from Fig. 4.2. The measured frequency change data was fit using a liquid phase BET adsorption isotherm, Eq. 4.2 [200] shown in Figure 4.3.

$$q = q_m * \frac{K_S C_{eq}}{(1-K_L C_{eq})*(1-K_L C_{eq}+K_S C_{eq})} \qquad (4.2)$$

where q_m is the monolayer adsorption capacity, K_S is the equilibrium adsorption constant for the first layer, and K_L is the equilibrium constant for the upper adsorbed layers. The maximum monolayer adsorption capacity was found to give a QCM response of 16.2 Hz, which corresponds to a monolayer mass of 287 ng/cm^2 using the Sauerbrey relation (Equation 3.1). Adsorption constants were determined to be 1.92 mM^{-1} (K_S) and 0.01 mM^{-1} (K_L). The equilibrium adsorption frequency meaured at 15.3 mM was found to be 19.6 Hz, which is higher than the monolayer adsorption capacity (16.2 Hz) suggests that multilayer binding or surfactant clustering occurs on the cellulose surface. Using the adsorption capacity value, the area occupied by each molecule in a monolayer on the cellulose surface was calculated to be 75.9 Å^2. Kirby et al. studied the adsorption of

Tween-80 at oil/water interface by surface tension measurements and estimated the surface coverage of Tween-80 to be 137.1 $Å^2$. The lower area per molecule of Tween-80 suggest larger adsorption of Tween-80 on cellulose surface, either because of more close packing at the solid surface, or the slight roughness of the surface.

Figure 4.4 shows the typical QCM-D frequency profiles of LiCl/DMAc and NMMO cellulose films during hydrolysis with a 200x diluted *T. reesei* cellulase solution. A detailed explanation of the frequency and dissipation profiles is provided elsewhere [98]. In short, the cellulose films are equilibrated in buffer medium in the QCM-D chamber until no significant change in frequency was observed. The first frequency shift corresponds to the adsorption of cellulase onto the cellulose surface after cellulase injection into the QCM-D module followed by an increase in frequency due to hydrolysis of cellulose substrate by cellulases and then leveling off as the hydrolysable substrate is consumed. These results are in agreement with Ahola *et al* [96] who studied the effects of cellulose surface structure on enzymatic hydrolysis by QCM-D.

From the frequency profile, the minimum frequency attained due to adsorption (F_{min}), maximum hydrolysis rate, and the maximum frequency upon reaching a plateau (F_{max}) were quantified. When only cellulase was introduced into the QCM-D chamber the minimum frequency should be due to the amount of cellulase adsorbed. The maximum hydrolysis rate was determined by plotting the absolute slope of the frequency change between two consecutive time points ($d\Delta F/dt$) and observing the time where the maximum is attained (Figure S4.1 (Appendix IV) shows an example plot of frequency change and derivative with time to determine the maximum rate). It was observed that

slope initially increases and reaches a maximum and then decrease, but that because of noise in the data the maximum slope is not at a single point but spread over a range of the time interval, the maximum hydrolysis rate was quantified by measuring the slope from the frequency profile over the corresponding time interval. However, it was found that the minimum frequency change due to adsorption, the maximum hydrolysis rate and maximum frequency value after hydrolysis varied from film to film. The amount of cellulose mass coated on the surface of sensor was estimated by measuring the fundamental frequency of the sensors before and after cellulose coating using QCM-D. From the ratio of maximum value of frequency after hydrolysis and mass of cellulose coated on the surface the extent of reaction was quantified. It was found that the quantified values varied from batch to batch and there were large variations as reported in Table 4.1. Since no standard methods are available to normalize the QCM-D data and compare between batches, the results of further experiments are compared among each batch of cellulose films to determine trends in quantified data. Variations in results were found for both LiCl/DMAc and NMMO cellulose films.

The effect of Tween-80 on hydrolysis of cellulose surfaces was investigated by changing the addition sequence of Tween-80 by: 1) Sequential adsorption in which Tween-80 was adsorbed onto cellulose surface prior to cellulase introduction and 2) Co-adsorption in which cellulase and Tween-80 are introduced as a mixture in the same buffered solution.

Figures 4.5 show the frequency profile of cellulose hydrolysis with and without Tween-80 during sequential adsorption using 0.76 mM Tween-80. Qualitatively similar

frequency response profiles were observed at different Tween-80 concentrations, but it is difficult to represent the differences among experiments using raw data, so the data will be reported in terms of processed quantities. It was observed that from Figure 4.5 that upon exchange of buffer with Tween-80 the frequency dropped due to adsorption of Tween-80 on the cellulose surface until an equilibrium frequency was reached consistent with the adsorption studies (Figure 4.2). After Tween-80 adsorption reached equilibrium, the Tween-80 solution was replaced with a cellulase solution (free of Tween-80) and adsorption and hydrolytic activity of cellulases was measured. For comparison purposes the hydrolytic activity of cellulases in the presence and absence of Tween-80 are shown together (Figure 4.5). Cellulase adsorption on the Tween-80 adsorbed cellulose surface was measured by quantifying the difference between the minimum frequency (F_{min}) and frequency change due to Tween-80 adsorption after equilibrium was attained.

Figure 4.6 shows the frequency change due to cellulase adsorption on both NMMO and LiCl/DMAc cellulose films with varying concentrations of Tween-80 (0-8 mM) for different trials (where each trial represents a new set of films prepared from the same cellulose solution). It was found that the frequency change decreased with increasing concentration of Tween-80. This frequency can be regarded as a measure of cellulase adsorption. Taking the difference between the minimum frequency change during sequential adsorption and the frequency change associated with pre-adsorption of Tween-80 alone as a lower bound on the frequency change due to cellulase adsorption, reduction in bound cellulase was found to increase from 16% at 0.76 mM to 33% at 7.6 mM Tween-80 for NMMO films and 25% at 0.76 mM to 44% at 7.6 mM Tween-80 for LiCl films. Due to large variation in the hydrolysis rates among trials, the hydrolysis rate

was normalized using the minimum frequency due to adsorption, which is assumed to be proportional to the amount of cellulase adsorbed. In Figure 4.7, the normalized rates are reported as ratios of the normalized rates with Tween-80 to that without Tween-80. It was found that for NMMO cellulose films the hydrolysis rate decreased with increasing concentration of Tween-80 for all trials, whereas LiCl/DMAc cellulose films showed no significant trend in the effect of Tween-80 on hydrolysis rate for all trials. While there is variability in the ratio of the normalized hydrolysis rate, it is clear from these studies that pre-adsorption of Tween-80 leads to both a reduction in bound cellulase on both types of films, and a reduction in hydrolysis rate per bound cellulase on NMMO films.

Figure 4.8 shows the frequency profile during cellulose hydrolysis for an NMMO film in contact with a mixture of 0.76 mM Tween-80 and cellulase. The frequency profiles looks similar with and without Tween-80. It should be noted that both cellulase and Tween-80 adsorb onto the cellulose surface and the minimum frequency change due to adsorption is a combined effect which is not directly distinguishable by QCM-D. To study the effect of Tween-80 on cellulase adsorption, the minimum frequency due to adsorption was quantified and plotted. Figure 4.9 shows the plot of quantified adsorption values for both NMMO and LiCl/DMAc cellulose films. Both films show a similar trend: cellulase adsorption slightly decreased at the lowest Tween-80 concentrations (0.76 mM) suggesting that Tween-80 decreased the cellulase binding on cellulose surfaces. At higher concentrations of Tween-80, the frequency change was higher than for only cellulase adsorption. However, it should be noted that the minimum frequency in case of co-adsorption is a combined effect of cellulase and Tween-80 binding and the higher change might be due large amounts of Tween-80 adsorbed on the surface. If the difference

between the frequency change during coadsorption and the frequency change associated with Tween-80 alone is taken as a lower bound on the frequency change due to cellulase adsorption, the average reduction in bound cellulase was found to be 11±3% on NMMO films and 21±2% on LiCl films. Figure 4.10 shows plots of the normalized hydrolysis rate vs. hydrolysis without Tween-80 as function of Tween-80 concentration. The hydrolysis rate decreased with increasing concentration of Tween-80 for NMMO cellulose films for all trials, and showed no trend for the LiCl/DMAc cellulose films across all trials.

Overall, these results show that the most consistent effect of adding Tween-80 (either before or with cellulase) is to reduce binding of cellulase. Hydrolysis rate decreases for partially crystalline films derived from NMMO, and does not change significantly for amorphous films derived from LiCl / DMAc. In bulk studies, the conclusions for enhancement of cellulose hydrolysis by surfactants were primarily based on the conversion of cellulose measured at a certain time by the amount of sugars produced. In the present study, the conversion of cellulose cannot be measured due to the nature of the QCM-D system. Therefore a quantity extent of reaction based on the ratio maximum frequency (plateau after hydrolysis) and amount of cellulose coated was quantified. The extent of reaction for both co-adsorption and sequential adsorption studies are represented in Figures S4.2 and S4.3 (Appendix IV) for NMMO and LiCl/DMAc cellulose films respectively. It was found that using this approach a consistent trend was not observed suggesting extents for these model films are unaffected by Tween-80 within the experimental uncertainties.

The mechanism underlying the enhancement of cellulose hydrolysis by the addition of surfactants has been a topic of extensive research. Most bulk studies have reported that the increase of free enzymes in solution due to reduction of non-productive adsorption of cellulase onto lignin contributes to the enhancement of cellulose conversion in lignocellulosic substrates [59, 60, 180]. From the findings in this study it was found that Tween-80 adsorbs to cellulose surfaces and, from Figures 4.6 and 4.9, decreases cellulase adsorption onto cellulose. This result is in agreement with the investigations of cellulase adsorption in the presence of surfactants on pure cellulose substrates in which it was reported that the amount of free enzyme in solution was larger in the case of surfactants than with no surfactant [61, 184, 192, 193]. A key difference in this case is that because a flow through system is used, the concentration of cellulase in solution is unaffected by the change in adsorbed amount.

In contrast to prior investigations on enhancement of hydrolysis of pure cellulose substrates with surfactants, the current results indicate that Tween-80 inhibited the hydrolysis rate of NMMO-derived cellulose films. A possible explanation for the negative effect of surfactant on hydrolysis rate is due to substrate–surfactant interactions. The surface of a cellulose is known to contain hydrophobic and hydrophilic regions [201], and it is hypothesized that the binding of surfactants onto cellulose through hydrophobic interactions prevents the productive binding of cellulases onto cellulose resulting in a decreased hydrolysis rate. Zhou *et al.*[187] studied the effect of surfactant concentration on hydrolysis of microcrystalline cellulose and filter paper and they reported that high concentration of surfactant decrease cellulose conversion. They proposed the possible mechanism was due to the interaction between surfactant and

enzymes forming surfactant-enzyme aggregates at later stages of hydrolysis, thus limiting productive adsorption of cellulases. However, in this study we found that the decrease in hydrolysis rate was significant when surfactant was introduced as a mixture and when pre-adsorbed on cellulose surface suggesting that the substrate-surfactant interactions might be the reason for a decrease in hydrolysis rate.

The finding that the LiCl/DMAc cellulose films show no effect in presence of Tween-80 suggests that the effect is not universal, and structural features of cellulose might affect the action of surfactant on cellulose hydrolysis. The lack of an effect for amorphous cellulose either reflects the high availability of free chain ends in these films, or that because the rate of hydrolysis is high already, Tween-80 has little effect. Another factor to be noted in bulk studies is that the enzyme is added in a limited amount and the substrate is in excess during hydrolysis. The conversion in bulk studies does not reach 100%, and addition of surfactants helps to attain higher conversion (but not necessarily higher rate). In this study cellulose thin films were used which have a limited amount of cellulose available for hydrolysis and a continuous supply of enzyme in a flow through module. If all the cellulose was consumed the conversion would reach 100% across all materials (in presence or absence of Tween-80). As a result no difference in conversion would be observed.

The effect of surfactants has been reported to be dependent on various factors such as surfactant type, concentration, biomass substrate features and hydrolysis conditions [187, 202, 203]. This study supports the mechanism on the positive effect of surfactant on lignocellulosic substrates is based on the reduction of non-productive

binding. Although no evidence for the enhancement of cellulose conversion was observed in this study, it is believed that the interactions between surfactant and biomass surfaces (cellulose and lignin) play a significant role in reducing the cellulase binding and at higher concentration surfactants inhibit the hydrolysis rate.

4.5 Conclusions

The effects of Tween-80 on the adsorption and hydrolysis of *T. reesei* cellulases on model cellulose surfaces was investigated. Two kinds of model cellulose surfaces (NMMO and LiCl/DMAc) with different surface morphology and crystallinity were prepared and characterized. Tween-80 was found to adsorb onto the cellulose surface according to a BET (multilayer) isotherm mostly reversibly, but that some residual Tween-80 remained upon rinsing. Cellulase binding decreased in the presence of Tween-80 on both NMMO and LiCl/DMAc cellulose films. With pre-adsorption of Tween-80 on cellulose, the reduction in bound cellulase was found to increase from 16% at 0.76 mM to 33% at 7.6 mM Tween-80 for NMMO films and 25% at 0.76 mM to 44% at 7.6 mM Tween-80 for LiCl films. Co-adsorption of Tween-80 and cellulase resulted in a net reduction in the amount of cellulase adsorbed by 11±3% on NMMO films and 21±2% on LiCl/DMAc films.

The hydrolysis rate was observed to decrease with added Tween-80 for NMMO cellulose films while no significant effect was observed on the hydrolysis of LiCl/DMAc cellulose films. This is surprising in light of some prior studies which suggested an increase in conversion of cellulose due to Tween-80 addition. This study clarifies that this effect may not be a result of a direct enhancement in hydrolytic activity, but instead

due to increased desorption of cellulase (which would allow it to redistribute in the system and thus drive towards higher conversions) and looking at conversion rather than rate of hydrolysis. The high affinity of Tween-80 to lignin rather than cellulose (see Chapter 5 for more details) suggests that the reduction in non-productive cellulase binding onto hydrophobic surfaces is the best explanation for the enhancement of cellulose conversion in lignocellulose substrates. The effect of Tween-80 on hydrolysis of pure cellulose was found to be dependent on the cellulose substrate type and surfactant concentration, which may also help to explain variance in the literature as a function of cellulose pretreatment conditions.

4.6 Figures and Tables

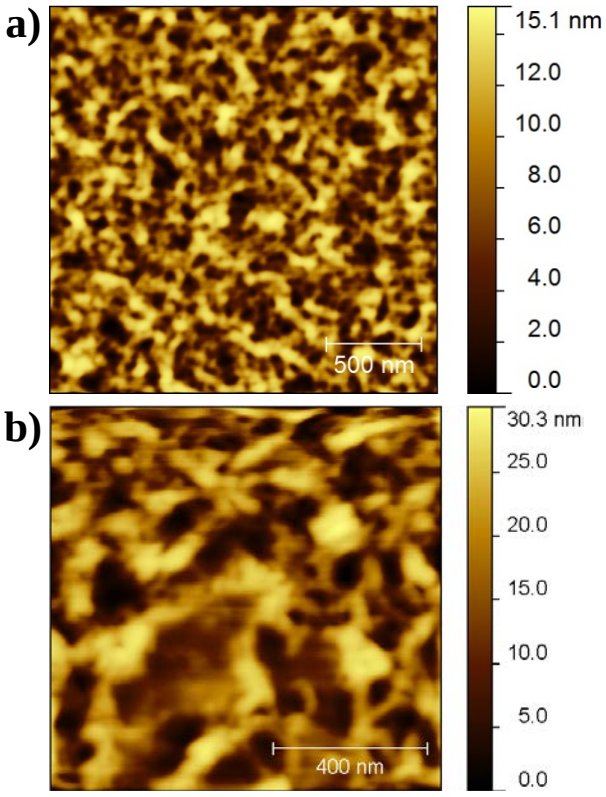

Figure 4.1. Atomic force microscopy topography images of a) LiCl/DMAc and b) NMMO cellulose surfaces

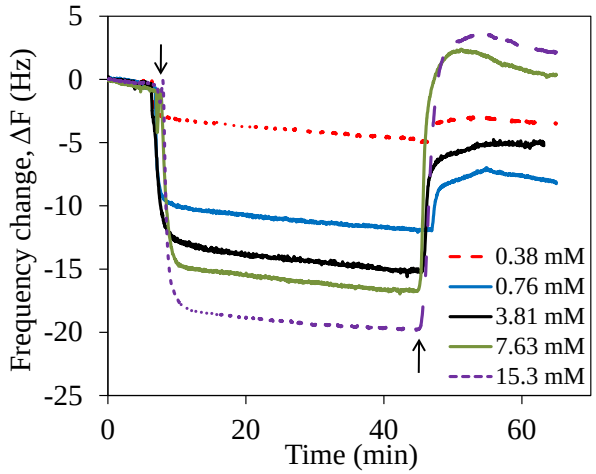

Figure 4.2. Frequency changes of the cellulose coated gold sensor due to adsorption of Tween-80. The arrow to the left indicate the time at which Tween-80 was injected and the arrow to the right indicate the time at which buffer was introduced.

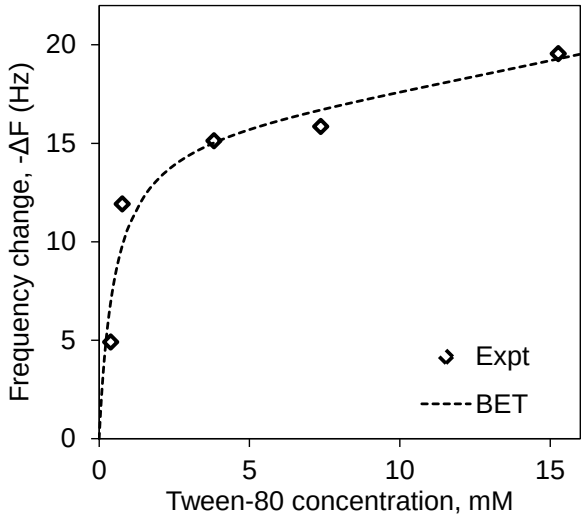

Figure 4.3. Adsorption isotherms of Tween-80 on cellulose surface, Langmuir model equation (dotted line) and BET model equation (solid line)

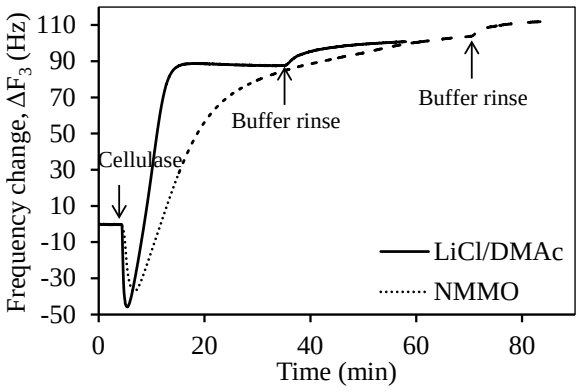

Figure 4.4. Frequency profiles during the enzymatic hydrolysis of cellulose films by a 200x diluted *T. reesei* cellulase cocktail in pH 4.7 acetate buffer (0.1M) on NMMO and LiCl cellulose films

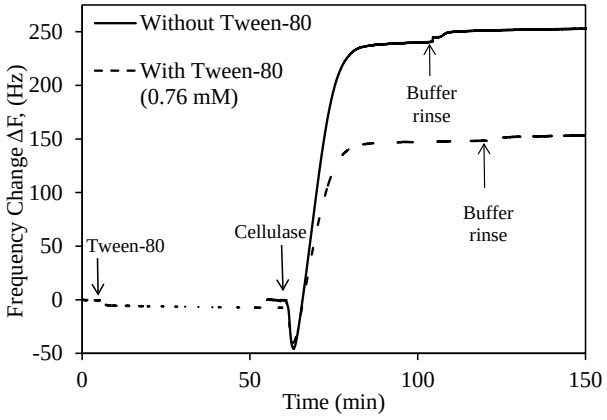

Figure 4.5. Frequency profile of cellulose hydrolysis with Tween-80 adsorption and without Tween-80 adsorption followed by cellulase hydrolysis

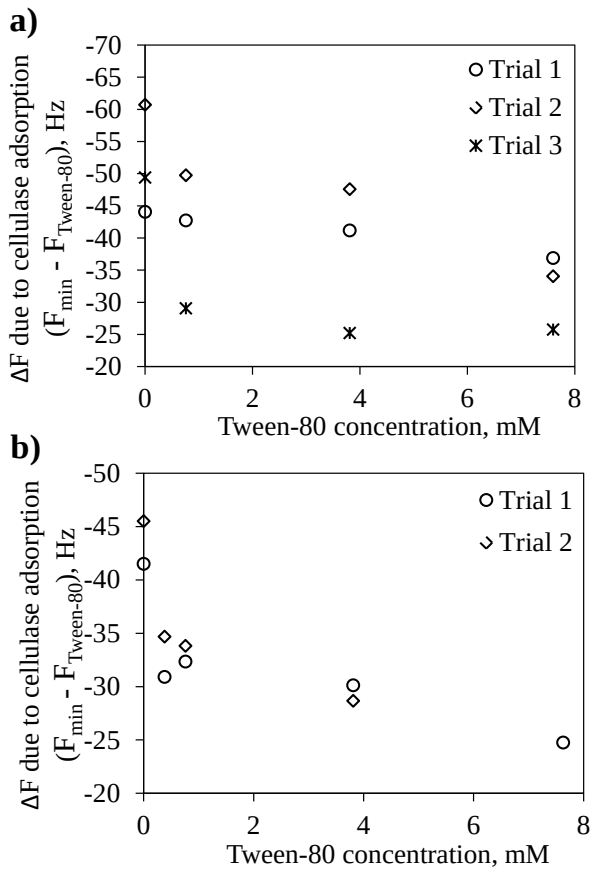

Figure 4.6. Plot of quantified frequency change due to cellulase adsorption with Tween-80 pre-adsorbed on a) NMMO cellulose films and b) LiCl/DMAc cellulose films with varying concentration of Tween-80 (0-8 mM).

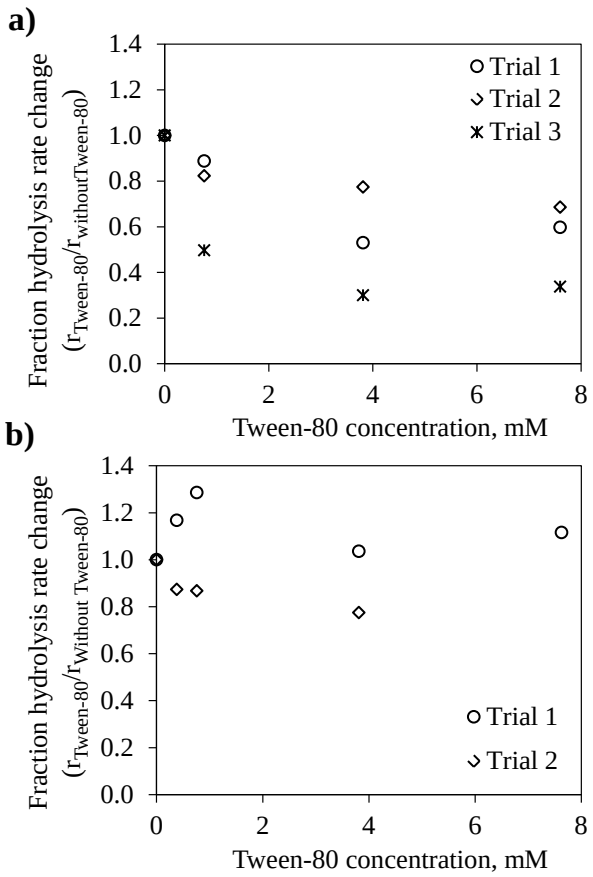

Figure 4.7. Plot of fraction of hydrolysis rate change during sequential adsorption for, a) NMMO cellulose films and b) LiCl/DMAc cellulose films with varying concentration of Tween-80 (0-8 mM).

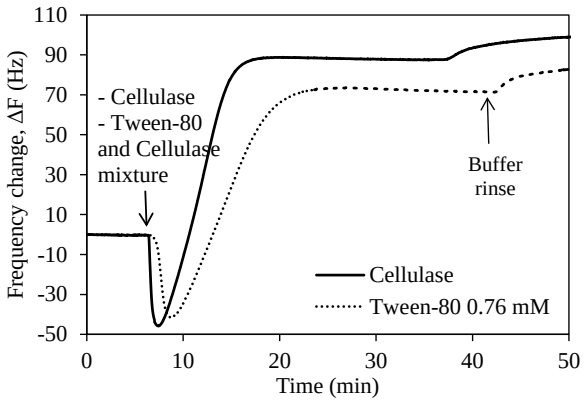

Figure 4.8. Frequency profile of cellulose hydrolysis with co-adsorption of Tween-80 (0.76 mM) and cellulase, and cellulose hydrolysis

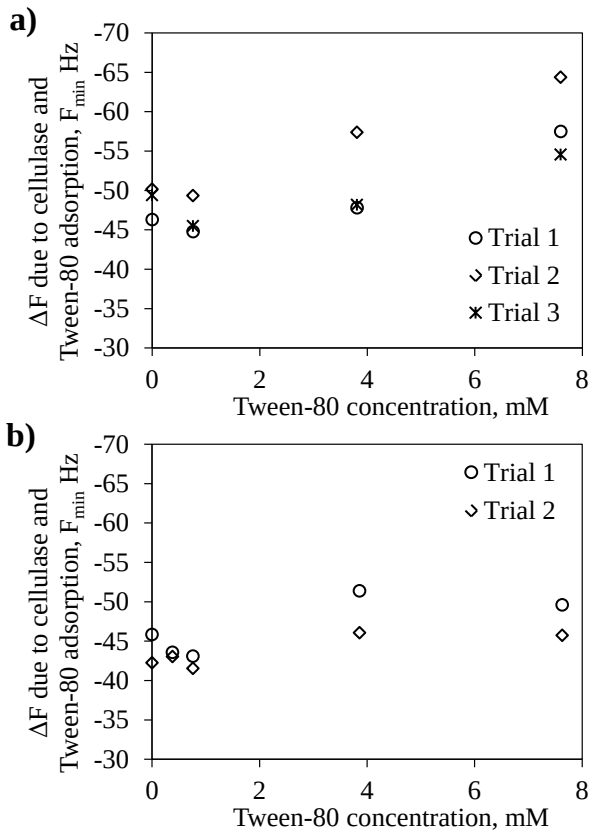

Figure 4.9. Plot of quantified frequency change due to cellulase and Tween-80 co-adsorption on a) NMMO cellulose films and b) LiCl/DMAc cellulose films with varying concentration of Tween-80 (0-8 mM).

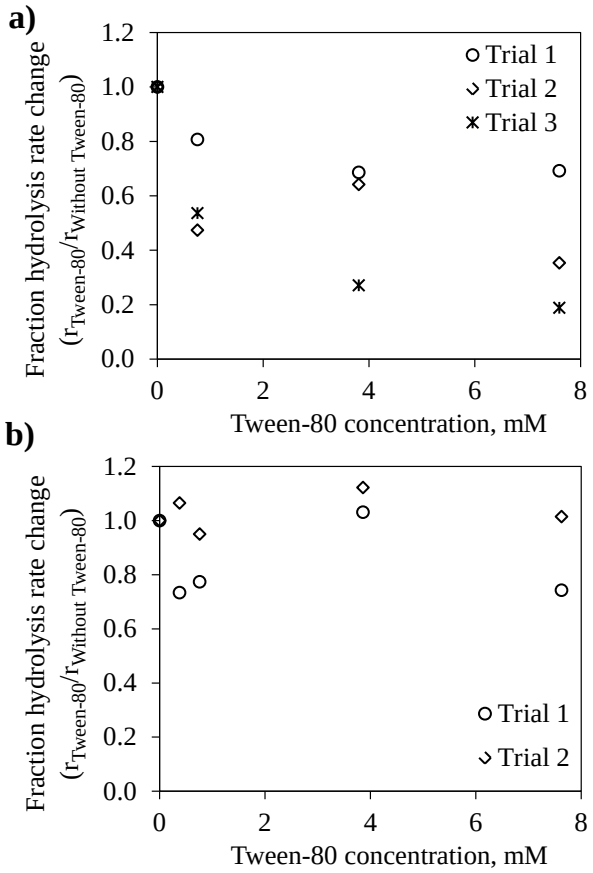

Figure 4.10. Plot of fraction of hydrolysis rate change during co-adsorption for, a) NMMO cellulose films and b) LiCl/DMAc cellulose films with varying concentration of Tween-80 (0-8 mM).

Table 4.1. Variation in F_{min}, maximum hydrolysis rate, F_{max}, cellulose mass coated and extent of reaction values from batch to batch for LiCl/DMAc cellulose films.

Batch	Frequency change cellulase adsorption (Hz)	Maximum hydrolysis rate (Hz/min)	Rate normalized by F_{min} (min^{-1})	Frequency after hydrolysis F_{max} (Hz)	Cellulose Mass coated (Hz)	(F_{max})/Mass (Hz)
1	-46	21	0.45	89	106	0.84
2	-42	13	0.31	201	248	0.81
3	-45	25	0.54	241	166	1.45
4	-36	14	0.38	80	102	0.79

CHAPTER 5

QCM-D STUDY OF THE EFFECTS OF TWEEN-80 ON CELLULASE ENZYME BINDING TO LIGNIN

5.1 Summary

Bulk studies on hydrolysis of cellulosic substrates have suggested that additives such as nonionic surfactants enhance both conversion of sugars and enzyme recovery when lignin is present. However, the specific mechanism underlying the use of surfactants is not well understood. In this study the effect of nonionic surfactant Tween-80 on the interactions of cellulases with model lignin thin films was investigated using a Quartz Crystal Microbalance with Dissipation monitoring. In-situ studies of single-component binding show that cellulase is bound to the lignin surface irreversibly, while Tween-80 is partially reversible upon rinsing with buffer. Co-adsorption of Tween-80 and cellulase resulted in a net reduction in the amount of cellulase adsorbed on lignin – e.g. 43±2% less cellulase bound with a monolayer of Tween-80. Sequential adsorption experiments were carried out by varying the order and concentration of Tween-80 and cellulase introduction to lignin surfaces which suggested that Tween-80 was able to displace adsorbed cellulases.

Keywords: Cellulase, Lignin, Nonproductive binding, Tween-80, Enzymatic hydrolysis

5.2 Introduction

Depolymerization of sugar based components of lignocellulosic biomass into monomeric sugars by pretreatment and enzymatic hydrolysis is a key enabling technology for the production of bioethanol from renewable plant-based resources. However, the recalcitrant nature of cellulose, hemicellulose and lignin in biomass presents a major challenge and hindrance to enzymatic hydrolysis [148]. Lignin is believed to be an obstacle to efficient enzymatic hydrolysis, not only by restricting access of cellulases to cellulose, but also by providing sites for non-specific adsorption of cellulases resulting in reduced efficacy of cellulase enzymes [32, 55, 67]. Therefore, understanding and overcoming the barriers of enzymatic hydrolysis of biomass is essential for development of economically viable cellulosic ethanol processes.

Lignin is the most abundant non-carbohydrate component of biomass. It is a heterogeneous phenolic copolymer, containing mainly aromatic functional groups and is closely associated with cellulose and hemicellulose to form the structural framework of plant cell walls, thus protecting the organism from microbial attack by forming a physical and chemical barrier [204]. The inhibitory effect of lignin on enzymatic hydrolysis has been widely studied [51, 54, 67]. Rahikainen et al. [54] showed that lignin residues isolated by enzymatic and acid hydrolysis from softwood reduce the degree of hydrolysis of Avicel and that hydrolysis yield is inversely proportional to lignin content. Removal of lignin from steam pretreated Douglas fir substrate was shown to improve the enzymatic hydrolysis of cellulose, an effect attributed to improved accessibility of the cellulose to the cellulases [67]. Inhibition of cellulases by two lignin preparations was studied by Berlin et al. [51] who reported 11 - 84% reduction in hydrolysis rate by

dissolved lignin and 8 - 58% reduction in hydrolysis rate by lignin isolated by extensive hydrolysis of biomass (enzyme residual lignin). They suggested that higher surface hydrophobicity due to lower content of carboxyl and aliphatic hydroxyl groups of dissolved lignin was the reason for the range of inhibitory effects observed. Adsorption of cellulases to lignin has also been investigated by several groups; adsorption of cellulase enzymes on two kinds of lignin isolated from lodgepole pine (steam-expolded and ethanol pretreated) was studied by Tu et al. [56] and they reported that cellulase had a higher affinity for ethanol pretreated lignin with higher hydrophobic nature than steam exploded lignin. The adsorption capacities and binding affinities of cellulase have been found to differ widely among various lignins from pretreated materials suggesting that the pretreatment process has a significant effect on cellulase adsorption [205]. Binding of *Trichoderma reesei* cellulase components on lignin using enzymes with and without their carbohydrate binding module (CBM) were investigated [58], and it has been reported that enzymes with a CBM have higher affinities to lignin than enzyems without CBM, suggesting hydrophobic interactions mediated by CBM to be the major driving force for non-productive enzyme adsorption on lignin. In addition to hydrophobic interactions, electrostatic interactions have been suggested to influence enzyme adsorption onto lignin pretreated in the presence of sulfates [206]. Thus, while the negative effects of lignin in reducing the activity of cellulases are not fully understood, it has been suggested in several prior studies that hydrophobic interactions between cellulase and lignin play a important role in reducing cellulase activity by non-prodcutively binding enzymes.

Enhancement of enzymatic hydrolysis of lignocellulose has been shown in the presence of surface-active additives such as non-ionic surfactants [56, 60, 68, 184, 192],

polyethyleneglycol (PEG) [59] and bovine serum albumin (BSA) [64]. A seven-fold increase in hydrolysis of Sigmacell 100 cellulose by Tween-80 addition was reported by Helle et al. [184] who speculated that surfactants enhance enzyme hydrolysis by altering the cellulose structure and facilitating release of bound enzyme. Castanon and Wilke [192] also reported a 14% increase in extent of hydrolysis from newspaper cellulose and also found about three times more recoverable cellulase could be recycled in the presence of Tween-80. The effects of various surfactants on enzymatic hydrolysis of steam pretreated spruce were compared by Eriksson et al. [60] and the results showed that non-ionic surfactants had the greatest positive effect. They proposed that the mechanism of surfactant action is the steric hindrance of enzyme interactions with lignin, thus preventing non-productive binding of cellulase to lignin. This mechanism has been supported by experiments showing enhanced hydrolysis in the presence of PEG [59] and BSA [64]. Furthermore, the adsorption of cellulase to residual lignin has been implicated in low recovery of cellulase following hydrolysis [207]. Recycling of enzymes with addition of surfactants by re-adsorption onto fresh lignocellulosic substrates was investigated by Tu et al. [208]. They found that up to 96% of the total enzyme could be recycled by addition of Tween-80, but the reversibility of cellulase binding is dependent on the lignin content and nature of the substrate. Hence, the strategy of reducing non-productive enzyme binding to lignin by addition of additives not only maximizes hydrolysis, but it is anticipated that this approach would also increase the efficiency of enzyme recycling. However, the above hypothesis is based on adsorption measurements of cellulase to lignocellulose and lignin residues over the period of hydrolysis reaction. A

direct measurement of the binding of cellulase to lignin in the presence of additives would insights into the mechanism and kinetics of enzyme - lignin interactions.

The quartz crystal microbalance with dissipation (QCM-D) technique has been used to study the adsorption of proteins and macromolecules [209], enzymatic degradation of cellulosic [96] and lignocellulosic [97] films. It enables real-time measurements of molecular adsorption and interactions on various surfaces. Previously, lignin thin films developed using methods such Langmuir-Blodgett deposition [210] and spin coating [211, 212] have been used to investigate the molecular interactions at lignin surfaces using QCM-D. Adsorption of different lacasses on cellulose and lignin surfaces was studied by Saarinen et al. [103] and the measurements confirmed that laccases are highly surface specific. The interactions (electrostatic and hydrophobic) between the protein and surface were believed to induce major differences in adsorption depending on the substrate. During adsorption of soy proteins on lignin and hydrophobic self-assembled monolayer (SAM) surfaces, the adsorbed mass was higher when the proteins were in their native state compared to that after chemical denaturation [213]. These results suggest that strong nonspecific interactions between the protein and the substrates exist, favoring conformational changes at the interface that contribute to exposure and rearrangement of hydrophobic and hydrophilic amino acid residues. The effect of lignin chemistry on cellulase adsorption was studied using lignin films prepared from steam pretreated and non-treated spruce and wheat straw lignin preparations using QCM-D [55]. The results showed that *Trichoderma reesei* Cel7A binds more onto lignin isolated from steam pretreated biomass than onto lignin isolated from non-treated lignocellulosic biomass. Recently, Lou *et al.* [214] investigated the effect of anionic surfactant polymers

with different weight fractions and molecular structure on CTec2 cellulase binding to lignin films. They showed that the anionic polymers reduced non-productive cellulase adsorption on lignin, but that the additives also reduced efficiency of enzymatic hydrolysis of cellulose. Because of this, they suggested non-ionic surfactants to be potentially more effective as blocking agents.

In the present work, we investigate the molecular interactions of *T. reesei* cellulase with lignin in the presence of non-ionic surfactant additive Tween-80 using QCM-D, to understand the mechanism of reduction of non-productive cellulase binding. Spin coated Kraft lignin films [211] are employed to directly measure cellulase and Tween-80 binding on lignin, to test the ability of Tween-80 to prevent cellulase binding to lignin, and to quantify the reduction in non-productive binding under different surface exposure scenarios.

5.3 Material and Methods

5.3.1 Materials

Sodium acetate (>99%), acetic acid (>99.7%), aqueous ammonium hydroxide (1 N concentration, <3% w/v), hydrogen peroxide (30%), concentrated ammonium hydroxide (25%) and deionized ultrafiltered (DIUF) water were purchased from Fisher Scientific; Kraft lignin powder, non-ionic surfactant Tween-80 (average molecular weight 1310, viscous liquid) from Sigma Aldrich; and polyethyleneimine (average M_n~1200, 50 wt. % in water) from Acros Organics. Commercial cellulase (Celluclast®) derived from *Trichderma reesei* (> 700 EGU/g) in the form of an aqueous solution purchased Sigma-Aldrich was used as the enzyme source. Gold coated quartz sensors

supplied by Q-Sense AB, Gothenburg, Sweden were used as base supports for lignin thin films.

5.3.2 Lignin films dissolution and deposition procedure

The lignin thin films were obtained by depositing a 1.25 % solution of Kraft lignin in aqueous ammonia onto polymer coated quartz sensors by using a modification of the spin coating technique described by Norgren et al [211]. In short, 50 mg of Kraft lignin powder was dissolved in 4 ml of 1 N aqueous ammonia, by continuous stirring for 24 hours at room temperature to ensure complete dissolution. The sensors were first cleaned by UV ozone plasma treatment for 10 minutes, and then cleaned with a 5:1:1 mixture of water, concentrated ammonia (25%) and hydrogen peroxide (30%) at 75°C for 15 minutes, and finally rinsed with deionized water. The sensors were then dried under a stream of nitrogen and underwent another 10 minutes of UV ozone plasma treatment. This was consistent with the sensor cleaning protocols recommended by the manufacturer, Q-sense. Cleaned quartz sensors were then immersed in a diluted polyethyleneimine (PEI) solution (0.1 g/L in water) for 15 minutes before spin coating, which served as an anchoring layer for lignin deposition [212]. Finally, the lignin solution was spin coated onto the PEI-coated sensors with a WS-400BZ-6NPP/Lite (Laurell Technologies Corporation) spin coater at 2000 rpm for 1 minute.

5.3.3 Characterization

Imaging of the lignin films was performed in air using tapping mode atomic force microscopy (AFM, model 5500 SPM, Agilent Technologies) to determine the surface morphology and roughness. The images were acquired using silicon cantilevers (supplied by Budget Sensors) with drive frequency 300 Hz and tip radius less than 10 nm. Images

were analyzed using Gwyddion software (version 2.20) to measure the roughness. The thickness of the films was measured with a spectroscopic ellipsometer (model M-2000V, J.A. Woollam Co. Inc.) with a spectral range from 370 nm to 1700 nm. The thickness of the films was estimated by fitting the raw data to a Cauchy model using the software provided with the instrument.

5.3.4 Quartz crystal microbalance measurements

The interactions of the cellulase enzyme and the non-ionic surfactant Tween-80 with lignin surfaces was studied using a commercial QCM-D system (model E-4, Q-sense). QCM-D measures simultaneously changes in resonance frequency (Δf) and dissipation (ΔD) at the fundamental resonant frequency (f = 5 MHz) and at overtones of that fundamental frequency. The change in resonance frequency relates to the amount of adsorbed mass according, as a first approximation, to the Sauerbrey relation:

$$\Delta m = \frac{-C\Delta f}{n} \qquad (5.1)$$

In Equation 1, Δm is the adsorbed mass, C is a constant characteristic of the crystal (C = 17.7 ng cm^{-2} Hz^{-1} for the crystals at 5 MHz), Δf is the change in the resonance frequency of the crystal, and n is the overtone number (n = 1, 3, 5...). The experiments were carried out in continuous mode at a flow rate of 0.2 mL/min and at a temperature of 25±0.02 °C. Initially, sodium acetate buffer solution (pH 4.7) flowed through the module into which a lignin coated sensor was mounted to attain equilibrium in the buffer medium. The interpretation of the data is described in detail elsewhere [139, 214]. A frequency drop lower than 2 Hz per hour was used as criteria for equilibrium. Once equilibrium was attained the buffer solution was replaced by enzyme/surfactant solutions and monitored

for changes in frequency (Δf), and energy dissipation (ΔD). Concentrations and order of addition of surfactant and enzyme solutions will be described below.

5.4 Results and Discussion

The lignin thin films deposited onto the quartz sensor by spin-coating were imaged using AFM prior to use in QCM-D measurements. Figure S5.1 (Appendix V) shows a tapping mode AFM topography image of a lignin surface over a 1μm × 1 μm area. The lignin films were found to be continuous with uniformly spaced pores. The films were relatively smooth with an RMS surface roughness of 0.56 ± 0.1 nm measured for 1 μm × 1 μm images. The thickness of the lignin films was determined by ellipsometry to be 32 ± 0.3 nm. The refractive index was found to be in the range of 1.4 - 1.6 for wavelengths in the range of 350 – 800 nm. Kraft lignin films prepared by spin coating on silica substrates have been found to exhibit a wide range of thicknesses from 20 - 140 nm and RMS roughness values between 0.5 – 1.1 nm, depending on the solution concentration and spinning rate [211]. The current thickness and roughness measurements are consistent with the previous lignin films prepared by a similar approach, and were used to study the cellulase/surfactant – lignin interactions without further modification. The stability of the lignin films was investigated by recording the frequency change upon transition from air to buffer in the QCM-D cell and found that the lignin films were firmly attached to the base substrate (Figure S5.2, Appendix V).

The adsorption of cellulase enzymes on the lignin surface was monitored by QCM-D. QCM-D measures simultaneously changes in resonance frequency (Δf) and dissipation (ΔD), which are related to the mass and viscoelastic properties of adsorbed

layer, respectively. The binding of cellulase to lignin film was measured by diluting the cellulase enzyme solution with acetate buffer (pH – 4.7) 200 times, which is equal to a protein concentration of 45 mg/ml determined by Bradford assay. The rapid decrease in frequency upon injection of cellulase (Fig. 5.1) suggests that cellulase enzymes adsorbed onto the lignin surface without significant transport limitations. The frequency drop was accompanied by a dissipation rise due to the soft nature of the hydrated enzyme. The maximum frequency drop was measured to be -45 Hz for the cellulase solution without Tween-80. An adsorption plateau was reached within a few minutes, after which desorption of the enzymes was examined by rising with the cellulase-free acetate buffer. Upon buffer rinsing, only a small increase in frequency was observed, indicating that the adsorption of cellulase enzymes to the lignin surface is almost completely irreversible after ~20 minutes of contact with the lignin surface. This result agrees with previous reports by Hoeger *et al*. [97] and Lou *et al*. [214] who studied cellulase interactions with lignin surfaces and found evidence for limited reversibility of the binding.

The adsorption behavior of Tween-80 alone at the lignin interface is important to measure in order to interpret the effects of the surfactant on enzyme–lignin interactions. Therefore, we investigated the adsorption of various concentrations of Tween-80 onto lignin films, which were freshly prepared for each measurement. Figure 5.2a shows the adsorption and desorption kinetics of Tween-80 at the lignin interface. Tween-80 adsorbed quickly onto the lignin surface, with a slight “overshoot” in frequency change observed for higher concentrations. This overshoot is most likely due to trapping water with the Tween-80 at the lignin surface, which was lost shortly after contact. The extent of adsorption measured by the plateau frequency reached at long times after surfactant

introduction increased with an increase in the concentration of Tween-80 (the changes in frequency due to adsorption were measured to be -13.17, -14.75, -17.05, -20.16 and -37.62 Hz for Tween-80 concentrations of 0.38, 0.76, 3.18, 7.63 and 15.27 mM, respectively). Upon rinsing with buffer, the frequency increased until reaching a final frequency value of -8.04 ± 0.97 Hz for all concentrations of Tween-80, suggesting that the adsorption was mostly reversible, but that some residual Tween-80 remained. The adsorption of non-ionic surfactant was studied previously on cellulose and lignocellulosic substrates and showed Langmuir type adsorption isotherms for Tween-20 suggesting the formation of monolayers [202, 215]. Here, the adsorbed amount was quantified by the measured change in frequency values after reaching a plateau frequency, and the results are plotted in Figure 5.2b. An initial increase in adsorbed amount with increasing bulk concentration is observed, and seems to start to plateau (consistent with a Langmuir-type isotherm) below a Tween-80 concentration of 5 mM. However, increasing the Tween-80 concentration further results in increasing adsorption of Tween-80, which is more consistent with multilayer adsorption. Figure 2b shows the measured frequency change data fit using a liquid phase BET adsorption isotherm in the form given by Equation 2 [200],

$$q = q_m * \frac{K_S C_{eq}}{(1-K_L C_{eq}) * (1-K_L C_{eq}+K_S C_{eq})} \qquad (5.2)$$

where q_m is the monolayer adsorption capacity, K_S is the equilibrium adsorption constant for the first layer, and K_L is the equilibrium constant for the upper adsorption layers. The maximum monolayer adsorption capacity was found to be 14.3 Hz, and adsorption constants were determined to be 33.05 mM^{-1} (K_S) and 0.04 mM^{-1} (K_L). These parameters suggest that even at the lowest concentration studied, the coverage at equilibrium

corresponds to 94% of a monolayer, and that the concentration required to form a monolayer is only 0.84 mM Tween-80. Kirby et al.[216] studied the adsorption of Tween-80 at oil/water interface by surface tension measurements and estimated the surface coverage of Tween-80 to be 1.21 μmol/m^2 corresponding to a minimum area of 137.1 $Å^2$/molecule of Tween-80. In this study, using the monolayer adsorption capacity and Sauerbrey realtion the monolayer surface coverage was estimated to be 253 ng/cm^2 (1.93 μmole/m^2) corresponding to a minimum area of 85.93 $Å^2$ per molecule of Tween-80, suggesting larger adsorption of Tween-80 on lignin surface, either because of more efficient packing at the solid surface, or the slight roughness of the surface (since the sensor area is the relevant quantity in the Sauerbrey equation).

To evaluate the effect of Tween-80 on cellulase binding to lignin, experiments were performed in which Tween-80 was either introduced together with cellulase (co-adsorption) or after cellulase introduction (which may result in the displacement of the adsorbed enzymes). For these experiments the cellulase enzyme concentration was fixed (diluted 200X with acetate buffer) and variable concentrations of Tween-80 (0.76, 3.81, 7.63 and 15.3 mM) were used.

To investigate the ability of Tween-80 to prevent non-productive cellulase binding to lignin and the mechanism of interaction, experiments were first performed by introducing cellulase and Tween-80 together. Figure 5.3 displays the shift in frequency due to adsorption and desorption of cellulase on lignin when introduced together with Tween-80. The frequency change due to coadsorption of both cellulase and Tween-80 was measured based on the final plateau frequency ~20 min after introduction of the mixture in Figure 5.3. As shown in Figure 5.4, Tween-80 initially decreases the

magnitude of the frequency change upon coadsorption, but it increases for higher concentrations compared to single component cellulase adsorption. Reduction in the magnitude of the frequency change upon initial adsorption suggests that Tween-80 reduces the amount of cellulase that can bind to lignin, although adsorption of the surfactant itself increases the observed frequency change for high concentrations of Tween-80. The point at which the balance shifts corresponds to where multilayer adsorption of Tween-80 is observed in the adsorption isotherm (~5 mM Tween-80). If the difference between the frequency change during coadsorption and the frequency change associated with Tween-80 alone is taken as a lower bound on the frequency change due to cellulase adsorption, the lower three Tween-80 amounts all give the same value, -25.6±0.7 Hz. This represents a reduction in bound cellulase of 43±2%. At the highest Tween-80 concentration, the frequency difference is -15.3 Hz, which represents a 66% reduction in bound cellulase, although these are upper bounds and may be smaller if less Tween-80 binds in the presence of cellulase.

The frequency change associated with desorption (upon rinsing with buffer) was also quantified by taking the difference in the frequency after equilibration was reached upon mixing and the frequency at the previous plateau. As also shown in Figure 5.4, the frequency changes observed due to Tween-80 desorption have much smaller magnitudes than those due to adsorption, because adsorption of cellulase is irreversible so only a fraction of the cellulase can be removed. Comparing the frequency changes due to desorption of single component Tween-80 (Figure 5.2a) to that of cellulase and Tween-80 together (Figure 5.3) suggests that Tween-80 dominates the frequency change upon adsorption. For desorption, as the concentration of Tween-80 in the mixture increased,

the amount of cellulase that could be desorbed also increased. Not only does the change in frequency upon buffer rinsing increase with increasing Tween-80, but the general trend observed in Figure 5.3 is that the residual frequency after buffer rinsing (at the end of the experiments) is smaller in magnitude as the Tween-80 concentration used increases. The residual frequency was nearly constant in the experiments with only Tween-80 (at -7 to -9 Hz, Figure 5.2a), which suggests that the differences observed at the end of the co-adsorption experiment in Figure 5.3 are due to differences in adsorbed cellulase. Assuming that this is the case, and that Tween-80 always contributes -8 Hz to the frequency after rinsing, the three lowest Tween-80 concentrations all give similar changes in the amount of residue: 36±3% less residual cellulase after rinsing compared to the case without surfactant. At the highest concentration (15.3 mM Tween-80), the residual cellulase is reduced by 48%. These results are consistent with introducing Tween-80 together with cellulase being an effective way to reduce nonproductive binding, which would potentially enhance saccharification effectiveness in lignin-containing biomass.

In order to explore the ability of Tween-80 to displace the bound cellulase from lignin for recovery, QCM-D experiments were performed similar to those in Figure 5.3, but with introduction of cellulase, followed by a solution of only Tween-80, followed with a final buffer rinse (Figure 5.5). Similar amounts of cellulase adsorbed initially in each case suggest that the lignin films are uniform and comparable in surface characteristics. After reaching a steady state for cellulase adsorption, each cellulase solution was replaced with a Tween-80 solution containing no added cellulase. For the smallest Tween-80 concentration (0.763 mM), the frequency increased when it was

introduced, suggesting net displacement of material (cellulase) from the surface. For larger concentrations (3.82-15.3 mM), an initially a drop in frequency was observed due to the adsorption of Tween-80 on the lignin surface followed by an increase in frequency consistent with removal of adsorbed cellulase. After rinsing with buffer, the final frequency was less than that measured prior to Tween-80 addition and this suggests that the adsorbed cellulase may have been displaced by Tween-80. The frequency change associated with displacement upon rinsing with buffer was quantified (the difference in plateau frequency values after Tween-80 adsorption and after buffer rinsing) and plotted along with the co-adsorption results in Figure 5.5. Despite the difference in order of introduction of components, the frequency change measured for the displacement experiments (Figure 5.5) are roughly the same as for the desorption experiments (Figure 5.3), which suggests that Tween-80 not only prevents cellulase from binding to lignin when introduced at the same time, but also can displace cellulase to allow it to be recovered and reused.

To further elucidate the role of Tween-80 in reducing cellulase adsorption at the lignin interface, the adsorption of cellulase on lignin surfaces pre-contacted with Tween-80 was performed, giving the frequency profiles shown in Figure 5.6. For the lower concentrations of Tween-80 (0.76-7.63 mM), a drop in frequency was observed upon switching from the Tween-80 solution to a solution containing only surfactant-free cellulase. However, for the solution containing 15.3 mM Tween-80, an increase in frequency was observed before a slight decrease. For the lower three concentrations, the trends are consistent with a net addition of mass to the surface upon cellulase introduction, and a net decrease for the highest Tween-80 concentration. Despite

differences in the sign of the frequency change upon switching to cellulase, the absolute value of the frequency after cellulase introduction is approximately the same (-31 to -34 Hz). This can be explained by the desorption measurements for Tween-80 alone, which showed that the same amount of residual surfactant is left on the lignin surface upon buffer rinsing for all concentrations (Figure 5.2a). When cellulase is introduced along with the buffer (Figure 5.6), adsorption of the cellulase onto lignin surfaces with the same amount of residual surfactant (regardless of the concentration initially present), so the same frequency is reached. Note that the frequency at this point is less than the frequency observed upon cellulase adsorption in the absence of Tween-80 (-42 to -45 Hz from Figure 5.1 and 5.5). This indicates a concentration-independent reduction in cellulase adsorption on the lignin surface of 37±2% compared to expected contributions from pure components (-8 Hz from Tween-80 and -44.7 Hz from cellulase) due to the presence of residual Tween-80 at the interface. Moreover, a very small change in frequency after rinsing with buffer following cellulase adsorption suggests that the cellulase is strongly bound to the lignin film despite the presence of the residual Tween-80. The magnitude of the final frequency after buffer rinsing is 36±3% less than that the sum of the residual amounts from adsorption of pure cellulase and Tween-80.

Cellulase enzymes produced from *Trichoderma reesei* have a two-domain structure consisting of a catalytic domain and carbohydrate binding domain attached by a peptide linker. The carbohydrate binding domain targets the enzyme to the cellulose substrate. These binding domains are characterized by hydrophobic amino acids exposed on the surface, which may result in non-productive adsorption to the hydrophobic lignin surface [217]. As non-productive binding of cellulase enzymes to lignin has been

identified as an obstacle restricting hydrolysis, the results observed here supports the hypothesis that irreversible binding of cellulase enzymes to lignin is one source of reduced efficacy of cellulase enzymes. Addition of non-ionic surfactants is known to enhance enzymatic hydrolysis of lignocelluloses [56, 60, 68, 184, 192]. Different mechanisms have been proposed that cause the enhancement effect, including increased enzyme stability, increased accessibility to substrates, and preventing non-productive binding of cellulases to lignin [60, 184]. The mechanism of surfactants in reducing the non-productive binding was explained by the hydrophobic tail of the non-ionic surfactant binding to lignin through hydrophobic interactions and the hydrophilic head group of the surfactant providing a barrier towards binding of the binding domain to lignin [60]. The current study provides direct evidence to support the idea that Tween-80 competes with cellulase for adsorption onto lignin so that cellulase binding is reduced by either co-adsorption or pre-exposing the lignin to a Tween-80 solution. Co-adsorption is most effective with moderate concentrations of Tween-80 but the pre-exposure only depends on the residual Tween-80 left behind, which is independent of surfactant concentration over the range studied – perhaps because strong binding of Tween-80 to lignin gives close to monolayer coverage ($q/q_m > 94\%$) even at the lowest concentrations used.

The interaction of Tween-80 with lignin is also strong enough to partially displace cellulases from the lignin surface upon switching from cellulase to surfactant solution, suggesting that Tween-80 can be utilized for enzyme recovery and recycling. The results indicate that the addition of Tween-80 to a lignocellulosic hydrolysis system at concentrations sufficient for monolayer coverage (0.84 mM) could significantly reduce enzyme adsorption onto lignin by as much as 43±2% and potentially improve the

enzymatic hydrolysis and enzyme recycling. However, it has been reported that the lignin sources were found to affect the enzyme adsorption through differences in their physiochemical properties as a result of different pretreatment methods [56, 218]. The approach used in this study to understand the mechanism that drives the interactions between cellulase enzymes and lignin from different pretreatments will help us design suitable strategies for effective enzymatic hydrolysis and cellulase recovery.

5.5 Conclusions

The effects of Tween-80 on interactions between cellulase and spin coated kraft lignin films were studied using QCM-D. Cellulase adsorbed to lignin almost irreversibly, while Tween-80 adsorbed strongly but more reversibly. Coadsorption of cellulase and Tween-80 reduced the material adsorbed upon adsorption (e.g. 43±2% less cellulase adsorption at monolayer Tween-80 coverage). Tween-80 also reduced bound cellulase by both displacement from lignin and pre-adsorption (36±3% less residue after rinsing in both cases). These results show that competitive reduction of cellulase binding to lignin is a likely mechanism for Tween-80 enhancement of hydrolysis extent and cellulase recovery from biomass.

5.6 Figures and Tables

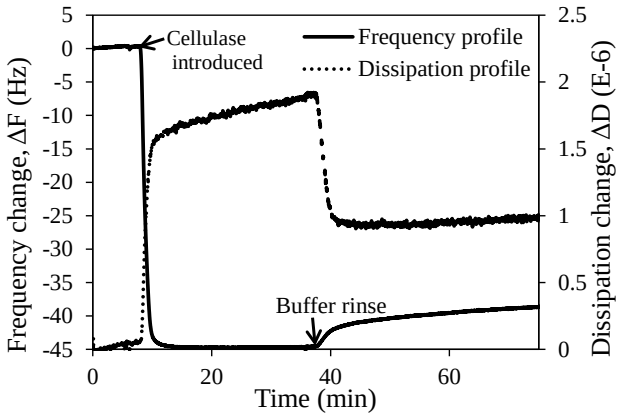

Figure 5.1. Frequency and dissipation shifts of the third overtone of the QCM crystal during cellulase adsorption onto model lignin film, and upon rinsing with buffer.

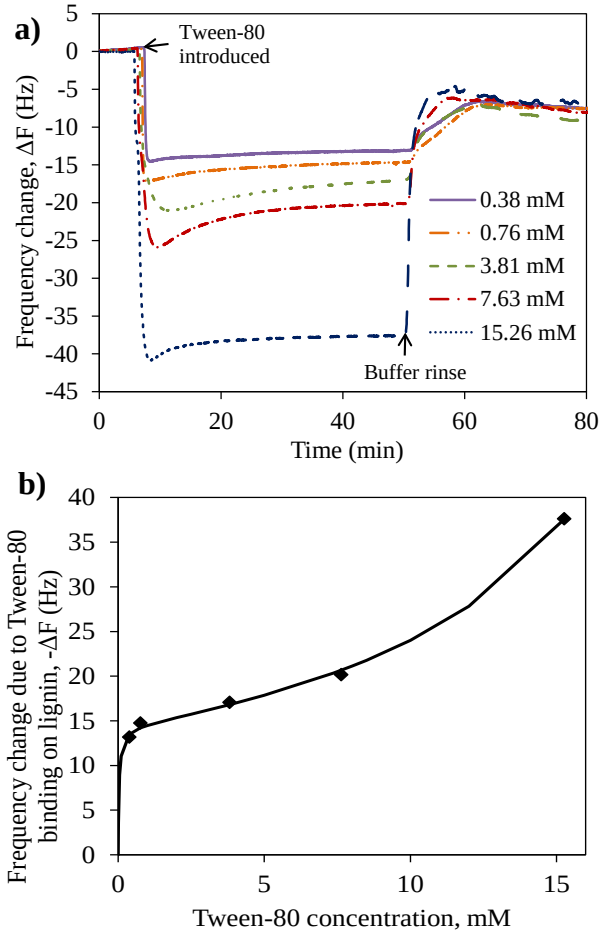

Figure 5.2. (a) Frequency profiles of Tween-80 adsorption onto model lignin films as a function of surfactant concentration and (b) adsorption isotherm of Tween-80 on lignin surface based on the frequency change attained after reaching equilibrium (points). In part (b), the curve is a fit of the BET model equation with a regression coefficient of R^2 = 0.99.

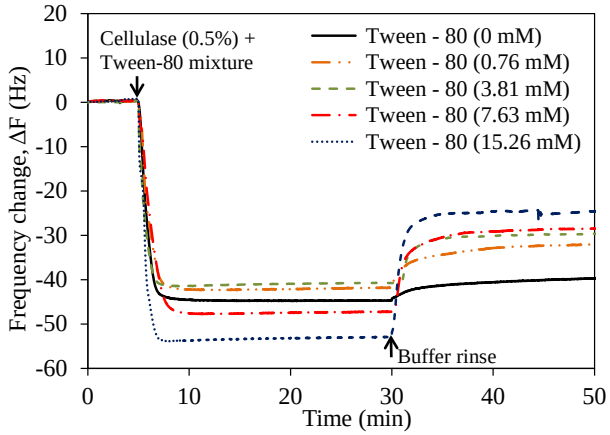

Figure 5.3. Evolution of the frequency shifts measured by QCM-D due to co-adsorption of cellulase and varying concentrations of Tween-80 together onto lignin coated quartz sensors.

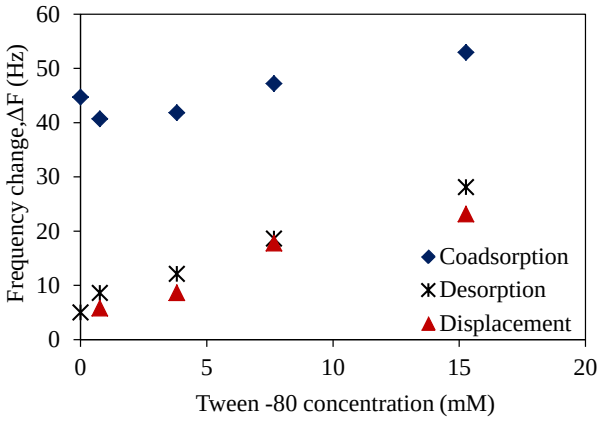

Figure 5.4. Effect of Tween-80 on frequency changes measured between plateaus in the QCM-D measurements on lignin-coated sensors. Magnitudes of frequency changes are reported for co-adsorption of cellulase with Tween-80 (a negative change), desorption into buffer after co-adsorption, and displacement of cellulase by Tween-80 introduced after cellulose binding.

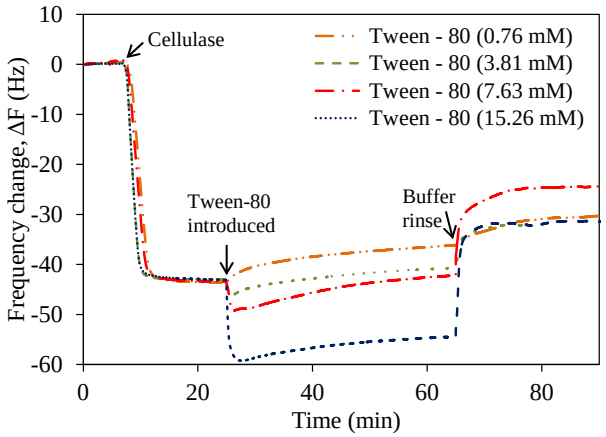

Figure 5.5. Frequency changes measured by QCM-D due to adsorption of cellulase on lignin followed by introduction of Tween-80.

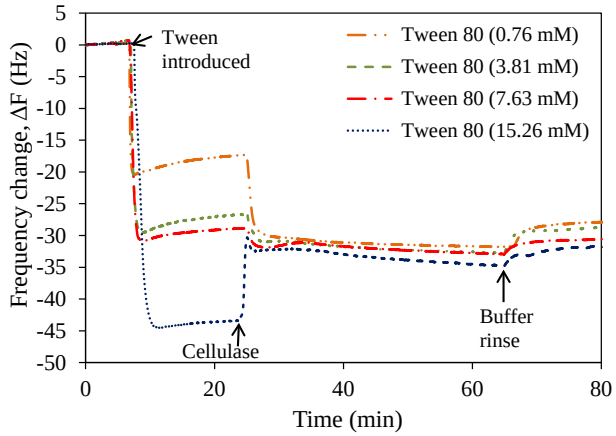

Figure 5.6. Frequency shifts measured by QCM-D due to adsorption of Tween-80 on lignin followed by introduction of cellulase.

CHAPTER 6

QUARTZ CRYSTAL MICROBALANCE KINETICS AND MODELING OF THE EFFECTS OF CELLULASE CONCENTRATION ON HYDROLYSIS OF MODEL CELLULOSE THIN FILMS

6.1 Summary

Cellulose is an insoluble structured material recalcitrant to enzymatic hydrolysis because of its highly self-associated inter-and intra-molecular hydrogen bonding network. The cellulose hydrolysis reaction is heterogeneous in nature (i.e. it occurs between a soluble enzyme and an insoluble substrate) and involves more steps than classical enzyme kinetics. In this work, QCM-D (a surface based assay technique) has been used to study the dynamic interactions between model type II cellulose thin films and cellulase enzymes with the goal of establishing a better understanding of the mechanism of hydrolysis. The adsorption of cellobiose inhibited cellulases from *T. reesei* on cellulose surface was studied. The frequency decrease due to binding was fitted to a Hill's isotherm model. The effect of cellulase concentration on the hydrolysis of cellulose films was then investigated using QCM-D. A kinetic model was developed that predicts adsorption and hydrolysis trends as a function of cellulase concentration and fitted to the QCM-D data. The model provides useful insights into the impact of substrate surface area on the hydrolysis rate. When the generation of new interfacial enzyme accessible cellulose surface from bulk sites during hydrolysis was considered and represented by a term describing rate of exposure in cylindrical cellulose particles, the model achieved

*The QCM-D experiments were performed by Hsin-Fen Li, former graduate student Department of Chemical and Materials Engineering

surface kinetic model, the dynamic behavior of enzyme-substrate complex and change in cellulose concentration during hydrolysis was captured, and the rate constants governing the hydrolysis mechanism were obtained.

6.2 Introduction

Lignocellulosic biomass is considered to be a sustainable non-food feedstock that can be utilized to produce biofuels and commodity chemicals [219]. Production of bioethanol from lignocellulosic biomass is based on using enzymes from organisms capable of digesting biomass to degrade structural polysaccharides into fermentable sugars. The efficient utilization of enzymes to degrade cellulose has been hindered by several factors such as high cost of enzymes, reduction of hydrolysis rates by a variety of factors, and limited understanding of heterogeneous enzyme catalysis [32, 86, 148]. Economically competitive biofuels can be produced by improving the performance of cellulase enzymes through protein engineering and optimizing the physicochemical factors that limit the rate of cellulose hydrolysis [106, 220-223].

Cellulose is an insoluble structured material recalcitrant to enzymatic hydrolysis because of its highly self-associated inter-and intra-molecular hydrogen bonding network. Cellulase enzymes with multiple components and distinct modes of action have evolved to combat this recalcitrance by synergistic action [42, 224-226]. High solids enzymatic hydrolysis is at present considered a technological target for biomass conversion to improve the process economics by increasing product concentration and decreasing capital costs [227, 228]. However, the main drawback in the implementation of this approach is that the cellulose conversion decreases with increasing solids concentration

[229-231]. Enzymatic hydrolysis of cellulose in nature is confronted by a number of obstacles; one of the key challenges is the slow kinetics of hydrolysis, and the subsequent reduction in rate as reaction proceeds. This effect is accentuated in high solids systems. Experimental data on cellulose hydrolysis by cellulases have led to divergent interpretations of the decline in cellulase activity as hydrolysis proceeds including thermal instability of cellulases [232], product inhibition by cellobiose/glucose [73, 233-235], inactivation of the adsorbed enzyme [76, 236, 237], transformation of the substrate into a less digestible form, and nonproductive binding due to the heterogeneous nature of the substrate [32, 238-240].

The cellulose hydrolysis reaction is heterogeneous in nature (i.e. it occurs between a soluble enzyme and an insoluble substrate) and may involve more steps than classical enzyme kinetics. Models based on Michaelis-Menten (MM) kinetics have been used to describe the enzymatic hydrolysis, and display a good ability to fit bulk kinetic measurements under conditions for which they are developed [86]. Bezerra and Dias[241] investigated kinetics of hydrolysis of Avicel by *T. reesei* Cel7A using different enzyme to substrate ratios. It was found that a MM model with competitive inhibition by cellobiose fit the data best. Despite this successful application, strictly speaking the MM model is derived by applying a steady state assumption that does not necessarily hold true for the hydrolysis of heterogeneous lignocellulose substrates. The MM model is also only truly valid if all substrate is fully accessible at all times, which is not necessarily the case during enzyme catalyzed hydrolysis of a solid material [242].

Various mechanistic kinetic models of enzymatic hydrolysis of insoluble cellulose have been proposed based on knowledge of the mechanism of action of cellulase

enzymes [86, 243, 244]. Gan *et al*. [234] proposed a model in which the complex structure of cellulose is divided into hydrolysable and non-hydrolysable regions defined by an inert substrate fraction coefficient. It was found that the inert substrate fraction increased during the course of reaction leading to reduction in hydrolysis rate. Xu and Ding [245] formulated models incorporating fractal and jamming theories to the MM model to describe the interaction between the reactant and catalyst that are different from the homogeneous system, because of the limitations imposed by confining the enzyme to the cellulose surface. The models were applied to bulk kinetics of the hydrolysis of cellulose by cellobiohydrolase and found to capture the hydrolysis profile. However, the models incorporate parameters such as a time-dependent fractal dimension that are not readily interpreted mechanistically or quantitatively predictive of the hydrolysis process. Griggs *et al.* [92] developed a mechanistic model using continuously distributed substrate populations and suggested that the surface availability of cellulose is a key rate determining factor during hydrolysis. Westh and co-workers [246, 247] proposed a model based on the processive kinetics of cellobiohydrolase Cel7A from *Trichoderma reesei* on amorphous cellulose and showed that the slowdown can be explained by the relative rates of the sequential reactions in the hydrolysis process and the occurrence of obstacles for the processive movement along a cellulose strand. This model was not tested widely on different enzymes and substrates. The effect of product inhibition has been studied widely with a focus on determination of inhibition mechanism and inhibition constants [73, 74, 235]. Although bulk kinetic data indicate that product inhibition profoundly decreases the rate of hydrolysis, the actual inhibition mechanism is

a subject of ongoing debate and its magnitude depends strongly on variety of operating conditions (pH, temperature), sources of enzymes and the nature of the substrate.

While the previous models in literature do not give a complete mechanism of cellulose hydrolysis they help in understanding the key factors (substrate and enzyme related) that determine the rate of hydrolysis. Despite ongoing studies of enzymatic hydrolysis of cellulose, the effect of simple process parameters, such as enzyme concentration, on hydrolysis has not been investigated extensively. The effect of enzyme concentration has been studied in bulk experiments by Sattler *et al*. [75] and they reported that the formation of glucose can be described by summation of two parallel pseudo-first order reactions. The cellulose substrate Sigmacell 50 was defined to consist of two cellulose components of easily and difficult hydrolysable cellulose to model the product yield as a function of hydrolysis time and enzyme dosage. The results were evaluated only for substrate concentration less than 2% substrate and the use of this model is limited by the inadequate representations of enzyme-substrate interactions. Most kinetic studies are based on utilizing bulk assays and they do not explain the surface interactions between the cellulase surface and enzymes. Further, the action of the cellulases depends on the availability and accessibility of cellulose substrate to enzymes that differs from the total cellulose in a reaction mixture due to the super-molecular organization of cellulose chains, which needs careful consideration in developing mechanistic models.

In this work, a surface based assay technique has been used to study the dynamic interactions between model cellulose surfaces and enzymes with the goal of establishing a better understanding of the mechanism of hydrolysis. Due to the complexity of the

lignocellulosic substrates and their composition, model cellulose surfaces have been developed for investigation of dynamics of enzymatic hydrolysis and surface activities. The model surfaces offer heterogeneous substrate features that can mimic conditions encountered by enzymes during the hydrolysis of lignocellulosic biomass [97] but are amenable to processing into thin films. Previously, substrates consisting of thin films of pure cellulose have been used to evaluate the dynamics of cellulase activity using ellipsometry [248], quartz crystal microbalance with dissipation (QCM-D) [96, 98, 172], and atomic force microscopy [249]. Of these, QCM-D has been applied most often because it allows one to monitor the in-situ adsorption and hydrolysis during enzymatic reactions on deposited cellulose films by detecting minute changes in mass adsorbed/desorbed to a quartz sensor via changes in the resonance frequency of a quartz crystal. Ahola *et al*. [96] studied the interaction of cellulase enzymes with different cellulose surfaces using QCM-D. They used empirical equations to separately model the binding and enzyme activities on different surfaces and found that the nature of cellulose substrate strongly influence the dynamics of enzymatic degradation. Empirical models are based on data correlation without explicit definitions for enzyme substrate interactions and provide limited mechanistic insight or predictive capability. In contrast, Maurer *et al.* [172] [172] [172] developed a mechanistic two-enzyme surface kinetic model of cellulase activity elucidated using QCM-D including competitive adsorption, irreversible binding, complexation and hydrolytic activity for a binary mixture of cellobiohydrolase I and endoglucanase I, and found surface chain end concentration to be a major predictor of cellobiohydrolase activity. They used a pseudo-steady-state Langmuir-Michaelis-Menten kinetic model to predict the transient trends in the QCM-D

experimental data by determining the kinetic constants from single enzyme experimental data. They also reported that the cellulose films were degrade completely at a constant rate upon exposure to cellulase for 12 -24 hr. However, other QCM-D studies reported multiphasic degradation kinetics of cellulose hydrolysis [96, 98] which are consistent with those observed in the present study.

In the present work, a comprehensive model applicable during both adsorption and hydrolysis is developed that account for the accessibility of cellulose substrate and represents the multiphasic cellulose degradation as a function of bulk cellulase concentration. The model is validated with experimental QCM-D data for cellulases derived from *T.reesei* acting on NMMO (model Type II) cellulose surfaces as a function of cellulase concentration.

6.3 Materials and Methods

6.3.1 Materials. Microcrystalline cellulose (MCC, 20 μm) was purchased from Aldrich. N-methylmorpholine-N-oxide (NMMO, 50% w/w aqueous solution), dimethyl sulfoxide (DMSO, ≥99.8%), and polyethyleneimine (PEI, approx. M.W. 60,000, 50 wt. % aqueous solution branched) were obtained from Acros Organics. Acetate buffer (0.1 M, pH 5) was prepared by diluting glacial acetic acid (Fisher Scientific) in deionized ultrafiltered water (Fisher Scientific). Celluclast® cellulase cocktail (an aqueous mixture consisting of *endo*-glucanases, *exo*-glucanases, cellobiohydrolases, and *β*-glucosidases) from *Trichoderma reesei* 26921 was purchased from Sigma Aldrich and diluted in acetate buffer (0.1 M, pH 5) to the desired final concentration of 0.01, 0.05, 0.1, 0.5, and 1 % v/v. The protein content of cellulase (E_o, 3.4 μM) was determined by the Peterson

method [250] with the protocol provided by Sigma. Based on protein content, the cellulase concentrations correspond to 0.34 µM, 1.7 µM, 3.4 µM, 17 µM and 34 µM respectively.

6.3.2 Preparation of Cellulose Thin Films. Cellulose thin films were prepared based on the method described by Gunnars *et al*. [168]. A solution of microcrystalline cellulose in N-methylmorpholine-N-oxide (NMMO, 50 wt. % aqueous solution in water) was prepared by adding cellulose (2 wt. %) at 115 °C. After a clear solution was obtained, dimethyl sulfoxide (DMSO, ≥99.8%) was slowly added to the mixture to make a final solution of 0.5 wt. % cellulose. The temperature of the cellulose solution was reduced to 70° C, prior to spin coating.

Gold-coated QCM-D resonators (QSX 301, Q-Sense AB, Göteborg, Sweden) were cleaned prior to coating with an ultraviolet cleaner (BioForce, Ames, IA) for 10 minutes to decompose and volatilize organic contaminants on the sensor surface. The UV-treated QCM-D sensors were immersed in diluted (0.2 % v/v) polyethyleneimine (PEI, 50 wt. % aqueous solution) for 15 minutes. PEI was used as an anchoring polymer, as described by Aulin *et al*., [167] to attach the cellulose to the QCM-D sensor. The QCM-D sensors were contacted with de-ionized water for an additional 10 minutes, and then dried using nitrogen gas. Cellulose solution was spin-coated (WS-400BZ-6NPP/Lite, Laurell Technologies) onto the PEI-coated QCM-D sensors at 4500 rpm for 40 sec. After spin-coating, the sensors were immersed in deionized water (30 min), and then dried in an oven (50° C, 30 min). The cellulose-coated sensors were stored in a desiccator at room temperature prior to use.

6.3.3 Cellulose Thin Film Characterization by Spectroscopic Ellipsometry and Atomic Force Microscopy (AFM). The thickness of model cellulose thin film was measured using a variable angle spectroscopic ellipsometer (M-2000, JA Woollam Co., Inc.). The surface topography and material distribution of the cellulose thin film on QCM sensor (QSX301) was characterized by AFM (Series 4500, Agilent Technologies). The support base and the cellulose thin layer coating on the sensor were scanned in air in tapping mode using a silicon cantilever (TAP 300AI-G, Budget Sensors) with a spring constant of 40 N/m and a driving frequency of 300 kHz.

6.3.4 Cellulose Thin Films/ Cellulase Interactions Measured by Quartz Microbalance with Dissipation (QCM-D). A quartz crystal microbalance (Q-Sense model E4) equipped with four temperature controlled flow modules was used to measure changes in mass per unit area and in the viscoelasticity properties of the cellulose thin films from the change in frequency (Δf) and dissipation (D) of the cellulose-coated quartz crystal resonator. The oscillation frequency and dissipation energy were measured simultaneously from the application of an AC voltage across the electrode, causing the piezoelectric quartz crystal vibrate. The resonance frequency change ($\Delta \boldsymbol{f}$) is proportional to the mass absorbed on the crystal surface by the Sauerbrey equation [138]. The QCM-D acquires frequency signal at the fundamental resonance (5 MHz) and at a multiple of resonance (overtone frequency). The third overtone frequency was used to avoid edge effects (unstable frequency signal at the edge of the sensor measured at the fundamental frequency).

The mass change of cellulase thin films in response to cellulase concentration (0.34 µM, 1.7 µM, 3.4 µM, 17 µM and 34 µM) was measured by QCM. Prior to contacting the cellulose thin films with cellulase, the cellulose-coated QCM sensors were

equilibrated with the acetate buffer (0.1 M, pH 5) at a flow rate of 0.2 ml min^{-1} until a constant baseline frequency measurement was reached (< 2 Hz hr^{-1}), which was obtained in approximately 30 min. The temperature of the QCM chamber was controlled at 30 ±0.02 °C. All liquid solutions were degassed for 30 min using an ultra-sonicator (Cole-Parmer 8890, IL) prior to injection into the flow cell. When enzyme solutions (concentration as indicated) were injected (0.2 ml min^{-1}) into the QCM flow module containing the cellulose thin films, both cellulase binding and cellulose hydrolysis were monitored simultaneously. The change in oscillation frequency and dissipation energy was recorded throughout the experiment. When the frequency signal and dissipation had no significant change (< 2 Hz h^{-1}), the injection solution was switched to acetate buffer to rinse and remove any remaining hydrolysate on the sensor surface.

6.3.5 Model fitting and error analysis. To verify the proposed kinetic model (see below), the experimentally measured frequency change was fitted to the modeled frequency by nonlinear regression using the *lsqcurvefit* function in Matlab. The rate parameters in the model k_1, k_{-1}, k_2, n, α_0, S_T, A, and B were estimated as explained in the Results section. The confidence intervals (95%) of the fitted parameters were determined using the *nlparci* function in Matlab and standard errors are reported.

6.4 Kinetic Model

The objective was to develop a kinetic model appropriate to cellulase enzymes on model cellulose thin films measured by QCM-D [96, 172]. The frequency change response by QCM-D is assumed to be proportional to the responses due to the concentration of bound enzyme-substrate complex (ES) and the amount of cellulose

substrate (S) present on the quartz sensor surface. Therefore, the frequency change (Δf) can be represented by Equation (1):

$$\Delta f = \underbrace{-\mathrm{A}[ES]}_{Enzyme\ adsorption} + \underbrace{\mathrm{B}([S_T]_0 - [S_T])}_{Hydrolysis} \qquad (6.1)$$

where, A and B are constants representing the frequency response to enzyme and cellulose units on the surface, respectively; [ES] is the concentration of cellulose-bound enzyme on the sensor; $[S_T]_0$ is the initial total concentration of cellulose on the sensor; and $[S_T]$ is the total concentration on the sensor at a given time. Equation (1) is used to link the experimentally observed frequency changes to the changes in individual species at the sensor surface based on the model discussed below.

In spite of the heterogeneous nature of the enzymatic hydrolysis of cellulose, traditional Michaelis-Menten kinetic schemes coupled with a Langmuir adsorption model (given by Equation 2) are a reasonable starting point and have been used to explain the kinetics of cellulose hydrolysis in bulk systems [251].

$$E + S \underset{k_{-1}}{\overset{k_1}{\longleftrightarrow}} ES \overset{k_2}{\rightarrow} E + P \qquad (6.2)$$

However, for heterogeneous systems the classical chemical kinetics assumption of all substrate being accessible at all times to enzymes is not valid. Most models represent cellulase adsorption onto cellulose using a Langmuir equilibrium equation [252, 253], though the implicit assumptions of uniform binding sites and no interactions between adsorbing molecules are not consistent with experimental observations from the complex interaction between the enzyme and the substrate [244]. Based on the structure of cellulases and binding modes for adsorption, the binding capacity and distribution coefficients were evaluated using the Hill isotherm [254]

$$\Delta f_b = \frac{\Delta f_{max}^{ads} * E_f^n}{\left(K_{ad}^{-1} + E_f^n\right)} \qquad (6.3)$$

where Δf_{max}^{ads} represents the adsorption capacity (in Hz), Δf_b is the frequency change due to bound enzyme (Hz), E_f is the free enzyme concentration (μM), K_{ad} is the apparent association constant and n is a cooperativity parameter.

In the current proposed model, unlike the traditional enzyme kinetic scheme in which the enzyme (*E*) binds to the substrate (*S*) to form a substrate-bound enzyme (*ES*), and the enzyme is recovered after the product (*P*) is formed, the kinetic model is developed based on the processive mechanism of cellulase enzymes. Several cellulase components form a cellulase cocktail which synergistically hydrolyses cellulosic substrates, and the nature of the cellulolytic enzyme system employed determines the mode of action of cellulase, activity of each enzyme component, and synergistic action among the enzyme components [173]. As it is difficult to distinguish the function of each component by QCM, the cellulase system is assumed to have a single combined activity in the hydrolysis of cellulose and is represented as a single enzyme (E). Because 80% of the cellulase consistent of processive enzymes, the model is developed based on current theoretical understanding of processive cellulase action: first, the enzyme (*E*) binds to the unoccupied cellulose substrate (*S*) to form a productive enzyme substrate complex *(ES)*, where the enzyme is threaded with the cellulose chain and completes catalytic cycles releasing the product (*P*) until eventually the complex dissociates. The binding scheme may be reversible for the formation and dissociation of complex *ES*.

An important distinction of the model proposed here is that rather than assuming that the substrate is easily accessible and that all sites are always available for binding and reaction, the cellulose substrate is considered to consist of interior and exterior

accessible surfaces with only a portion of cellulose substrate being accessible to enzymes at a given time and gradually exposed as hydrolysis proceeds. The interfacial surface sites concentration is given by S_i. The surface concentration of cellulose is modeled to change with time as the hydrolysis progresses. As layers of substrate are solubilized, the reaction interface moves towards the inside of the substrate, new surface is exposed, and the total substrate concentration is reduced. Translation of this reaction scheme is presented in equations 6.4, 6.5 and 6.6 and the instantaneous concentration of available substrate (*S*) for enzyme binding is given by substrate balance at the interface in equation 6.7.

$$E + S \underset{k_{-1}}{\overset{k_1}{\longleftrightarrow}} ES \qquad (6.4)$$

$$ES \overset{k_2}{\rightarrow} ES + P - S_i \qquad (6.5)$$

$$S_{bulk} \rightarrow S_i \qquad (6.6)$$

$$[S_i] = [\mathrm{S}] + [ES] \qquad (6.7)$$

This reaction scheme leads to differential equations for enzyme-bound and total interfacial sites (equations 6.8 and 6.9) where enzyme adsorption on the cellulose surface is described by a reaction with apparent order *n*.

$$\frac{\mathrm{d[ES]}}{\mathrm{dt}} = \mathrm{k_1[E]}^n\mathrm{[S]} - \mathrm{k_{-1}[ES]} \qquad (6.8)$$

$$\frac{\mathrm{d}[S_i]}{\mathrm{dt}} = -\mathrm{k_2} * [ES] + \text{rate of exposure} \qquad (6.9)$$

Assuming that the cellulose fibers are cylindrical in shape, the rate of exposure of the new surface accessible sites from bulk is given by equation 6.10 (for the derivation see Appendix I)

$$rate\ of\ \ exposure = \mathrm{k_2} * \left(1 - \frac{[S_i]}{[S_T]}\right)^{1/2} * [ES] \qquad (6.10)$$

As the total cellulose substrate is considered to consist of interfacial and bulk sites (*i.e.*, $S_T = S_i + S_b$), the initial proportion of interfacial substrate to the total substrate concentration, $\alpha_{0,}$ is defined by equation 6.11 and the conversion of the total substrate at any time 't' is given by equation 6.12.

$$\alpha_0 = \left[\frac{S_{i,0}}{S_{T,0}}\right] \qquad (6.11)$$

$$X_T = \frac{[(S_{T,0})-(S_T)]}{[S_{T,0}]} \qquad (6.12)$$

6.5 Results and Discussion

The as-prepared cellulose films were characterized using ellipsometry to determine their thickness. They exhibited a thickness of 51±1 nm and refractive index varying from 1.45 to 1.6 over a wavelength range of 370 – 1000 nm. An AFM image of the spin coated cellulose film deposited is displayed in Figure 6.1. The films consisted of aggregates of cellulose fibrils deposited on the flat sensor surface. The rms surface roughness of the films was estimated from the AFM image to be about 7.7 ± 0.5 nm. The cellulose films were found to be non-uniform and the sizes of the cellulose domains suggest that they are agglomerates of cellulose fibrils and not individual fibrils. Incomplete coverage of the surface by cellulose is most likely due to the low concentration of the cellulose solutions (0.5 wt% cellulose) from which the films are deposited. Cellulose thin films deposited using a similar procedure were reported to have an average roughness of 5 nm and thickness in the range of 20-270 nm controlled by changing the concentration of cellulose solution, [168] which is consistent with the results obtained in this study.

QCM-D measurements were performed to study the hydrolysis of the model cellulose surfaces by a commonly used enzyme cocktail derived from *Trichoderma reesei*. After equilibrating the sensor in the chamber with flowing acetate buffer (pH 5) at 30 °C, the change in frequency with time was measured when a cellulase solution (1.7 µM concentration, diluted in 0.1 M acetate buffer, pH 5) was introduced into the QCM-D chamber. Figure 6.2 shows the frequency profile for this representative case that reflects changes due to enzyme adsorption onto the cellulose surface followed by the hydrolysis of the cellulose thin film. Initially, a decrease in frequency (increase in mass) was observed as the cellulases adsorbed to and complexed with the cellulose surface followed by an increase in frequency (decrease in mass) indicating hydrolysis of the substrate. Enzyme adsorption and hydrolysis occurs simultaneously, and the change in the frequency curve after reaching a minimum (ΔF = -23 Hz) indicates that point at which the rate of adsorption on the cellulose surface was surpassed by the rate of mass change due to the hydrolytic reaction. As hydrolysis proceeded, the slope of the frequency curve slowly decreased, and eventually flattened, suggesting that the thin film surface remains unchanged due to substrate depletion. Similar qualitative results were presented by Turon *et al*.[98].

To determine the maximum cellulase adsorption capacity on the model cellulose surface, adsorption of inactivated cellulases on cellulose was studied using QCM-D. Figure 6.3a displays the frequency response during adsorption of cellulase under inhibition by 5 g/L cellobiose at cellulase concentrations of 0.34 µM to 34 µM in acetate buffer. The kinetics of the inactive cellulase adsorption was found to be very similar for all cellulase concentrations studied and attained equilibrium within 60 min. Upon

introduction of the inactive cellulase onto cellulose surface a fast initial frequency drop followed by a slow change was observed. This pattern suggests initial direct binding of enzymes to the cellulose surface followed by additional binding (frequency decrease) due to multilayer adsorption or clustering of cellulases on the cellulose surface. The disspation (ΔD) vs. time plot (Figure 6.3b), showed a sharp increase in energy dissipation during the initial cellulase binding that ended with a plateau. Subsequently, an inflection was observed associated with an accelerated increase in ΔD, indicating structural changes on the cellulose surface due to cellulose clustering.

The dissipation value is roughly related to the viscosity of the adsorbed layer and is caused by a combination of protein adsorption and hydration of the cellulose thin film. The hydrolysis rate depends on the concentration of enzyme substrate complex formed by direct binding of cellulase; therefore the amount of enzyme adsorbed was quantified using the frequency change during the initial adsorption phase. The change in frequency profile before the acceleration in dissipation increase and deceleration in frequency change due to the effects of clustering and hydration was used as a criterion to determine the initial adsorption phase. The time frame with this initial stage (~15-30 min) is also more consistent with the time scale for the adsorption stage of the experiments with active cellulase than the complete timescale required for clustered cellulase binding in Figure 6.3b. The magnitude of frequency was measured at the end of this stage to quantify the enzyme binding. Hill's equation was fit to the data to obtain the cooperativity parameter and maximum cellulase adsorption capacity on the cellulose surface. Figure 6.4 shows cellulase adsorption as a function of cellulase concentration in solution. The dotted line shows the fit using Hill's model (R^2 = 0.97) and the maximum

adsorption capacity Δf_{max}^{ads} was determined to be 64.5 Hz. The cooperativity parameter *n* providing the best fit to the data was determined to be 0.49, indicating negative cooperativity on binding which suggests the occurrence of steric hindrance effects among the cellulases on cellulose surfaces. Negative cooperativity in enzyme binding was also reported for adsorption studies of CBH I and CBH II and cellulose binding domains from *Trichoderma reesei* on cellulose [254, 255].

Figure 6.5 shows the frequency response measured using QCM-D on cellulose surfaces with variable cellulase concentrations of 0.34 μM to 34 μM. Quantitatively, a larger reduction in the initial frequency drop (ΔF = -20 to -35 Hz) was observed with increasing cellulase concentration suggesting adsorption of more cellulase on surfaces with comparable site concentrations. After the minimum value was reached the frequency started to increase at a steady rate after a short ramp up period and the slope of the linear region yielded the initial hydrolysis rate (illustrated by the dashed line in Figure 6.2). From Figure 6.5, the least amount of enzyme adsorption and the lowest hydrolysis rate occurred at the lowest enzyme concentration of 0.34 μM. However, with increasing enzyme concentration more complex effects on the QCM-D frequency response were observed with respect to hydrolysis and extent of reaction (corresponding to the maximum in the frequency response).

Figure 6.6 displays the measured initial hydrolysis rate as a function of cellulase concentration. The hydrolysis rate increases with the cellulase concentration until a plateau is reached at 3.4 μM cellulase. These QCM-D results are in good agreement with the findings of cellulase adsorption and degradation of cellulose films reported previously

by Maurer *et al*. [248] and Eriksson *et al*. [99] , where the hydrolysis rates showed a strong dependence on the cellulase concentration at low to intermediate concentrations, but displayed a tendency to level off at higher cellulase concentrations. This suggests that at high cellulase concentrations the enzyme loaded onto the surface fully cover the available adsorption sites and the apparent hydrolysis rate reaches a maximum level. However, the observed frequency response trends reflect a combination of enzyme adsorption and hydrolysis events, and the overall conversion is strongly influenced by the cellulase and substrate concentrations. Therefore, the data was fit to the kinetic model developed to interpret the raw QCM-D data.

The effect of cellulase concentration on the hydrolysis of cellulose was initially modeled using Michaelis-Menten kinetics as represented by equation 6.2, assuming all the substrate is fully accessible for binding and hydrolysis, and enzyme is released after hydrolysis. The kinetic model was fit to 90% of the extent of reaction (estimated from the maximum in frequency measured) to avoid a large effect on fitting due to the flat frequency profile at the end of each measurement. The model parameters were determined by fitting the experimental frequency response data. From the preliminary evaluation it was found that MM kinetic model showed deviations between the model prediction and experimental frequency, and also coupling between the model parameters was observed resulting in large uncertainties (fitting plots and fitted model parameters are shown in Figure S6.1 and Table S 6.1 (Appendix VI). The best-fit MM kinetic model frequency profiles showed a linear increase in frequency suggesting a constant degradation rate of cellulose at the lower enzyme concentrations, and low conversions of cellulose were predicted over the course of the experiments.

The amount of surface bound cellulases has been shown to be directly correlated to cellulose hydrolysis [79, 256], but the role of cellulose structure on cellulase activity is not clear. Therefore, a model based on the processive cellulase kinetics and the role of cellulose structure on the relationship between cellulase binding and activity detailed in the Model Development section was fitted to explain the results obtained in Figure 6.5, and to determine the model parameters for cellulose hydrolysis. In order to capture and understand the qualitative characteristics of cellulase binding, the parameters that affect binding were evaluated independently of cellulose degradation. To capture the adsorption kinetics accurately at various cellulase concentrations, the frequency response data during the initial adsorption and hydrolysis period were analyzed to obtain the adsorption/desorption rate constants (k_1 and k_{-1}). Thus, only data at short exposure times (t < 10 min) during which cellulase adsorption and initial degradation occur (the linear initial region of QCM response) were used to determine the sorption kinetics from the experiments without inhibitor. It should be noted that while some enzymatic hydrolysis may occur during the initial adsorption period, the adsorption rate is much greater than the hydrolysis rate. It was assumed that the surface concentration of available cellulose binding sites was constant during short exposure times, and the value of the parameter *A* associated with the frequency change due to enzyme adsorption was fixed to the maximum adsorption capacity obtained from the adsorption isotherm of inhibited enzyme (64.45 Hz). The order of the reaction (*n*) with respect to enzyme concentration was fitted, as opposed to first order assumed in MM kinetics. From the fit of the initial kinetic data the adsorption rate parameters were determined to be $k_1 = 2.88 \pm 0.03$ (mM^{-n} min^{-1}), $k_{-1} = 0.88 \pm 0.01$(min^{-1}) and $n = 0.22$ (Fitting of the initial hydrolysis data shown in Figure

S6.2 (Appendix VI)). The value of *n* from this kinetic analysis (0.22) was observed to be less than the value of *n* obtained from the adsorption isotherm (0.49). A comparison of adsorption isotherm with parameters obtained from initial adsorption kinetics, Hill's isotherm fit and experimental data for inhibited enzyme are shown in Figure S6.3 (Appendix VI). It was observed that the predicted results from the initial adsorption kinetics do not match the adsorption model that was fitted independent of the kinetic experiments. The differences in the adsorption isotherm fittings may be due to the differences in the binding characteristics of the active and inactive enzymes.

Using the initial adsorption kinetic rate parameters (k_1, k_{-1}, and A) the complete frequency response data was fitted to determine the hydrolysis rate constant (k_2) and the other model parameters (B, S_{T0} and α_0). In this study, the amount of cellulose coated on the sensor surface (S_{T0}) was an unknown quantity and was estimated as a fitted parameter in the model, but was assumed to be constant for all the films. The cellulose substrates are typically deposited in the form of fibrils having both interior and exterior accessible surfaces with only a portion of cellulose substrate being accessible to enzymes at a given time and thus resulting in exposure of interior surface as the hydrolysis proceeds. In the proposed model it is considered that the cellulose substrate consists of interfacial surface and bulk sites, and the fraction of total binding sites accessible initially (α_0) was allowed to vary for each experiment as a fitting parameter. It is assumed that the cellulose fibrils cylindrical in structure and bulk sites are gradually exposed as hydrolysis proceeds. The frequency response data for five different cellulase concentrations was fitted to the proposed model equations (6.1, 6.8-6.11) and the parameters were obtained.

Figure 6.7 shows the fitting the surface kinetic model to the experimental frequency response. The proposed model shows excellent agreement with the experimental data for both adsorption and hydrolysis with varying cellulase concentrations. The estimated model parameters are summarized in Table 6.1. The total initial substrate concentration was found to be 2.81 and the values of α_0 varied between 0.33 and 0.39 which indicate the initial accessible surface site concentration. Variation in the value of α_0 reflects random variation in initial accessibility of cellulose in different coatings. The hydrolysis rate constant (k_2) was determined to be 0.219 ± 0.001 min^{-1}. Luterbacher *et al.* [257] developed a kinetic model based on the fluorescence intensity signal to model the depolymerization of bacterial microcrystalline cellulose immobilized on a glass surface using the β-glucosidase supplemented cellulase cocktail from *T. reesei*. Three models based on irreversible, reversible and instantaneous binding gave hydrolysis rate constant of k_2 = 0.068 ± 0.019 min^{-1}. Maurer *et al*. [248] developed a modified Langmuir-Michaelis-Menten model based on a pseudo steady state approximation for cellulose hydrolysis and found the hydrolysis rate coefficient to be 0.57 ± 0.08 s^{-1}. Comparing the results of the rate parameters obtained in this work to those in literature is difficult since cellulose enzyme behavior is expected to be specific to the type of substrate, cellulose preparation or pretreatment, and modeling approach used. However, the proposed model gives reasonable agreement in order of magnitude with prior kinetic studies and provides insights into the nature of enzyme substrate interactions and substrate changes occurring during the hydrolysis reaction. Earlier kinetic models in literature reported capture the progression of enzymatic hydrolysis of cellulose in the initial stages of hydrolysis, but fail to model later stages of the hydrolysis process. The modeling approach presented in this work extended the hydrolysis model to capture the kinetics to a near completion state and account for substrate morphology heterogeneity.Figure 6.8 shows the change in concentrations of *ES*, S_i and S_T determined from the rate equations with respect to time predicted with the optimal coefficients in Table 6.1. The

ES complex concentration initially increased due to binding of cellulase enzymes onto the cellulose surface and then decreased continuously as substrate availability decreased due to hydrolysis. It can also be seen that the magnitude of the concentration of ES complex formed increased with increase in cellulase concentration. The frequency profiles show a slow-down in the hydrolysis rates. The decline in hydrolysis rate has been observed in bulk studies and has been attributed to loss of enzyme activity due to inactivation or due to inhibition by hydrolysis products (cellobiose/glucose) [237, 244]. In the current model neither inactivation nor inhibition is modeled, but the model fits the experimentally measured frequency profile. Thus, the slow-down in hydrolysis may be expected as a result of factors such as declining in substrate reactivity caused by substrate heterogeneity or a decline in the surface area available for hydrolysis.

To explain the changes occurring in substrate concentrations, conversion defined based on the substrate depletion (equation 6.12) was plotted as a function of time in Figure 6.9 for the cellulase concentrations studied. The conversion of cellulose was found to increase with cellulase concentration but decreasing benefits from increasing the cellulase concentration were found, suggesting an optimum exists (17 μM) for making effective use of added cellulase. The conversion rate was initially fast and showed a slow down at longer duration due to substrate depletion. It was also observed that initially the conversion of substrate starts off at the same rate for all cellulase concentrations and as hydrolysis proceeds the conversion rate increased for high cellulase concentration before slowing down due to substrate depletion was seen. However, the level of details needed to explain such trends in conversion are not clear from the data but based on the mode of action of cellulase enzymes on cellulose surface it can be speculated that the slower conversion at low cellulase concentration might be limited by substrate availability to the enzymes.

The proposed model is considered not fully comprehensive in respect to lacking consideration of the synergistic actions of single enzyme components. Attempting to develop such a model was not justified by the level of information available with QCM-D data using a cellulase cocktail, although the cocktail is highly relevant to the practice of enzymatic hydrolysis and typical of what has been used for bulk experiments. Capturing this synergy with a more elaborate kinetic model would require a large set of kinetic experiments with purified cellulase enzymes and mixtures of cellulase enzymes. Nonetheless, the model developed in this work has been used successfully to fit the kinetics of cellulose degradation by considering the gradual generation of enzyme-accessible cellulose by cellulase action on a cylindrical particle comprised of cellulose chains. The model predicts that hydrolysis kinetics is strongly dependent on the initial substrate accessibility. This demonstrates that kinetic models constructed on the basis of QCM-D measurements can be useful in guiding the development of cellulase cocktails by improving our understanding of the key mechanisms and rate limiting steps that occur during cellulose degradation. An improved understanding of the cellulose degradation process can be achieved by incorporating solution kinetics, product inhibition and cooperative enzyme hydrolysis.

6.6 Conclusions

Model cellulose films were produced by spin coating using NMMO as solvent, and consistent with prior studies were found to partially cover gold QCM sensor surfaces with agglomerates of cellulose particles [168]. These films appeared to be composed of cellulose fibrils and were used to investigate the adsorption of cellulases and enzymatic

degradation of cellulose. The binding of cellobiose-inactivated cellulases on cellulose followed Hill's adsorption isotherm. Negative cooperativity (n = 0.49) on cellulase binding was determined suggesting steric hindrance effects among the cellulases on cellulose surface. The hydrolysis rate measured from the slope of the experimental QCM-D frequency curves showed strong dependence on the enzyme concentration with hydrolysis rate reaching a maximum at higher enzyme concentrations. Fitting a simple Langmuir-Michaelis-Menten kinetic model based on the assumption that all the substrate was accessible and that the enzyme was released after product formation was not successful due to both poor fitting and large uncertainties in the model parameters. Therefore, a surface based kinetic model for hydrolysis of cellulose was developed describing the adsorption, desorption and processive action of cellulases. When the generation of new interfacial enzyme-accessible cellulose surface sites from bulk sites during hydrolysis was considered and represented by a rate of exposure term in the kinetic model, the model achieved good agreement with the experimental data for all cellulase concentrations. Using the surface kinetic model, the dynamic behavior of enzyme-substrate complexes and the change in cellulose concentration during hydrolysis was captured using a first-order hydrolysis rate constant of $k_2 = 0.219 \pm 0.001$ min^{-1}. The order of magnitude of this coefficient agrees with prior bulk and QCM-D studies, but this kinetic model shows the importance of capturing the exposure of new accessible cellulose due to hydrolysis activity over the course of a saccharification experiment. The conversion of cellulose at a given time after enzyme introduction was found to increase with cellulase concentration but the increase in conversion was not proportional to the cellulase concentration suggesting an optimum exists for most effective utilization of

cellulase (17 μM) in this study. The current model provides a framework for further developments to investigate and elucidate the details of cellulase-cellulose interactions including synergistic action of single enzymes, product inhibition and structural heterogeneities within the substrate that play a significant role on the hydrolysis rate.

6.7 Figures and Tables

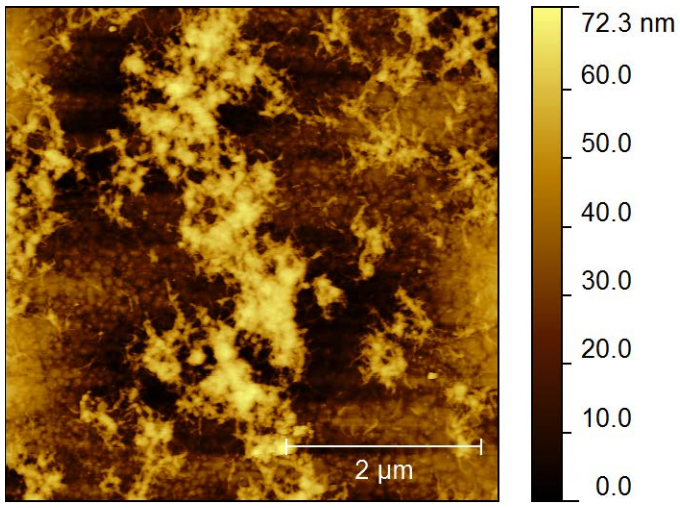

Figure 6.1 Tapping mode atomic force microscopy topography image of a representative cellulose film on the gold surface of a QCM sensor

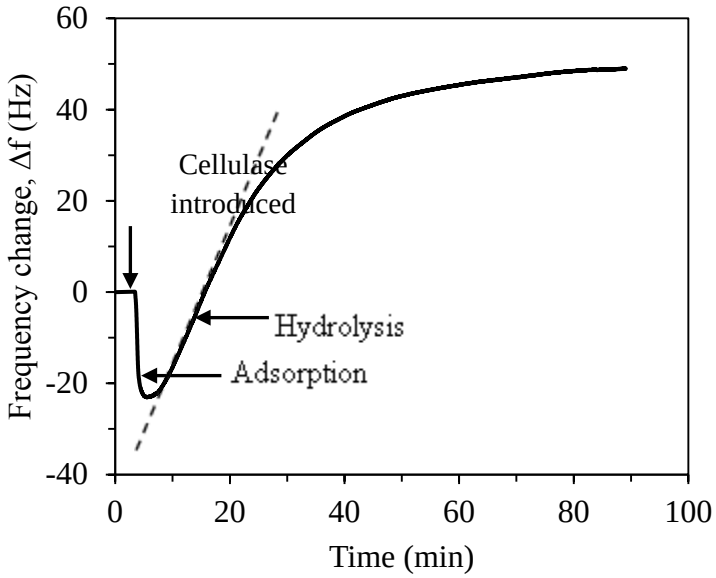

Figure 6.2 Representative QCM-D frequency profile during cellulose hydrolysis with a 1.7 µM cellulase solution at pH 5 and 30 °C. The dashes line illustrates the determination of initial hydrolysis rate as the maximum in the frequency change after the minimum in frequency is observed.

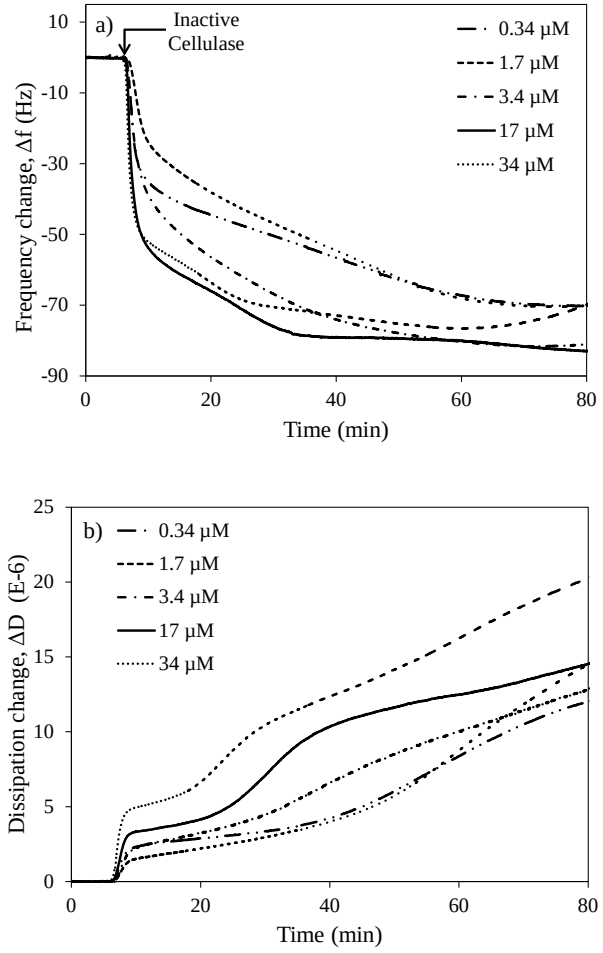

Figure 6.3 (a) Frequency profiles and (b) dissipation profiles during the binding of inactivated cellulase onto cellulose films at 25 °C measured by QCM-D. Hydrolysis activity was completely inhibited in all solutions by addition of 5 g/L of cellobiose.

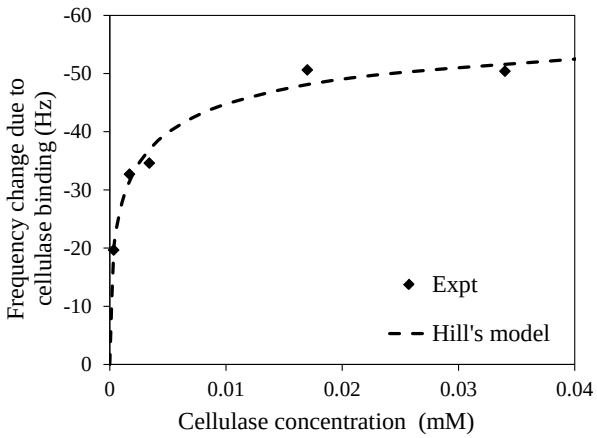

Figure 6.4 Adsorption isotherm of inactivated *T. reesei* cellulases on model cellulose surfaces at 25 °C. along with fitting of Hill's adsorption model (dashed curve) to the experimental data (♦).

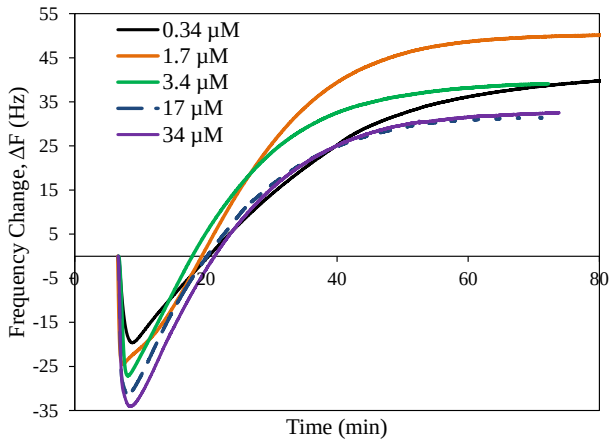

Figure 6.5 QCM-D frequency profile during cellulose film hydrolysis at indicated cellulase concentrations from 0.34 µM to 34 µM. The results for the third overtone are shown for experiments performed at pH 5 and 30 °C.

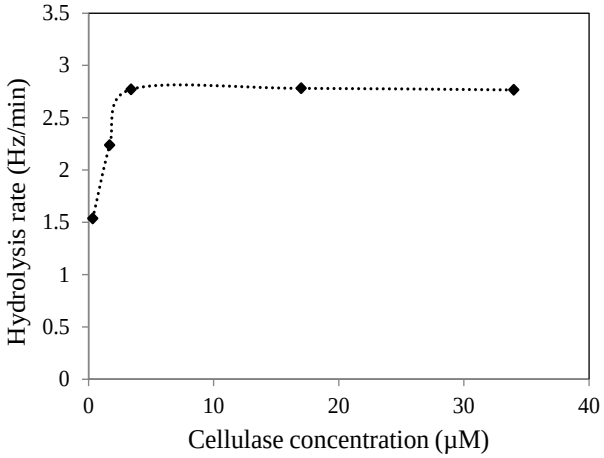

Figure 6.6 Initial hydrolysis rate of cellulose thin film determined directly from the experimental QCM-D frequency profiles in Figure 6.5 at different cellulase concentrations.

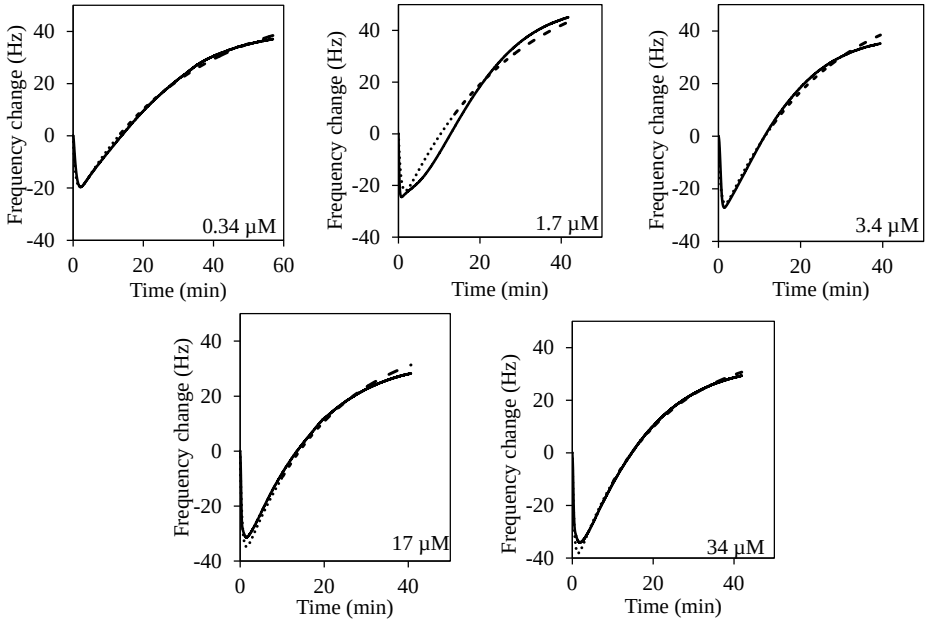

Figure 6.7 Fitting of the modified Michaelis-Menten kinetic model with accessible sites generated by hydrolysis (dotted curves) to experimental frequency response QCM-D data (solid curves). The results for the third overtone are shown for experiments performed at pH 5 and 30 °C.

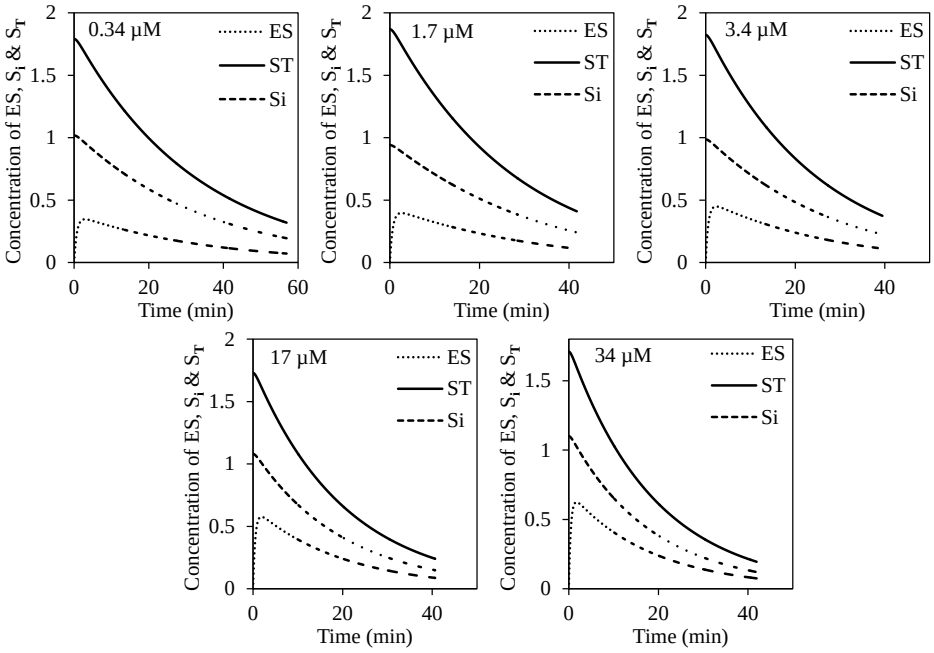

Figure 6.8 Predicted concentration profiles of intermediate enzyme substrate complex (ES), total interfacial sites (S_i), and total cellulose (S_T).

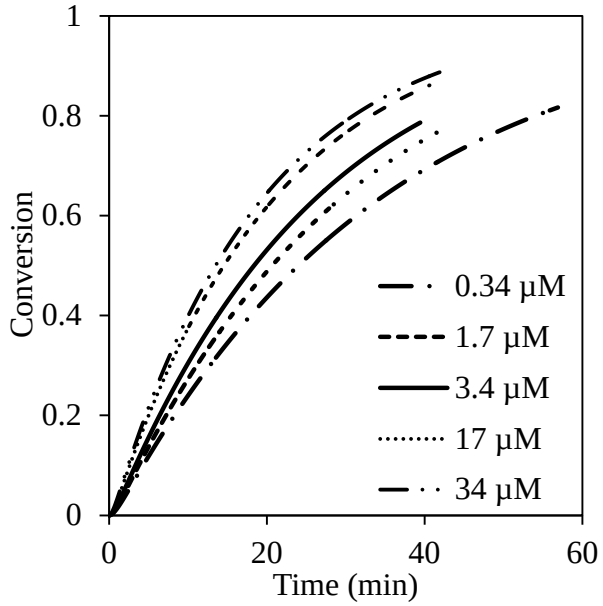

Figure 6.9 Cellulose conversion vs. time as a function of cellulase concentration calculated using the modified Michaelis-Menten model with parameters in Table 6.1.

Table 6.1 Parameter values obtained by fitting the experimental data to model (The error value is the uncertainty of that parameter determined using a 95% confidence interval).

Parameter	Value
k_1 (mM^{-n} min^{-1})	2.88 ± 0.03
k_{-1} (min^{-1})	0.88 ± 0.01
k_2 (min^{-1})	0.219 ± 0.001
S_{T0} (SU)	2.81 ± 0.021
A (Hz SU^{-1})	64.5
B (Hz SU^{-1})	66.4 ± 1.86
$\alpha_{1,0}$ (0.34 µM)	0.362 ± 0.003
$\alpha_{2,0}$ (1.7 µM)	0.335 ± 0.004
$\alpha_{3,0}$ (3.4 µM)	0.351 ± 0.003
$\alpha_{4,0}$ (17 µM)	0.385 ± 0.002
$\alpha_{5,0}$ (34 µM)	0.392 ± 0.002
n	0.22

SU - Substrate units

CHAPTER 7

CONCLUSIONS

Understanding and overcoming the barriers to efficient enzymatic hydrolysis of lignocellulosic biomass is essential for the development of economically competitive processes. The effects of process parameters including pretreatment, source of lignocellulose and exposure to additives are not fully understood and so developing a universal strategy for saccharification remains a goal in this field. The current work investigated several aspects associated with the conversion of cellulose, including binding and activity of cellulases, effect of nonionic surfactants and the development of a kinetic model for the hydrolysis of cellulose. Substrate properties have been speculated to be the limiting factor in hydrolysis of cellulose, model cellulose films (deposited using NMMO, LiCl and from a dispersion of cellulose nanocrystals, CNC) with different morphology and crystallinity were used to investigate the enzymatic hydrolysis cellulose substrates using QCM-D. In addition to the experimental studies, the hydrolysis was also approached from the modeling point of view. A mechanistic model coupling enzyme binding and hydrolysis with exposure of bulk sites from embedded cellulose was developed to study the effect of cellulose structure on hydrolysis rate. The experimental results showed that the hydrolysis rate of CNC films was much slower despite a hypothesized high level of accessible surface area for enzyme binding compared with NMMO and LiCl films. The hydrolysis rate constant obtained from modeling for amorphous LiCl-derived films was larger than for type II crystalline NMMO-derived films, and much larger than for CNC films. The study of the effect enzyme concentration

on adsorption and enzymatic degradation of cellulose on type II crystalline NMMO cellulose films showed a strong dependence on the adsorbed enzyme concentration, with hydrolysis rates increasing as the cellulase concentration increased at low to intermediate concentrations, but displayed a tendency to level off at higher cellulase concentrations. The model developed predicted the complete hydrolysis kinetics at initial and later stage of hydrolysis over wide range of cellulase concentrations.

This approach of coupling experimental methods with mechanistic modeling not only provide insights on enzyme activity, understanding of the underlying mechanism and the nature of enzyme-substrate interaction but is also more likely to be capable of moving backwards from understanding binding to understanding how to best pretreat biomass for effective hydrolysis. The current study results demonstrated that while accessibility to cellulase is certainly important, the crystallinity of the films plays a greater role in determining enzyme hydrolysis rate suggesting effective pretreatment strategies would be expected to be those able both to increase accessibility and reduce crystallinity of cellulose. In addition, the modeling approach presented in this work opens up new perspectives to explore many hypothesized causes of kinetic slowdown in the cellulosic hydrolysis process such as product inhibition and enzyme inactivation which are commonly experienced in industrial applications.

This dissertation work also investigated experimental methods to directly determine how cellulase enzymes interact with biomass components in presence of non-ionic surfactants. The results showed that cellulase binding decreased in the presence of

non-ionic surfactant Tween-80 on both NMMO and LiCl cellulose films. However, the hydrolysis rate was observed to decrease for NMMO cellulose films due to Twen-80 addition while no significant effect was observed on the hydrolysis of LiCl/DMAc cellulose films.

The studies on cellulase enzyme-lignin interactions in the presence of non-ionic surfactant Tween-80 showed that adsorption of cellulase on lignin was strong and irreversible, while Tween-80 adsorption was partially reversible. Coadsorption of cellulase and Tween-80 reduced the material adsorbed upon adsorption. Tween-80 also reduced bound cellulase by both displacement from lignin and pre-adsorption. The results also suggested that introducing enough Tween-80 to give monolayer coverage is adequate to reduce cellulase binding to displace cellulase from the lignin surface. The results obtained from this work showed definitively using direct in situ kinetic measurements that control of nonproductive binding of enzymes will contribute to reduce required cellulase dosage. This approach also acts as a tool to move backwards from understanding binding to understanding how to best pretreat biomass to favor the appropriate surface for controlled binding. Based on these findings it can be suggested that additives such as Tween-80 do not directly enhance hydrolysis, but may be beneficial under real hydrolysis conditions (where a limited concentration of enzyme is present to partition between the solution and cellulose surface) by helping to desorb and redistribute cellulases which in turn maximize hydrolysis activity.

The studies on effects of surfactant-cellulose/lignin interactions suggested that the positive effect of Tween-80 is most likely due to the binding of surfactants to the

lignin surface of lignocellulose and hence reduction in the inhibitory effects of lignin. Although QCM-D measurements suggested that Tween-80 can not only reduce cellulase binding but can also displace bound cellulases on lignin, quantifying the amount of cellulase displaced was indirect with QCM-D as it measures the net change in frequency due to mass adsorbed and desorbed on the sensor. In the future, further experiments with quantification of the cellulase adsorbed on the lignin surface would be beneficial to confirm the ability of surfactants to prevent binding of and displace cellulases. For this, X-ray photoelectron spectroscopy (XPS) can be used as an analytical technique. XPS has been used to analyze and quantify the surface chemical composition of thin films. From the binding energy and intensity of a photoelectron peak, the elemental identity, chemical state, and quantity of an element are determined. Lignin and non-ionic surfactant Tween-80 do not contain nitrogen, whereas nitrogen is intrinsic in the amino acids of proteins such as cellulase enzymes. The nitrogen in the enzymes structure enables the study of the adsorption of cellulase by XPS. High resolution scans of the N(1s) region (BE ~400 eV) can be used to determine the nitrogen content and used as a means of characterizing the relative amount of cellulase on lignin as a function of Tween-80 concentration. From the XPS data, the reduction in adsorption of cellulase to lignin in the presence of Tween-80 and the ability of Tween-80 to displace adsorbed cellulase can be quantified to confirm the conclusions of the QCM-D measurements.

APPENDIX I

Cellulose fibril based enzyme hydrolysis kinetic model - derivation of rate of exposure

Let R be the radius of the cellulose microfibril, R_o be the radius of interfacial cellulose layer, L be length of the cylinder and ρ be the density of cellulose. Then
Total volume of cellulose $S_T = \pi\rho R^2 L$

Volume of interfacial layer $S_i = 2\pi L \int_{R-R_o}^{R} R dR = 2\pi L \left[\frac{R^2}{2}\right]_{R-R_o}^{R}$

$$= 2\pi L \left[\frac{R^2 - (R - R_o)^2}{2}\right]$$

Mass of interfacial layer $S_i = \pi\rho L[R^2 - (R - R_o)^2] = \pi\rho L\left[2RR_o - {R_o}^2\right]$

As the hydrolysis progress, the change in interfacial mass is due to the rate of exposure of new surface sites and change in total cellulose mass [92].

$$\frac{d[S_i]}{dt} = \frac{d[S_T]}{dt} + \text{rate of exposure}$$

$S_T = \pi\rho R^2 L$ $\quad\quad \frac{d[S_T]}{dt} = 2\pi\rho LR\frac{dR}{dt}$

$S_i = \pi\rho L\left[2RR_o - {R_o}^2\right]$ $\quad\quad \frac{d[S_i]}{dt} = 2\pi\rho LR_o\frac{dR}{dt}$

$$2\pi\rho R_o L\frac{dR}{dt} = 2\pi\rho RL\frac{dR}{dt} + \text{rate of exposure}$$

$$\text{rate of exposure} = 2\pi\rho L(R_o - R)\frac{dR}{dt}$$

$$\frac{d[S_T]}{dt} = 2\pi\rho LR\frac{dR}{dt}$$

$$\text{rate of exposure} = \left(\frac{R_o - R}{R}\right) * \frac{d[S_T]}{dt}$$

$$\text{rate of exposure} = \left(\frac{R_o}{R} - 1\right) * \frac{d[S_T]}{dt}$$

$$\text{rate of exposure} = -\left(1 - \frac{R_o}{R}\right) * \frac{d[S_T]}{dt}$$

$$S_T = \pi\rho R^2 L$$

$$S_i = \pi\rho L\left[2RR_o - {R_o}^2\right]$$

$$\frac{S_i}{S_T} = \frac{\pi\rho L[R^2 - (R - R_o)^2]}{\pi\rho R^2 L}$$

$$\frac{S_i}{S_T} = 1 - \left(1 - \frac{R_o}{R}\right)^2$$

$$\left(1-\frac{R_o}{R}\right)=\left(1-\frac{S_i}{S_T}\right)^{1/2}$$

Rate of change of cellulose mass due to hydrolysis

$$\frac{d[S_T]}{dt}=-k_2 ES$$

$$\text{rate of exposure} = k_2 * \left(1-\frac{S_i}{S_T}\right)^{1/2} * ES$$

APPENDIX II

Cellulose nanocrystal network hydrolysis model – derivation of rate of exposure

Cellulose film is considered to be made of porous network of cellulose nanocrystals with pores of radius 'r', length 'l' and number of particles per unit volume of film (n/m^3) be N_p

Surface area of particles per volume of film (m^2/m^3) $Area = N_p 2\pi rl$

Surface density of cellulose, (g of cellobiose units/ m^2) $\rho_{surface}$

Surface site concentration of cellulose S_i (g/ m^3) $S_i = \rho_{surface} * N_p 2\pi rl$

Rate of change of surface sites, $\frac{dS_i}{dt} = \rho_{surface} * N_p 2\pi l \frac{dr}{dt}$

Bulk density of cellulose film, (g/ m^3) $\rho_{cellulose}$

Total site concentration S_T (g/ m^3) $S_T = \rho_{cellulose}(N_p \pi r^2 l)$

Rate of change of total concentration, $\frac{dS_T}{dt} = \rho_{cellulose} * N_p 2\pi rl \frac{dr}{dt}$

As the hydrolysis progress, the change in interfacial mass is due to the rate of exposure of new surface sites and change in total cellulose mass.

$$\frac{d[S_i]}{dt} = \frac{d[S_T]}{dt} + rate\ of\ \ exposure$$

$$\rho_{surface} * N_p 2\pi l \frac{dr}{dt} = \rho_{cellulose} * N_p 2\pi rl \frac{dr}{dt} + rate\ of\ generation\ of\ new\ sites$$

$$rate\ of\ \ exposure = N_p 2\pi l(\rho_{surface} - \rho_{cellulose} r)\frac{dr}{dt}$$

Rate of hydrolysis, $\frac{dS_T}{dt} = -k_2 ES = \rho_{cellulose} * N_p 2\pi rl \frac{dr}{dt}$

$$\frac{dr}{dt} = \frac{-k_2 ES}{\rho_{cellulose} * N_p 2\pi rl}$$

$$rate\ of\ \ exposure = k_2 ES\left(1 - \frac{\rho_{surface}}{\rho_{cellulose} r}\right)$$

APPENDIX III

Supporting information for chapter 3

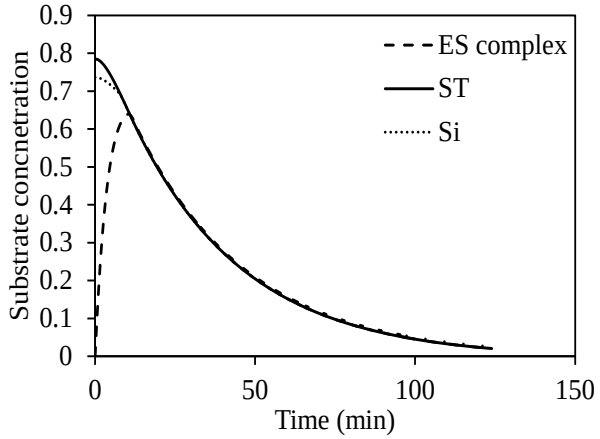

Figure S3.1 Cellulose nanocrystal network model - Model concentration profile of ES complex (dashed line), interfacial substrate concentration S_i (dotted line) and total substrate concentration S_T (solid line) for CNC film hydrolysis by cellulase (0.5 %v/v).

Calculation of surface density ($\rho_{surface}$)

The 110 lattice plane for monoclinic cellulose dimensions of 0.78 nm and 0.795 nm were used for calculation of planar density of cellulose[258] assuming the lattice structure was made of cellobiose units.

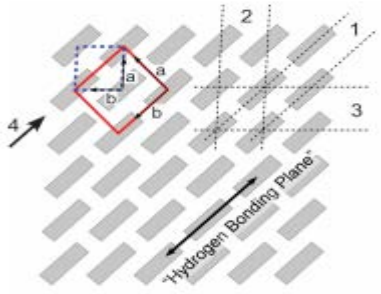

Figure S3.2 Unit cell structure of cellulose[258].

a = 0.78 nm b = 0.795 nm

Surface density = 2(cellobiose unit)/(0.78 nm)*(0.79 nm) = $3.22*10^{18}$ cellobiose units/m^2
Surface density = $3.22*10^{18}$ cellobiose units/m^2* (342.29 g/mole)/$6.023*10^{23}$ (cellobiose units/mole) =$182.99*10^{-5}$ g/m^2

APPENDIX IV

Supporting information for chapter 4

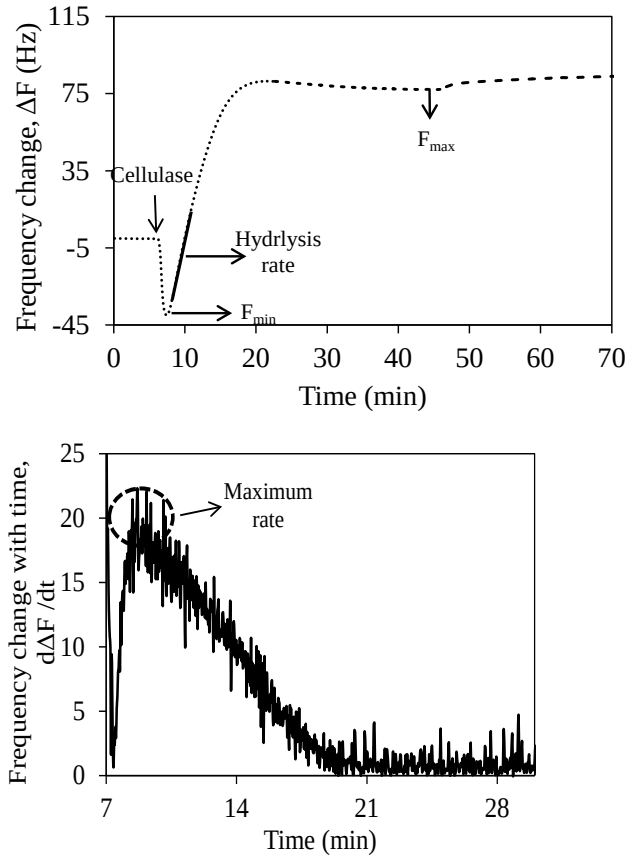

Figure S4.1 Plot of frequency change (absolute) with time vs time to determine the maximum rate.

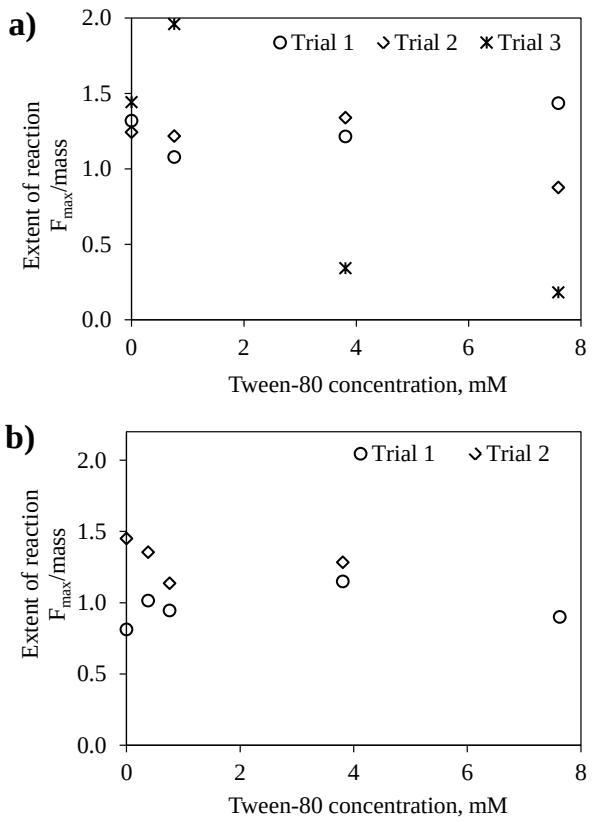

Figure S4.2 Plot of extent of reaction for co-adsorption, a) NMMO cellulose films and b) LiCl/DMAc cellulose films with varying concentration of Tween-80 (0-8 mM).

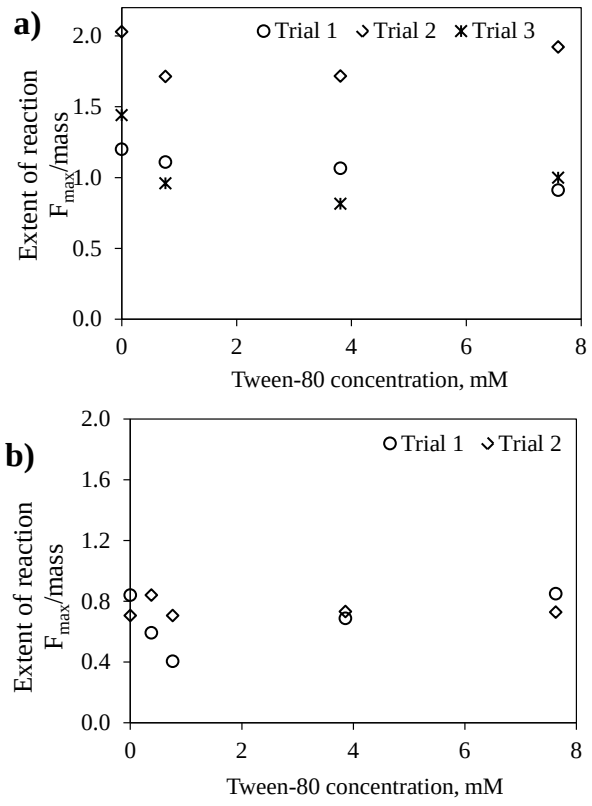

Figure S4. 3 Plot of extent of reaction for sequential adsorption, a) NMMO cellulose films and b) LiCl/DMAc cellulose films with varying concentration of Tween-80 (0-8 mM).

APPENDIX V

Supporting information for chapter 5

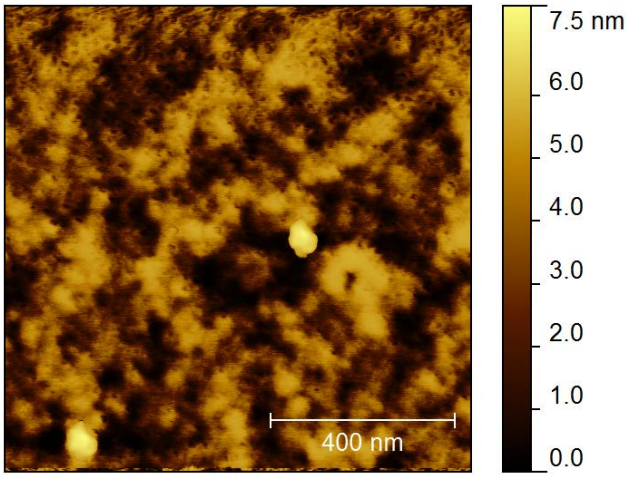

Figure S5.1. AFM topography image of model lignin thin film prepared by spin coating Kraft lignin dispersion onto a PEI-coated gold sensor (1µm × 1µm size with Z scale range).

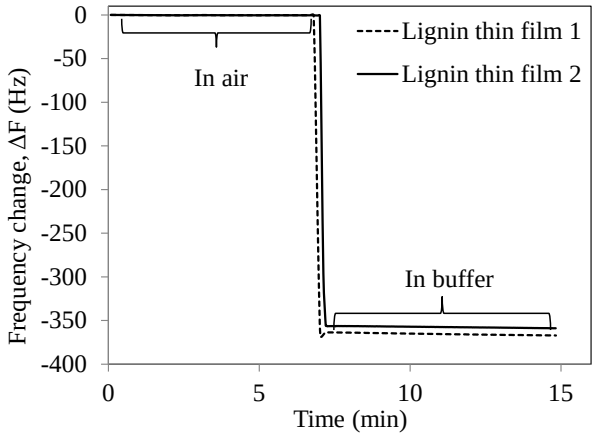

Figure S5.2. Stability of lignin films -Frequency change associated with transition from air to buffer

In order to test the stability of the lignin films prepared the frequency change upon transition from air to buffer was recorded. It was found that, initially a large drop in frequency is observed due to change in the medium and after that no increase in frequency was observed, implying that films are not detached from the base substrate and stable under the given environment.

APPENDIX VI

Supporting information for chapter 6

Table S6.1. Parameter values obtained by fitting the Michaelis-Menten model assuming all the substrate is fully accessible for binding and hydrolysis, and enzyme is released after hydrolysis to experimental data (The error value is the uncertainty of that parameter determined using a 95% confidence interval).

Parameter	Value
k_1 (mM min^{-1})	1.68 ± 5.36
k_{-1} (min^{-1})	0.36 ± 7.3
k_2 (min^{-1})	2.33 ± 7.36
A (Hz SU^{-1})	1805 ± 3513
B (Hz SU^{-1})	52.55 ± 175.04
S(0.34 µM) (SU)	42.62 ± 143.81
S(01.7 µM) (SU)	15.92 ± 53.68
S(3.4 µM) (SU)	7.17 ± 24.16
S(17 µM) (SU)	1.3 ± 2.56
S(34 µM) (SU)	0.77 ± 4.37

SU - Substrate units

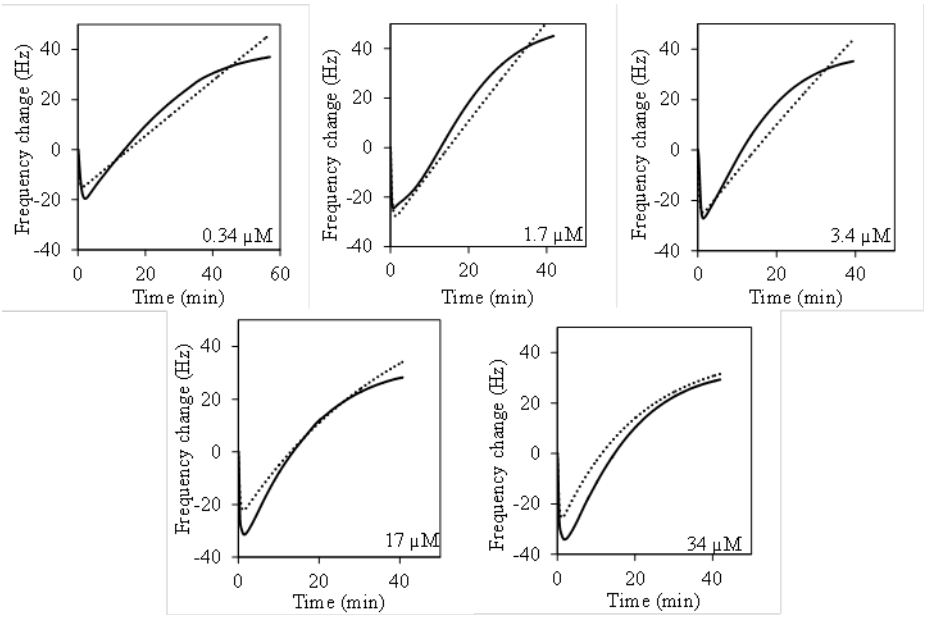

Figure S6.1. Comparison of experimental frequency response QCM-D data and Michaelis-Menten model prediction assuming all the substrate is fully accessible for binding and hydrolysis, and enzyme is released after hydrolysis of cellulose hydrolysis by cellulases. Solid line represents the experimental measured frequency; dotted line represents the modeled frequency.

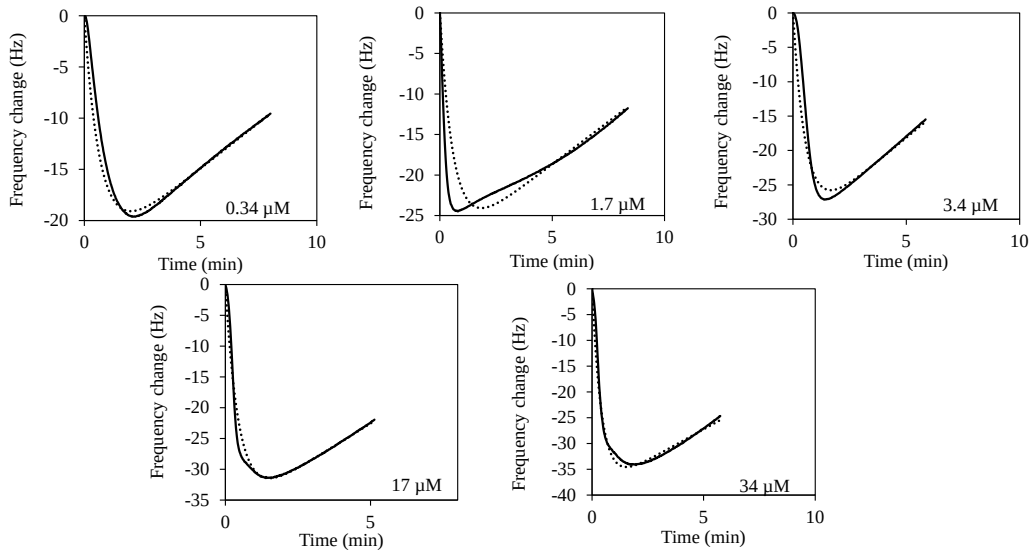

Figure S6.2. Initial kinetic hydrolysis data fitting. Comparison of experimental frequency response data and model prediction of cellulose hydrolysis by cellulases. Solid line represents the experimental measured frequency; dotted line represents the modeled frequency.

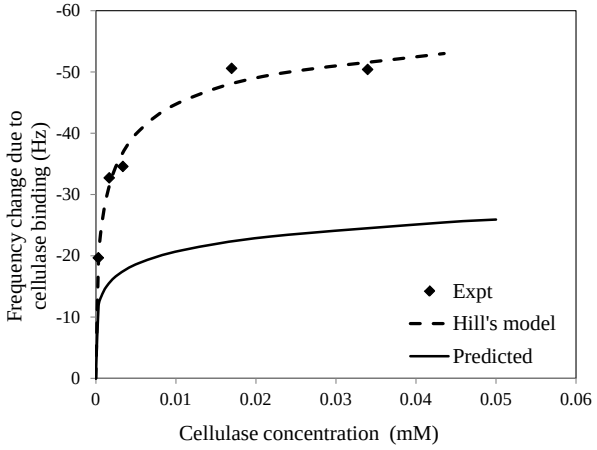

Figure S6.3. Adsorption of *T. reesei* cellulases to model cellulose surface. Comparison of Hills model (dashed line), Predicted adsorption from rate parameters obtained from initial adsorption kinetics (solid line) and experimental data are shown by symbol (♦).

References

1. Ragauskas, A.J., et al., *The path forward for biofuels and biomaterials.* science, 2006. **311**(5760): p. 484-489.
2. Lang, X., D. Macdonald, and G. Hill, *Recycle bioreactor for bioethanol production from wheat starch II. Fermentation and economics.* Energy Sources, 2001. **23**(5): p. 427-436.
3. Demain, A.L., M. Newcomb, and J.D. Wu, *Cellulase, clostridia, and ethanol.* Microbiology and molecular biology reviews, 2005. **69**(1): p. 124-154.
4. Lewis, S., *Fermentation alcohol.* Industrial enzymology, 1996: p. 11-48.
5. Lynd, L.R., et al., *Fuel ethanol from cellulosic biomass.* Science(Washington), 1991. **251**(4999): p. 1318-1323.
6. Independence, E., *Security Act of 2007 (EISA).* Pub L, 2007(110-140).
7. Sun, Y. and J. Cheng, *Hydrolysis of lignocellulosic materials for ethanol production: a review.* Bioresource technology, 2002. **83**(1): p. 1-11.
8. Association, R.F., *Climate of opportunity: 2010 ethanol industry outlook*. 2010: Renewable Fuels Association.
9. Jørgensen, H., J.B. Kristensen, and C. Felby, *Enzymatic conversion of lignocellulose into fermentable sugars: challenges and opportunities.* Biofuels, Bioproducts and Biorefining, 2007. **1**(2): p. 119-134.
10. Zhao, X., L. Zhang, and D. Liu, *Biomass recalcitrance. Part I: the chemical compositions and physical structures affecting the enzymatic hydrolysis of lignocellulose.* Biofuels, Bioproducts and Biorefining, 2012. **6**(4): p. 465-482.
11. Chang, M.C., *Harnessing energy from plant biomass.* Current opinion in chemical biology, 2007. **11**(6): p. 677-684.
12. Somerville, C., *Cellulose synthesis in higher plants.* Annu. Rev. Cell Dev. Biol., 2006. **22**: p. 53-78.
13. Hu, G., J.A. Heitmann, and O.J. Rojas, *Feedstock pretreatment strategies for producing ethanol from wood, bark, and forest residues.* BioResources, 2008. **3**(1): p. 270-294.
14. Perlack, R.D., et al., *Biomass as feedstock for a bioenergy and bioproducts industry: the technical feasibility of a billion-ton annual supply*. 2005, DTIC Document.
15. Somerville, C., *Cellulose Synthesis in Higher Plants.* Annual Review of Cell and Developmental Biology, 2006. **22**(1): p. 53-78.
16. O'SULLIVAN, A.C., *Cellulose: the structure slowly unravels.* Cellulose, 1997. **4**(3): p. 173-207.
17. Kontturi, E., T. Tammelin, and M. Österberg, *Cellulose—model films and the fundamental approach.* Chemical Society Reviews, 2006. **35**(12): p. 1287-1304.

18. Saha, B.C., *Hemicellulose bioconversion.* Journal of Industrial Microbiology and Biotechnology, 2003. **30**(5): p. 279-291.
19. Preiss, J., *The biochemistry of plants: A comprehensive treatise--3 Carbohidrates: Structure and function. ed.* 1980.
20. Mielenz, J.R., *Ethanol production from biomass: technology and commercialization status.* Current opinion in microbiology, 2001. **4**(3): p. 324-329.
21. Sticklen, M.B., *Feedstock crop genetic engineering for alcohol fuels.* Crop science, 2007. **47**(6): p. 2238-2248.
22. Chen, F., et al., *Multi-site genetic modulation of monolignol biosynthesis suggests new routes for formation of syringyl lignin and wall-bound ferulic acid in alfalfa (Medicago sativa L.).* The Plant Journal, 2006. **48**(1): p. 113-124.
23. Chandel, A.K., et al., *Economics and environmental impact of bioethanol production technologies: an appraisal.* Biotechnology and Molecular Biology Review, 2007. **2**(1): p. 14-32.
24. Himmel, M.E., et al., *Biomass recalcitrance: engineering plants and enzymes for biofuels production.* Science, 2007. **315**(5813): p. 804.
25. Galbe, M. and G. Zacchi, *Pretreatment of lignocellulosic materials for efficient bioethanol production*, in *Biofuels*. 2007, Springer. p. 41-65.
26. Alvira, P., et al., *Pretreatment technologies for an efficient bioethanol production process based on enzymatic hydrolysis: a review.* Bioresource technology, 2010. **101**(13): p. 4851-4861.
27. Mosier, N., et al., *Features of promising technologies for pretreatment of lignocellulosic biomass.* Bioresource technology, 2005. **96**(6): p. 673-686.
28. Hendriks, A. and G. Zeeman, *Pretreatments to enhance the digestibility of lignocellulosic biomass.* Bioresource technology, 2009. **100**(1): p. 10-18.
29. Xiang, Q., et al., *Heterogeneous aspects of acid hydrolysis of α-cellulose*, in *Biotechnology for Fuels and Chemicals*. 2003, Springer. p. 505-514.
30. Hamelinck, C.N., G. Van Hooijdonk, and A.P. Faaij, *Ethanol from lignocellulosic biomass: techno-economic performance in short-, middle- and long-term.* Biomass and bioenergy, 2005. **28**(4): p. 384-410.
31. Kim, S. and M.T. Holtzapple, *Delignification kinetics of corn stover in lime pretreatment.* Bioresource Technology, 2006. **97**(5): p. 778-785.
32. Mansfield, S.D., C. Mooney, and J.N. Saddler, *Substrate and enzyme characteristics that limit cellulose hydrolysis.* Biotechnology progress, 1999. **15**(5): p. 804-816.
33. Martín, C., et al., *Ethanol production from enzymatic hydrolysates of sugarcane bagasse using recombinant xylose-utilising Saccharomyces cerevisiae.* Enzyme and Microbial Technology, 2002. **31**(3): p. 274-282.

34. Cardona, C.A. and Ó.J. Sánchez, *Fuel ethanol production: process design trends and integration opportunities.* Bioresource technology, 2007. **98**(12): p. 2415-2457.
35. Reese, E. *History of the cellulase program at the US Army Natick Development Center*. in *Biotechnol. Bioeng. Symp.;(United States)*. 1976. Army Natick Development Center, MA.
36. Zhang, Y.-H.P. and L.R. Lynd, *Toward an aggregated understanding of enzymatic hydrolysis of cellulose: noncomplexed cellulase systems.* Biotechnology and bioengineering, 2004. **88**(7): p. 797-824.
37. Mullings, R., *Measurement of saccharification by cellulases.* Enzyme and Microbial Technology, 1985. **7**(12): p. 586-591.
38. Gruno, M., et al., *Inhibition of the Trichoderma reesei cellulases by cellobiose is strongly dependent on the nature of the substrate.* Biotechnology and Bioengineering, 2004. **86**(5): p. 503-511.
39. Henrissat, B., *A classification of glycosyl hydrolases based on amino acid sequence similarities.* Biochem. J, 1991. **280**: p. 309-316.
40. Lombard, V., et al., *The carbohydrate-active enzymes database (CAZy) in 2013.* Nucleic acids research, 2014. **42**(D1): p. D490-D495.
41. Linder, M. and T.T. Teeri, *The roles and function of cellulose-binding domains.* Journal of Biotechnology, 1997. **57**(1-3): p. 15-28.
42. Teeri, T.T., *Crystalline cellulose degradation: new insight into the function of cellobiohydrolases.* Trends in Biotechnology, 1997. **15**(5): p. 160-167.
43. Boraston, A., et al., *Carbohydrate-binding modules: fine-tuning polysaccharide recognition.* Biochem. J, 2004. **382**: p. 769-781.
44. Tomme, P., *Cellulose-binding domains: classification and properties.* The enzyme degradation of insoluble polysaccharides, 1995: p. 142-161.
45. Linder, M., et al., *Identification of functionally important amino acids in the cellulose-binding domain of Trichoderma reesei cellobiohydrolase I.* Protein Science, 1995. **4**(6): p. 1056-1064.
46. Tormo, J., et al., *Crystal structure of a bacterial family-III cellulose-binding domain: a general mechanism for attachment to cellulose.* The EMBO Journal, 1996. **15**(21): p. 5739.
47. Lehtiö, J., et al., *The binding specificity and affinity determinants of family 1 and family 3 cellulose binding modules.* Proceedings of the National Academy of Sciences, 2003. **100**(2): p. 484-489.
48. Liu, Y.-S., et al., *Cellobiohydrolase hydrolyzes crystalline cellulose on hydrophobic faces.* Journal of Biological Chemistry, 2011. **286**(13): p. 11195-11201.
49. Nimlos, M.R., et al., *Binding preferences, surface attachment, diffusivity, and orientation of a family 1 carbohydrate-binding module on cellulose.* Journal of Biological Chemistry, 2012. **287**(24): p. 20603-20612.

50. Palonen, H., M. Tenkanen, and M. Linder, *Dynamic interaction of Trichoderma reesei cellobiohydrolases Cel6A and Cel7A and cellulose at equilibrium and during hydrolysis.* Applied and environmental microbiology, 1999. **65**(12): p. 5229-5233.
51. Berlin, A., et al., *Inhibition of cellulase, xylanase and β-glucosidase activities by softwood lignin preparations.* Journal of Biotechnology, 2006. **125**(2): p. 198-209.
52. Chernoglazov, V.M., O.V. Ermolova, and A.A. Klyosov, *Adsorption of high-purity endo-1, 4-β-glucanases from Trichoderma reesei on components of lignocellulosic materials: cellulose, lignin, and xylan.* Enzyme and Microbial Technology, 1988. **10**(8): p. 503-507.
53. Ooshima, H., D.S. Burns, and A.O. Converse, *Adsorption of cellulase from Trichoderma reesei on cellulose and lignacious residue in wood pretreated by dilute sulfuric acid with explosive decompression.* Biotechnology and Bioengineering, 1990. **36**(5): p. 446-452.
54. Rahikainen, J., et al., *Inhibition of enzymatic hydrolysis by residual lignins from softwood—study of enzyme binding and inactivation on lignin-rich surface.* Biotechnology and bioengineering, 2011. **108**(12): p. 2823-2834.
55. Rahikainen, J.L., et al., *Inhibitory effect of lignin during cellulose bioconversion: the effect of lignin chemistry on non-productive enzyme adsorption.* Bioresource technology, 2013. **133**: p. 270-278.
56. Tu, M., X. Pan, and J.N. Saddler, *Adsorption of cellulase on cellulolytic enzyme lignin from lodgepole pine.* Journal of agricultural and food chemistry, 2009. **57**(17): p. 7771-7778.
57. Lee, D., A.H. Yu, and J.N. Saddler, *Evaluation of cellulase recycling strategies for the hydrolysis of lignocellulosic substrates.* Biotechnology and Bioengineering, 1995. **45**(4): p. 328-336.
58. Palonen, H., et al., *Adsorption of Trichoderma reesei CBH I and EG II and their catalytic domains on steam pretreated softwood and isolated lignin.* Journal of Biotechnology, 2004. **107**(1): p. 65-72.
59. Börjesson, J., R. Peterson, and F. Tjerneld, *Enhanced enzymatic conversion of softwood lignocellulose by poly (ethylene glycol) addition.* Enzyme and Microbial Technology, 2007. **40**(4): p. 754-762.
60. Eriksson, T., J. Börjesson, and F. Tjerneld, *Mechanism of surfactant effect in enzymatic hydrolysis of lignocellulose.* Enzyme and Microbial Technology, 2002. **31**(3): p. 353-364.
61. Ooshima, H., M. Sakata, and Y. Harano, *Enhancement of enzymatic hydrolysis of cellulose by surfactant.* Biotechnology and Bioengineering, 1986. **28**(11): p. 1727-1734.

62. Pan, X., *Role of functional groups in lignin inhibition of enzymatic hydrolysis of cellulose to glucose.* Journal of Biobased Materials and Bioenergy, 2008. **2**(1): p. 25-32.
63. Sewalt, V., W. Glasser, and K. Beauchemin, *Lignin impact on fiber degradation. 3. Reversal of inhibition of enzymatic hydrolysis by chemical modification of lignin and by additives.* Journal of Agricultural and Food Chemistry, 1997. **45**(5): p. 1823-1828.
64. Yang, B. and C.E. Wyman, *BSA treatment to enhance enzymatic hydrolysis of cellulose in lignin containing substrates.* Biotechnology and Bioengineering, 2006. **94**(4): p. 611-617.
65. Tu, M., R.P. Chandra, and J.N. Saddler, *Recycling cellulases during the hydrolysis of steam exploded and ethanol pretreated lodgepole pine.* Biotechnology progress, 2007. **23**(5): p. 1130-1137.
66. Wang, Z., T. Lan, and J. Zhu, *Lignosulfonate and elevated pH can enhance enzymatic saccharification of lignocelluloses.* Biotechnology for biofuels, 2013. **6**(1): p. 1-11.
67. Kumar, L., et al., *The lignin present in steam pretreated softwood binds enzymes and limits cellulose accessibility.* Bioresource technology, 2012. **103**(1): p. 201-208.
68. Qing, Q., B. Yang, and C.E. Wyman, *Impact of surfactants on pretreatment of corn stover.* Bioresource technology, 2010. **101**(15): p. 5941-5951.
69. Nidetzky, B., et al., *Synergism of Trichoderma reesei cellulases while degrading different celluloses.* Biotechnology letters, 1993. **15**(1): p. 71-76.
70. Henrissat, B., et al., *Synergism of cellulases from Trichoderma reesei in the degradation of cellulose.* Nature Biotechnology, 1985. **3**(8): p. 722-726.
71. Medve, J., J. Ståhlberg, and F. Tjerneld, *Adsorption and synergism of cellobiohydrolase I and II of Trichoderma reesei during hydrolysis of microcrystalline cellulose.* Biotechnology and bioengineering, 1994. **44**(9): p. 1064-1073.
72. Gusakov, A.V. and A.P. Sinitsyn, *A theoretical analysis of cellulase product inhibition: Effect of cellulase binding constant, enzyme/substrate ratio, and β-glucosidase activity on the inhibition pattern.* Biotechnology and bioengineering, 1992. **40**(6): p. 663-671.
73. Holtzapple, M., et al., *Inhibition of Trichoderma reesei cellulase by sugars and solvents.* Biotechnology and Bioengineering, 1990. **36**(3): p. 275-287.
74. Väljamäe, P., G. Pettersson, and G. Johansson, *Mechanism of substrate inhibition in cellulose synergistic degradation.* European Journal of Biochemistry, 2001. **268**(16): p. 4520-4526.

75. Sattler, W., et al., *The effect of enzyme concentration on the rate of the hydrolysis of cellulose.* Biotechnology and bioengineering, 1989. **33**(10): p. 1221-1234.
76. Converse, A.O., et al., *A model of enzyme adsorption and hydrolysis of microcrystalline cellulose with slow deactivation of the adsorbed enzyme.* Biotechnology and Bioengineering, 1988. **32**(1): p. 38-45.
77. Fan, L., Y.H. Lee, and D. Beardmore, *The influence of major structural features of cellulose on rate of enzymatic hydrolysis.* Biotechnology and Bioengineering, 1981. **23**(2): p. 419-424.
78. Fan, L., Y.H. Lee, and D.H. Beardmore, *Mechanism of the enzymatic hydrolysis of cellulose: effects of major structural features of cellulose on enzymatic hydrolysis.* Biotechnology and Bioengineering, 1980. **22**(1): p. 177-199.
79. Hall, M., et al., *Cellulose crystallinity–a key predictor of the enzymatic hydrolysis rate.* FEBS journal, 2010. **277**(6): p. 1571-1582.
80. Chen, Y., et al., *Effect of digestion by pure cellulases on crystallinity and average chain length for bacterial and microcrystalline celluloses.* Cellulose, 2007. **14**(4): p. 283-293.
81. Wang, L., et al., *Changes in the structural properties and rate of hydrolysis of cotton fibers during extended enzymatic hydrolysis.* Biotechnology and bioengineering, 2006. **93**(3): p. 443-456.
82. Converse, A., *Substrate factors limiting enzymatic hydrolysis.* Biotechnology in Agriculture, 1993: p. 93-93.
83. Grethlein, H.E., *The effect of pore size distribution on the rate of enzymatic hydrolysis of cellulosic substrates.* Nature Biotechnology, 1985. **3**(2): p. 155-160.
84. Thompson, D.N., H.-C. Chen, and H.E. Grethlein, *Comparison of pretreatment methods on the basis of available surface area.* Bioresource technology, 1992. **39**(2): p. 155-163.
85. Sinitsyn, A., A. Gusakov, and E.Y. Vlasenko, *Effect of structural and physico-chemical features of cellulosic substrates on the efficiency of enzymatic hydrolysis.* Applied Biochemistry and Biotechnology, 1991. **30**(1): p. 43-59.
86. Bansal, P., et al., *Modeling cellulase kinetics on lignocellulosic substrates.* Biotechnology advances, 2009. **27**(6): p. 833-848.
87. Gharpuray, M., Y.H. Lee, and L. Fan, *Structural modification of lignocellulosics by pretreatments to enhance enzymatic hydrolysis.* Biotechnology and bioengineering, 1983. **25**(1): p. 157-172.
88. Parajo, J., J. Alonso, and V. Santos, *Development of a generalized phenomenological model describing the kinetics of the enzymatic hydrolysis of NaOH-treated pine wood.* Applied biochemistry and biotechnology, 1996. **56**(3): p. 289-299.

89. Chang, V.S. and M.T. Holtzapple. *Fundamental factors affecting biomass enzymatic reactivity*. in *Twenty-First Symposium on Biotechnology for Fuels and Chemicals*. 2000. Springer.
90. Zhou, W., Y. Xu, and H.B. Schüttler, *Cellulose hydrolysis in evolving substrate morphologies III: Time-scale analysis.* Biotechnology and bioengineering, 2010. **107**(2): p. 224-234.
91. Levine, S.E., et al., *A mechanistic model of the enzymatic hydrolysis of cellulose.* Biotechnology and bioengineering, 2010. **107**(1): p. 37-51.
92. Griggs, A.J., J.J. Stickel, and J.J. Lischeske, *A mechanistic model for enzymatic saccharification of cellulose using continuous distribution kinetics I: depolymerization by EGI and CBHI.* Biotechnology and bioengineering, 2012. **109**(3): p. 665-675.
93. Beldman, G., et al., *Adsorption and kinetic behavior of purified endoglucanases and exoglucanases from Trichoderma viride.* Biotechnology and bioengineering, 1987. **30**(2): p. 251-257.
94. Chanzy, H., B. Henrissat, and R. Vuong, *Colloidal gold labelling of l, 4-β-D-glucan cellobiohydrolase adsorbed on cellulose substrates.* FEBS letters, 1984. **172**(2): p. 193-197.
95. Sticklen, M.B., *Plant genetic engineering for biofuel production: towards affordable cellulosic ethanol.* Nature Reviews Genetics, 2008. **9**(6): p. 433-443.
96. Ahola, S., et al., *Enzymatic hydrolysis of native cellulose nanofibrils and other cellulose model films: effect of surface structure.* Langmuir, 2008. **24**(20): p. 11592-11599.
97. Hoeger, I.C., et al., *Bicomponent lignocellulose thin films to study the role of surface lignin in cellulolytic reactions.* Biomacromolecules, 2012. **13**(10): p. 3228-3240.
98. Turon, X., O.J. Rojas, and R.S. Deinhammer, *Enzymatic Kinetics of Cellulose Hydrolysis: A QCM-D Study.* Langmuir, 2008. **24**(8): p. 3880-3887.
99. Eriksson, J., et al., *Enzymatic degradation of model cellulose films.* Journal of colloid and interface science, 2005. **284**(1): p. 99-106.
100. Cheng, G., et al., *Neutron reflectometry and QCM-D study of the interaction of cellulases with films of amorphous cellulose.* Biomacromolecules, 2011. **12**(6): p. 2216-2224.
101. Ma, A., et al., *The enzymatic hydrolysis rate of cellulose decreases with irreversible adsorption of cellobiohydrolase I.* Enzyme and Microbial Technology, 2008. **42**(7): p. 543-547.
102. Kumagai, A., S.-H. Lee, and T. Endo, *Thin film of lignocellulosic nanofibrils with different chemical composition for QCM-D study.* Biomacromolecules, 2013. **14**(7): p. 2420-2426.

103. Saarinen, T., et al., *Adsorption of different laccases on cellulose and lignin surfaces.* BioResources, 2008. **4**(1): p. 94-110.
104. USDOE, *Genomics:GTL Roadmap, DOE/SC-0090, US Department of Energy Office of Science* 2005. p. 204.
105. Davies, G. and B. Henrissat, *Structures and mechanisms of glycosyl hydrolases.* Structure, 1995. **3**(9): p. 853-859.
106. Limayem, A. and S.C. Ricke, *Lignocellulosic biomass for bioethanol production: current perspectives, potential issues and future prospects.* Progress in Energy and Combustion Science, 2012. **38**(4): p. 449-467.
107. Cara, C., et al., *Conversion of olive tree biomass into fermentable sugars by dilute acid pretreatment and enzymatic saccharification.* Bioresource Technology, 2008. **99**(6): p. 1869-1876.
108. Kumar, P., et al., *Methods for pretreatment of lignocellulosic biomass for efficient hydrolysis and biofuel production.* Industrial & Engineering Chemistry Research, 2009. **48**(8): p. 3713-3729.
109. Kim, S. and M.T. Holtzapple, *Lime pretreatment and enzymatic hydrolysis of corn stover.* Bioresource Technology, 2005. **96**(18): p. 1994-2006.
110. Zhao, Y., et al., *Enhanced enzymatic hydrolysis of spruce by alkaline pretreatment at low temperature.* Biotechnology and bioengineering, 2008. **99**(6): p. 1320-1328.
111. Lau, M.J., et al., *Ammonia fiber expansion (AFEX) pretreatment, enzymatic hydrolysis, and fermentation on empty palm fruit bunch fiber (EPFBF) for cellulosic ethanol production.* Applied biochemistry and biotechnology, 2010. **162**(7): p. 1847-1857.
112. Wyman, C.E., et al., *Coordinated development of leading biomass pretreatment technologies.* Bioresource technology, 2005. **96**(18): p. 1959-1966.
113. Teymouri, F., et al., *Optimization of the ammonia fiber explosion (AFEX) treatment parameters for enzymatic hydrolysis of corn stover.* Bioresource technology, 2005. **96**(18): p. 2014-2018.
114. Kim, T.H. and Y. Lee. *Pretreatment of corn stover by soaking in aqueous ammonia*. in *Twenty-Sixth Symposium on Biotechnology for Fuels and Chemicals*. 2005. Springer.
115. Papatheofanous, M., et al., *Two-stage acid-catalyzed fractionation of lignocellulosic biomass in aqueous ethanol systems at low temperatures.* Bioresource Technology, 1995. **54**(3): p. 305-310.
116. Sun, F. and H. Chen, *Organosolv pretreatment by crude glycerol from oleochemicals industry for enzymatic hydrolysis of wheat straw.* Bioresource technology, 2008. **99**(13): p. 5474-5479.

117. Ballesteros, I., et al. *Ethanol production from steam-explosion pretreated wheat straw*. in *Twenty-Seventh Symposium on Biotechnology for Fuels and Chemicals*. 2006. Springer.
118. Cara, C., et al., *Enhanced enzymatic hydrolysis of olive tree wood by steam explosion and alkaline peroxide delignification.* Process Biochemistry, 2006. **41**(2): p. 423-429.
119. Oliva, J.M., et al., *Effect of lignocellulosic degradation compounds from steam explosion pretreatment on ethanol fermentation by thermotolerant yeast Kluyveromyces marxianus*, in *Biotechnology for fuels and chemicals*. 2003, Springer. p. 141-153.
120. Wang, G., et al., *Sulfite pretreatment to overcome recalcitrance of lignocellulose (SPORL) for robust enzymatic saccharification of hardwoods.* Biotechnology Progress, 2009. **25**(4): p. 1086-1093.
121. Zhu, J., et al., *Sulfite pretreatment (SPORL) for robust enzymatic saccharification of spruce and red pine.* Bioresource Technology, 2009. **100**(8): p. 2411-2418.
122. Palonen, H., et al., *Evaluation of wet oxidation pretreatment for enzymatic hydrolysis of softwood.* Applied biochemistry and biotechnology, 2004. **117**(1): p. 1-17.
123. Banerjee, S., et al., *Alkaline peroxide assisted wet air oxidation pretreatment approach to enhance enzymatic convertibility of rice husk.* Biotechnology progress, 2011. **27**(3): p. 691-697.
124. Dias, A.A., et al., *Enzymatic saccharification of biologically pre-treated wheat straw with white-rot fungi.* Bioresource technology, 2010. **101**(15): p. 6045-6050.
125. Wan, C. and Y. Li, *Effectiveness of microbial pretreatment by Ceriporiopsis subvermispora on different biomass feedstocks.* Bioresource technology, 2011. **102**(16): p. 7507-7512.
126. Colton, R.J., *Procedures in scanning probe microscopies*. 1998: John Wiley & Sons.
127. Wiesendanger, R. and R. Wiesendanger, *Scanning probe microscopy and spectroscopy: Methods and applications*. Scanning probe microscopy and spectroscopy: Methods and applications. 1994: Cambridge University Press, 40 W. 20th Street, New York, New York 10011-4211, USA The Pitt Building, Trumpington Street, Cambridge CB2 1RP, England. xxii+637p.
128. Martin, Y., C. Williams, and H.K. Wickramasinghe, *Atomic force microscope–force mapping and profiling on a sub 100-Å scale.* Journal of Applied Physics, 1987. **61**(10): p. 4723-4729.
129. Santos, N.C. and M.A. Castanho, *An overview of the biophysical applications of atomic force microscopy.* Biophysical chemistry, 2004. **107**(2): p. 133-149.

130. Jalili, N. and K. Laxminarayana, *A review of atomic force microscopy imaging systems: application to molecular metrology and biological sciences.* Mechatronics, 2004. **14**(8): p. 907-945.
131. Fujiwara, H., *Spectroscopic ellipsometry: principles and applications*. 2007: John Wiley & Sons.
132. Liu, G. and G. Zhang, *QCM-D Studies on Polymer Behavior at Interfaces*. 2013: Springer.
133. Alder, J.F. and J.J. McCallum, *Piezoelectric crystals for mass and chemical measurements. A review.* Analyst, 1983. **108**(1291): p. 1169-1189.
134. Buttry, D.A. and M.D. Ward, *Measurement of interfacial processes at electrode surfaces with the electrochemical quartz crystal microbalance.* Chemical Reviews, 1992. **92**(6): p. 1355-1379.
135. O'sullivan, C. and G. Guilbault, *Commercial quartz crystal microbalances–theory and applications.* Biosensors and bioelectronics, 1999. **14**(8): p. 663-670.
136. Sauerbrey, G., *Use of quartz vibration for weighing thin films on a microbalance.* J. Physik, 1959. **155**: p. 206-212.
137. Höök, F., et al., *Variations in coupled water, viscoelastic properties, and film thickness of a Mefp-1 protein film during adsorption and cross-linking: a quartz crystal microbalance with dissipation monitoring, ellipsometry, and surface plasmon resonance study.* Analytical chemistry, 2001. **73**(24): p. 5796-5804.
138. Rodahl, M., et al., *Quartz crystal microbalance setup for frequency and Q-factor measurements in gaseous and liquid environments.* Review of Scientific Instruments, 1995. **66**(7): p. 3924-3930.
139. Höök, F., et al., *Energy dissipation kinetics for protein and antibody-antigen adsorption under shear oscillation on a quartz crystal microbalance.* Langmuir, 1998. **14**(4): p. 729-734.
140. Kanazawa, K.K. and J.G. Gordon, *Frequency of a quartz microbalance in contact with liquid.* Analytical Chemistry, 1985. **57**(8): p. 1770-1771.
141. Rodahl, M. and B. Kasemo, *On the measurement of thin liquid overlayers with the quartz-crystal microbalance.* Sensors and Actuators A: Physical, 1996. **54**(1): p. 448-456.
142. Voinova, M.V., et al., *Viscoelastic acoustic response of layered polymer films at fluid-solid interfaces: continuum mechanics approach.* Physica Scripta, 1999. **59**(5): p. 391.
143. Reviakine, I., D. Johannsmann, and R.P. Richter, *Hearing what you cannot see and visualizing what you hear: interpreting quartz crystal microbalance data from solvated interfaces.* Analytical chemistry, 2011. **83**(23): p. 8838-8848.
144. Barr, T.L., *Modern ESCAThe Principles and Practice of X-Ray Photoelectron Spectroscopy*. 1994: CRC press.

145. Brandon, D. and W.D. Kaplan, *Microstructural characterization of materials*. 2013: John Wiley & Sons.
146. Chabinyc, M.L., et al., *X-ray scattering study of thin films of poly (2, 5-bis (3-alkylthiophen-2-yl) thieno [3, 2-b] thiophene).* Journal of the American Chemical Society, 2007. **129**(11): p. 3226-3237.
147. Baker, J.L., et al., *Quantification of thin film crystallographic orientation using X-ray diffraction with an area detector.* Langmuir, 2010. **26**(11): p. 9146-9151.
148. Himmel, M.E., et al., *Biomass recalcitrance: engineering plants and enzymes for biofuels production.* science, 2007. **315**(5813): p. 804-807.
149. Mood, S.H., et al., *Lignocellulosic biomass to bioethanol, a comprehensive review with a focus on pretreatment.* Renewable and Sustainable Energy Reviews, 2013. **27**: p. 77-93.
150. Yang, B. and C.E. Wyman, *Pretreatment: the key to unlocking low-cost cellulosic ethanol.* Biofuels, Bioproducts and Biorefining, 2008. **2**(1): p. 26-40.
151. Rosgaard, L., et al., *Evaluation of minimal Trichoderma reesei cellulase mixtures on differently pretreated barley straw substrates.* Biotechnology progress, 2007. **23**(6): p. 1270-1276.
152. Park, S., et al., *Research cellulose crystallinity index: measurement techniques and their impact on interpreting cellulase performance.* Biotechnol Biofuels, 2010. **3**(10).
153. Zhang, Y.-H.P., et al., *A transition from cellulose swelling to cellulose dissolution by o-phosphoric acid: evidence from enzymatic hydrolysis and supramolecular structure.* Biomacromolecules, 2006. **7**(2): p. 644-648.
154. Lynd, L.R., et al., *Microbial cellulose utilization: fundamentals and biotechnology.* Microbiology and molecular biology reviews, 2002. **66**(3): p. 506-577.
155. Ooshima, H., M. Sakata, and Y. Harano, *Adsorption of cellulase from Trichoderma viride on cellulose.* Biotechnology and Bioengineering, 1983. **25**(12): p. 3103-3114.
156. Arantes, V. and J.N. Saddler, *Access to cellulose limits the efficiency of enzymatic hydrolysis: the role of amorphogenesis.* Biotechnol Biofuels, 2010. **3**(4): p. 1-11.
157. Arantes, V. and J.N. Saddler, *Cellulose accessibility limits the effectiveness of minimum cellulase loading on the efficient hydrolysis of pretreated lignocellulosic substrates.* Biotechnology for Biofuels, 2011. **4**(1): p. 1-17.
158. Chandra, R.P., A.R. Esteghlalian, and J.N. Saddler, *Assessing substrate accessibility to enzymatic hydrolysis by cellulases.* Characterization of lignocellulosic materials, 2008: p. 60-80.

159. Lee, D., et al., *Evaluation of the enzymatic susceptibility of cellulosic substrates using specific hydrolysis rates and enzyme adsorption.* Applied Biochemistry and Biotechnology, 1994. **45**(1): p. 407-415.
160. Hu, J., et al., *The Accessible Cellulose Surface Influences Cellulase Synergism during the Hydrolysis of Lignocellulosic Substrates.* ChemSusChem, 2015. **8**(5): p. 901-907.
161. Maurer, S.A., C.N. Bedbrook, and C.J. Radke, *Competitive sorption kinetics of inhibited endo-and exoglucanases on a model cellulose substrate.* Langmuir, 2012. **28**(41): p. 14598-14608.
162. Norgren, M., et al., *Smooth model surfaces from lignin derivatives. II. Adsorption of polyelectrolytes and PECs monitored by QCM-D.* Langmuir, 2007. **23**(7): p. 3737-3743.
163. Hu, G., J.A. Heitmann Jr, and O.J. Rojas, *In situ monitoring of cellulase activity by microgravimetry with a quartz crystal microbalance.* The Journal of Physical Chemistry B, 2009. **113**(44): p. 14761-14768.
164. Jiang, F., et al., *Effects of sulfate groups on the adsorption and activity of cellulases on cellulose substrates.* Langmuir, 2013. **29**(10): p. 3280-3291.
165. Zhou, W., et al., *Cellulose hydrolysis in evolving substrate morphologies I: a general modeling formalism.* Biotechnology and bioengineering, 2009. **104**(2): p. 261-274.
166. Zhou, W., et al., *Cellulose hydrolysis in evolving substrate morphologies II: Numerical results and analysis.* Biotechnology and bioengineering, 2009. **104**(2): p. 275-289.
167. Aulin, C., et al., *Nanoscale Cellulose Films with Different Crystallinities and Mesostructures□ Their Surface Properties and Interaction with Water.* Langmuir, 2009. **25**(13): p. 7675-7685.
168. Gunnars, S., L. Wågberg, and M.C. Stuart, *Model films of cellulose: I. Method development and initial results.* Cellulose, 2002. **9**(3-4): p. 239-249.
169. Fält, S., et al., *Model films of cellulose ID–improved preparation method and characterization of the cellulose film.* Cellulose, 2004. **11**(2): p. 151-162.
170. Dong, X.M., J.-F. Revol, and D.G. Gray, *Effect of microcrystallite preparation conditions on the formation of colloid crystals of cellulose.* Cellulose, 1998. **5**(1): p. 19-32.
171. Edgar, C.D. and D.G. Gray, *Smooth model cellulose I surfaces from nanocrystal suspensions.* Cellulose, 2003. **10**(4): p. 299-306.
172. Maurer, S., et al., *Surface kinetics for cooperative fungal cellulase digestion of cellulose from quartz crystal microgravimetry.* Journal of colloid and interface science, 2013. **394**: p. 498-508.

173. Nidetzky, B., et al., *Cellulose hydrolysis by the cellulases from Trichoderma reesei: a new model for synergistic interaction.* Biochem. J, 1994. **298**: p. 705-710.
174. Segal, L., et al., *An empirical method for estimating the degree of crystallinity of native cellulose using the X-ray diffractometer.* Textile Research Journal, 1959. **29**(10): p. 786-794.
175. Kittle, J.D., et al., *Equilibrium water contents of cellulose films determined via solvent exchange and quartz crystal microbalance with dissipation monitoring.* Biomacromolecules, 2011. **12**(8): p. 2881-2887.
176. Kostylev, M., et al., *Determination of the molecular states of the processive endocellulase Thermobifida fusca Cel9A during crystalline cellulose depolymerization.* Biotechnology and bioengineering, 2012. **109**(1): p. 295-299.
177. Beckham, G.T., et al., *Molecular-level origins of biomass recalcitrance: decrystallization free energies for four common cellulose polymorphs.* The Journal of Physical Chemistry B, 2011. **115**(14): p. 4118-4127.
178. Takashima, S., et al., *Correlation between cellulose binding and activity of cellulose-binding domain mutants of Humicola grisea cellobiohydrolase 1.* FEBS letters, 2007. **581**(30): p. 5891-5896.
179. Zheng, Y., et al., *Non-ionic surfactants and non-catalytic protein treatment on enzymatic hydrolysis of pretreated creeping wild ryegrass*, in *Biotechnology for Fuels and Chemicals*. 2008, Springer. p. 351-368.
180. Kristensen, J.B., et al., *Use of surface active additives in enzymatic hydrolysis of wheat straw lignocellulose.* Enzyme and Microbial Technology, 2007. **40**(4): p. 888-895.
181. Yang, B. and C.E. Wyman, *Pretreatment: the key to unlocking low-cost cellulosic ethanol.* Biofuels, Bioproducts and Biorefining, 2008. **2**(1): p. 26-40.
182. Marjamaa, K., et al., *Novel Penicillium cellulases for total hydrolysis of lignocellulosics.* Enzyme and microbial technology, 2013. **52**(6): p. 358-369.
183. Thongekkaew, J., et al., *Fusion of cellulose binding domain from Trichoderma reesei CBHI to Cryptococcus sp. S-2 cellulase enhances its binding affinity and its cellulolytic activity to insoluble cellulosic substrates.* Enzyme and microbial technology, 2013. **52**(4): p. 241-246.
184. Helle, S.S., S.J. Duff, and D.G. Cooper, *Effect of surfactants on cellulose hydrolysis.* Biotechnology and Bioengineering, 1993. **42**(5): p. 611-617.
185. Kaar, W.E. and M.T. Holtzapple, *Benefits from Tween during enzymic hydrolysis of corn stover.* Biotechnology and Bioengineering, 1998. **59**(4): p. 419-427.

186. Sipos, B., et al., *Hydrolysis efficiency and enzyme adsorption on steam-pretreated spruce in the presence of poly (ethylene glycol).* Enzyme and Microbial Technology, 2010. **47**(3): p. 84-90.
187. Zhou, Y., et al., *Non-ionic surfactants do not consistently improve the enzymatic hydrolysis of pure cellulose.* Bioresource technology, 2015. **182**: p. 136-143.
188. Steiner, W., W. Sattler, and H. Esterbauer, *Adsorption of Trichoderma reesei cellulase on cellulose: experimental data and their analysis by different equations.* Biotechnology and bioengineering, 1988. **32**(7): p. 853-865.
189. Linder, M. and T.T. Teeri, *The roles and function of cellulose-binding domains.* Journal of Biotechnology, 1997. **57**(1): p. 15-28.
190. Josefsson, P., G. Henriksson, and L. Wågberg, *The physical action of cellulases revealed by a quartz crystal microbalance study using ultrathin cellulose films and pure cellulases.* Biomacromolecules, 2007. **9**(1): p. 249-254.
191. Suchy, M., et al., *Quantitative assessment of the enzymatic degradation of amorphous cellulose by using a quartz crystal microbalance with dissipation monitoring.* Langmuir, 2011. **27**(14): p. 8819-8828.
192. Castanon, M. and C.R. Wilke, *Effects of the surfactant Tween 80 on enzymatic hydrolysis of newspaper.* Biotechnology and Bioengineering, 1981. **23**(6): p. 1365-1372.
193. Park, J.W., et al., *Effects of nonionic surfactant on enzymatic hydrolysis of used newspaper.* Biotechnology and bioengineering, 1992. **39**(1): p. 117-120.
194. Brinck, J., B. Jönsson, and F. Tiberg, *Kinetics of nonionic surfactant adsorption and desorption at the silica-water interface: one component.* Langmuir, 1998. **14**(5): p. 1058-1071.
195. Tiberg, F., et al., *Ellipsometry studies of the self-assembly of nonionic surfactants at the silica-water interface: equilibrium aspects.* Langmuir, 1994. **10**(7): p. 2294-2300.
196. Dixit, N., K.M. Maloney, and D.S. Kalonia, *Protein-silicone oil interactions: Comparative effect of nonionic surfactants on the interfacial behavior of a fusion protein.* Pharmaceutical research, 2013. **30**(7): p. 1848-1859.
197. Song, J., W.E. Krause, and O.J. Rojas, *Adsorption of polyalkyl glycol ethers and triblock nonionic polymers on PET.* Journal of colloid and interface science, 2014. **420**: p. 174-181.
198. Paria, S. and K.C. Khilar, *A review on experimental studies of surfactant adsorption at the hydrophilic solid–water interface.* Advances in colloid and interface science, 2004. **110**(3): p. 75-95.

199. Torn, L.H., et al., *Adsorption of nonionic surfactants on cellulose surfaces: Adsorbed amounts and kinetics.* Langmuir, 2005. **21**(17): p. 7768-7775.
200. Ebadi, A., J.S.S. Mohammadzadeh, and A. Khudiev, *What is the correct form of BET isotherm for modeling liquid phase adsorption?* Adsorption, 2009. **15**(1): p. 65-73.
201. Yamane, C., et al., *Two different surface properties of regenerated cellulose due to structural anisotropy.* Polymer journal, 2006. **38**(8): p. 819-826.
202. Seo, D.-J., H. Fujita, and A. Sakoda, *Effects of a non-ionic surfactant, Tween 20, on adsorption/desorption of saccharification enzymes onto/from lignocelluloses and saccharification rate.* Adsorption, 2011. **17**(5): p. 813-822.
203. Yang, M., et al., *Improvement of cellulose conversion caused by the protection of Tween-80 on the adsorbed cellulase.* Biochemical Engineering Journal, 2011. **56**(3): p. 125-129.
204. Achyuthan, K.E., et al., *Supramolecular self-assembled chaos: polyphenolic lignin's barrier to cost-effective lignocellulosic biofuels.* Molecules, 2010. **15**(12): p. 8641-8688.
205. Pareek, N., T. Gillgren, and L.J. Jönsson, *Adsorption of proteins involved in hydrolysis of lignocellulose on lignins and hemicelluloses.* Bioresource technology, 2013. **148**: p. 70-77.
206. Nakagame, S., et al., *The isolation, characterization and effect of lignin isolated from steam pretreated Douglas-fir on the enzymatic hydrolysis of cellulose.* Bioresource technology, 2011. **102**(6): p. 4507-4517.
207. Xue, Y., H. Jameel, and S. Park, *Strategies to recycle enzymes and their impact on enzymatic hydrolysis for bioethanol production.* Bioresources, 2011. **7**(1): p. 0602-0615.
208. Tu, M., R.P. Chandra, and J.N. Saddler, *Evaluating the distribution of cellulases and the recycling of free cellulases during the hydrolysis of lignocellulosic substrates.* Biotechnology progress, 2007. **23**(2): p. 398-406.
209. Speight, R.E. and M.A. Cooper, *A survey of the 2010 quartz crystal microbalance literature.* Journal of Molecular Recognition, 2012. **25**(9): p. 451-473.
210. Constantino, C., et al., *Langmuir-Blodgett films from lignins.* Thin Solid Films, 1996. **284**: p. 191-194.
211. Norgren, M., et al., *Smooth model surfaces from lignin derivatives. I. Preparation and characterization.* Langmuir, 2006. **22**(3): p. 1209-1214.
212. Tammelin, T., et al., *Preparation of lignin and extractive model surfaces by using spincoating technique-Application for QCM-D studies.* Nordic Pulp & Paper Research Journal, 2006. **21**(4): p. 444-450.

213. Salas, C., et al., *On the surface interactions of proteins with lignin.* ACS applied materials & interfaces, 2012. **5**(1): p. 199-206.
214. Lou, H., et al., *Reducing non-productive adsorption of cellulase and enhancing enzymatic hydrolysis of lignocelluloses by noncovalent modification of lignin with lignosulfonate.* Bioresource technology, 2013. **146**: p. 478-484.
215. Seo, D.-J., H. Fujita, and A. Sakoda, *Structural changes of lignocelluloses by a nonionic surfactant, Tween 20, and their effects on cellulase adsorption and saccharification.* Bioresource technology, 2011. **102**(20): p. 9605-9612.
216. Kirby, S.M., S.L. Anna, and L.M. Walker, *Sequential adsorption of an irreversibly adsorbed nonionic surfactant and an anionic surfactant at an oil/aqueous interface.* Langmuir, 2015. **31**(14): p. 4063-4071.
217. Reinikainen, T., O. Teleman, and T.T. Teeri, *Effects of pH and high ionic strength on the adsorption and activity of native and mutated cellobiohydrolase I from Trichoderma reesei.* Proteins: Structure, Function, and Bioinformatics, 1995. **22**(4): p. 392-403.
218. Guo, F., et al., *Differences in the adsorption of enzymes onto lignins from diverse types of lignocellulosic biomass and the underlying mechanism.* Biotechnology for biofuels, 2014. **7**(1): p. 1-10.
219. Wyman, C.E., *BIOMASS ETHANOL: Technical Progress, Opportunities, and Commercial Challenges.* Annual Review of Energy and the Environment, 1999. **24**(1): p. 189-226.
220. Schülein, M., *Protein engineering of cellulases.* Biochimica et Biophysica Acta (BBA)-Protein Structure and Molecular Enzymology, 2000. **1543**(2): p. 239-252.
221. Bommarius, A.S., et al., *Protein engineering of cellulases.* Current opinion in biotechnology, 2014. **29**: p. 139-145.
222. Chundawat, S.P., et al., *Deconstruction of lignocellulosic biomass to fuels and chemicals.* Annual review of chemical and biomolecular engineering, 2011. **2**: p. 121-145.
223. Sukumaran, R.K., et al., *Cellulase production using biomass feed stock and its application in lignocellulose saccharification for bio-ethanol production.* Renewable Energy, 2009. **34**(2): p. 421-424.
224. Divne, C., et al., *The three-dimensional crystal structure of the catalytic core of cellobiohydrolase I from Trichoderma reesei.* Science, 1994. **265**(5171): p. 524-528.
225. Kipper, K., P. Valjamae, and G. Johansson, *Processive action of cellobiohydrolase Cel7A from Trichoderma reesei is revealed as' burst'kinetics on fluorescent polymeric model substrates.* Biochem. J, 2005. **385**: p. 527-535.

226. Li, Y., D.C. Irwin, and D.B. Wilson, *Processivity, substrate binding, and mechanism of cellulose hydrolysis by Thermobifida fusca Cel9A.* Applied and environmental microbiology, 2007. **73**(10): p. 3165-3172.
227. Kristensen, J., C. Felby, and H. Jørgensen, *Determining Yields in High Solids Enzymatic Hydrolysis of Biomass.* Applied Biochemistry and Biotechnology, 2009. **156**(1-3): p. 127-132.
228. Modenbach, A.A. and S.E. Nokes, *Enzymatic hydrolysis of biomass at high-solids loadings–a review.* Biomass and Bioenergy, 2013. **56**: p. 526-544.
229. Kristensen, J.B., C. Felby, and H. Jørgensen, *Yield-determining factors in high-solids enzymatic hydrolysis of lignocellulose.* Biotechnology for Biofuels, 2009. **2**(1): p. 11.
230. Du, J., et al., *Factors to decrease the cellulose conversion of enzymatic hydrolysis of lignocellulose at high solid concentrations.* Cellulose, 2014. **21**(4): p. 2409-2417.
231. Nymand Olsen, S., et al., *The Role of Product Inhibition as a Yield-Determining Factor in Enzymatic High-Solid Hydrolysis of Pretreated Corn Stover.* Applied biochemistry and biotechnology, 2014.
232. Gonzàlez, G., et al., *A kinetic model for pretreated wheat straw saccharification by cellulase.* Journal of chemical technology and biotechnology, 1989. **44**(4): p. 275-288.
233. Lee, Y.H. and L. Fan, *Kinetic studies of enzymatic hydrolysis of insoluble cellulose:(II). Analysis of extended hydrolysis times.* Biotechnology and Bioengineering, 1983. **25**(4): p. 939-966.
234. Gan, Q., S. Allen, and G. Taylor, *Kinetic dynamics in heterogeneous enzymatic hydrolysis of cellulose: an overview, an experimental study and mathematical modelling.* Process Biochemistry, 2003. **38**(7): p. 1003-1018.
235. Gusakov, A.V. and A.P. Sinitsyn, *A theoretical analysis of cellulase product inhibition: Effect of cellulase binding constant, enzyme/substrate ratio, and β-glucosidase activity on the inhibition pattern.* Biotechnology and Bioengineering, 1992. **40**(6): p. 663-671.
236. Tanaka, M., et al., *Effect of pore size in substrate and diffusion of enzyme on hydrolysis of cellulosic materials with cellulases.* Biotechnology and bioengineering, 1988. **32**(5): p. 698-706.
237. Desai, S.G. and A.O. Converse, *Substrate reactivity as a function of the extent of reaction in the enzymatic hydrolysis of lignocellulose.* Biotechnology and bioengineering, 1997. **56**(6): p. 650-655.
238. Nidetzky, B. and W. Steiner, *A new approach for modeling cellulase–cellulose adsorption and the kinetics of the enzymatic hydrolysis of microcrystalline cellulose.* Biotechnology and bioengineering, 1993. **42**(4): p. 469-479.

239. Zhang, S., D.E. Wolfgang, and D.B. Wilson, *Substrate heterogeneity causes the nonlinear kinetics of insoluble cellulose hydrolysis.* Biotechnology and bioengineering, 1999. **66**(1): p. 35-41.
240. Lenz, J., et al., *Changes of structure and morphology of regenerated cellulose caused by acid and enzymatic hydrolysis.* Journal of Applied Polymer Science, 1990. **41**(5-6): p. 1315-1326.
241. Bezerra, R.M. and A.A. Dias, *Discrimination among eight modified Michaelis-Menten kinetics models of cellulose hydrolysis with a large range of substrate/enzyme ratios.* Applied biochemistry and biotechnology, 2004. **112**(3): p. 173-184.
242. Schnell, S. and P.K. Maini, *A Century of Enzyme Kinetics: Reliability of the KM and vmax Estimates.* Comm. Theoret. Biol, 2003. **8**: p. 169-187.
243. Sousa Jr, R., et al., *Recent trends in the modeling of cellulose hydrolysis.* Brazilian Journal of Chemical Engineering, 2011. **28**(4): p. 545-564.
244. Zhang, Y.H.P. and L.R. Lynd, *Toward an aggregated understanding of enzymatic hydrolysis of cellulose: noncomplexed cellulase systems.* Biotechnology and bioengineering, 2004. **88**(7): p. 797-824.
245. Xu, F. and H. Ding, *A new kinetic model for heterogeneous (or spatially confined) enzymatic catalysis: contributions from the fractal and jamming (overcrowding) effects.* Applied Catalysis A: General, 2007. **317**(1): p. 70-81.
246. Cruys-Bagger, N., et al., *Pre-steady-state kinetics for hydrolysis of insoluble cellulose by cellobiohydrolase Cel7A.* Journal of Biological Chemistry, 2012. **287**(22): p. 18451-18458.
247. Praestgaard, E., et al., *A kinetic model for the burst phase of processive cellulases.* Febs Journal, 2011. **278**(9): p. 1547-1560.
248. Maurer, S., C. Bedbrook, and C. Radke, *Cellulase adsorption and reactivity on a cellulose surface from flow ellipsometry.* Industrial & Engineering Chemistry Research, 2012. **51**(35): p. 11389-11400.
249. Andresen, M., et al., *Properties and characterization of hydrophobized microfibrillated cellulose.* Cellulose, 2006. **13**(6): p. 665-677.
250. Peterson, G.L., *A simplification of the protein assay method of Lowry< i> et al.</i> which is more generally applicable.* Analytical biochemistry, 1977. **83**(2): p. 346-356.
251. Kadam, K.L., E.C. Rydholm, and J.D. McMillan, *Development and validation of a kinetic model for enzymatic saccharification of lignocellulosic biomass.* Biotechnology progress, 2004. **20**(3): p. 698-705.
252. Peri, S., et al., *Modeling intrinsic kinetics of enzymatic cellulose hydrolysis.* Biotechnology progress, 2007. **23**(3): p. 626-637.

253. Wald, S., C.R. Wilke, and H.W. Blanch, *Kinetics of the enzymatic hydrolysis of cellulose.* Biotechnology and bioengineering, 1984. **26**(3): p. 221-230.
254. Sugimoto, N., et al., *Adsorption Characteristics of Fungal Family 1 Cellulose-Binding Domain from Trichoderma reesei Cellobiohydrolase I on Crystalline Cellulose: Negative Cooperative Adsorption via a Steric Exclusion Effect.* Langmuir, 2012. **28**(40): p. 14323-14329.
255. Medve, J., J. Ståhlberg, and F. Tjerneld, *Isotherms for adsorption of cellobiohydrolase I and II fromtrichoderma reesei on microcrystalline cellulose.* Applied biochemistry and biotechnology, 1997. **66**(1): p. 39-56.
256. Carrard, G., et al., *Cellulose-binding domains promote hydrolysis of different sites on crystalline cellulose.* Proceedings of the National Academy of Sciences, 2000. **97**(19): p. 10342-10347.
257. Luterbacher, J.S., L.P. Walker, and J.M. Moran-Mirabal, *Observing and modeling BMCC degradation by commercial cellulase cocktails with fluorescently labeled Trichoderma reseii Cel7A through confocal microscopy.* Biotechnology and bioengineering, 2013. **110**(1): p. 108-117.
258. Moon, R.J., et al., *Cellulose nanomaterials review: structure, properties and nanocomposites.* Chemical Society Reviews, 2011. **40**(7): p. 3941-3994.

VITA

Place of Birth:

India

Education:

Master of Science, Chemical Engineering, West Virginia University, August 2010

Bachelor of Technology, Chemical Engineering, Osmania University, India, April 2006

Publications:

Das, S., Wu, Q., Garlapalli, R., Nagpure, S., Strzalka, J., Jiang, Z., Rankin, S. E., "In-Situ GISAXS Investigation of Pore Orientation Effects on the Thermal Transformation Mechanism in Mesoporous Titania Thin Films", *J. Phys. Chem. C*, 118 (2), 968–976 (2014)

Garlapalli, R., Cho, E. H. and Yang, R., "Leaching of chalcopyrite with sodium hypochlorite", Metallurgical and Materials Transactions B, 41(2), 308-317(2010)

Cho, E. H., Chateker, P., Garlapalli, R., and Yang, R. Y. K., "Mercury removal from coal by leaching with SO_2", Energy & Fuels (American Chemical Society), 23, 774-778(2009)

Presentations:

Zhou, S, Garlapalli, R., Nokes, S. E., Rankin, S. E., and Knutson, B. L., "Quartz crystal microbalance investigation of cellulose hydrolysis by Clostridium Thermocellum on model cellulose films", AIChE Annual meeting, Atlanta, GA, (2014)

Garlapalli, R., Nokes, S. E., Knutson, B. L., and Rankin, S. E., "Role of Tween-80 in reduction of nonproductive cellulase binding to lignin", AIChE Annual meeting, Pittsburgh, PA, (2012)

Li, H., Garlapalli, R., Flythe, M. D., Nokes, S. E., Rankin, S. E., and Barbara, K. L., " Inhibition of enzymatic hydrolysis of soluble sugars on model cellulose films using quartz crystal microbalance", AIChE Annual meeting, Minneapolis, MN, (2011)

HONORS & AFFILIATIONS:

Recipient of BIACS Shashi Sathaye memorial scholarship (2013)

Recipient of best chemical engineering poster award, University of Kentucky (2012)